Report Documentation Page

Title and subtitle: **AISI/DOE Technology Roadmap Program: Development of Submerged Entry Nozzles that Resist Clogging**

Authors: **Jeffrey D. Smith and Kent D. Peaslee**

Performing Organization Names, Addresses:
University of Missouri-Rolla
1870 Miner Circle Dr.
Rolla, MO 65409-0330

Abstract:

Accretion formation and the associated clogging of SENs is a major problem for the steel industry leading to decreased strand speed, premature changing of SENs or strand termination and the associated reductions in productivity, consistency, and steel quality. A program to evaluate potentially clog resistant materials was initiated at the University of Missouri-Rolla. The main objective of the research effort was to identify combinations of steelmaking and refractory practices that would yield improved accretion resistance for tundish nozzles and submerged entry nozzles. A number of tasks were identified during the initial kick-off meeting and each was completed with two exceptions, the thermal shock validation and the industrial trials. Not completing these two tasks related to not having access to industrial scale production facilities. Though much of the results and information generated in the project is of proprietary nature, the main results can be summarized as follows:

1. The cathodoluminescence (CL) microscopy technique was found to be uniquely suited to study the nozzle clogging phenomenon.
2. Although all of the steel compositions investigated had significantly different equilibrium contact angles (with idealized refractory substrates) compared to pure iron, steel chemistry overall had a limited effect on wetting.
3. The predominant oxide inclusion in Al-killed steels was alumina, with some magnesium aluminate ($MgO.Al_2O_3$) and calcium hexa-aluminate ($CaO.6Al_2O_3$).
4. Both the microscopy data and the thermodynamic predictions indicated that the graphite-containing refractories resulted in the greatest degree of interactions between the molten steel and the refractory material. All of the carbon-free and impurity-free refractories resulted in significantly fewer interactions.
5. A series of nozzle clogging simulation design of experiments indicated the following trends:
    - Carbon content is the most important factor in determining clogging; lower the carbon, higher is the clogging tendency.
    - Titanium had the lowest effect on clogging.
    - Superheat appears to be beneficial for clogging.

Sponsor TBD Report No.:_____

AISI/DOE Technology Roadmap Program

Final Report

Development of Submerged Entry Nozzles That Resist Clogging

by

Jeffrey D. Smith
and
Kent D. Peaslee

October 14, 2002

Work Performed under Cooperative Agreement
No. DE-FC07-97ID13554

Prepared for
U.S. Department of Energy

Prepared by
American Iron and Steel Institute
Technology Roadmap Program Office
Pittsburgh, PA 15220

DISCLAIMER

"Any opinions, findings, and conclusions or recommendations expressed in this material are those of the author(s) and do not necessarily reflect the views of the US Department of Energy."

Number of pages in this report: 229

DOE and DOE contractors can obtain copies of this report FROM: Office of Scientific and Technical Information, P. O. Box 62, Oak Ridge, TN 37831. (615) 576-8401.

This report is publicly available from the Department of Commerce, National Technical Information Service, 5285 Port Royal Road, Springfield, VA 22161. (703) 487-4650.

TABLE OF CONTENTS

LIST OF FIGURES

Figure **Page**

LIST OF TABLES

Figure **Page**

EXECUTIVE SUMMARY

Accretion formation and the associated clogging of SENs is a major problem for the steel industry leading to decreased strand speed, premature changing of SENs or strand termination and the associated reductions in productivity, consistency, and steel quality. A program to evaluate potentially clog resistant materials was initiated at the University of Missouri-Rolla. The main objective of the research effort was to identify combinations of steelmaking and refractory practices that would yield improved accretion resistance for tundish nozzles and submerged entry nozzles. A number of tasks were identified during the initial kick-off meeting and each was completed with two exceptions, the thermal shock validation and the industrial trials. Not completing these two tasks related to not having access to industrial scale production facilities. Though much of the results and information generated in the project is of proprietary nature, the main results can be summarized as follows:

1. The cathodoluminescence (CL) microscopy technique was found to be uniquely suited to study the nozzle clogging phenomenon.
2. Although all of the steel compositions investigated had significantly different equilibrium contact angles (with idealized refractory substrates) compared to pure iron, steel chemistry overall had a limited effect on wetting.
3. The predominant oxide inclusion in Al-killed steels was alumina, with some magnesium aluminate ($MgO.Al_2O_3$) and calcium hexa-aluminate ($CaO.6Al_2O_3$).
4. Both the microscopy data and the thermodynamic predictions indicated that the graphite-containing refractories resulted in the greatest degree of interactions between the molten steel and the refractory material. All of the carbon-free and impurity-free refractories resulted in significantly fewer interactions.
5. A series of nozzle clogging simulation design of experiments indicated the following trends:
    - Carbon content is the most important factor in determining clogging; lower the carbon content, higher is the clogging tendency.
    - Titanium had the lowest effect on clogging.

- Superheat appears to be beneficial for clogging.

ACKNOWLEDGEMENT

"This material is based upon work supported by the U.S. Department of Energy and American Iron and Steel Institute under Award No. DE-FC07-97ID13554".

1.0 Introduction

Submerged Entry Nozzles (SENs) are used in the steelmaking process to prevent reoxidation of the molten steel directly from stream contact with the surrounding environment and from air entrainment and splashing when the molten stream strikes the liquid surface in the mold. Accretion formation and the associated clogging of SENs is a major problem for the steel industry leading to decreased strand speed, premature changing of SENs or strand termination and the associated reductions in productivity, consistency, and steel quality.

A program to evaluate potentially clog resistant materials was initiated at the University of Missouri-Rolla. The program was to involve post-mortem analysis of current nozzle systems and high temperature simulation of nozzle clogging, including wetting behavior studies.

2.0 Statement of Project Objectives

Proposed is a comprehensive refractory research program consisting of (1)Detailed post-mortem microstructural characterization of multiple nozzle accretions from steelmaking facilities using a range of casting conditions, (2)Development of a high temperature simulation that accurately reproduces the accretion so that materials can be evaluated under controlled conditions (temperature, steel chemistry, atmosphere, etc.) using a design of experiments approach, (3)Mathematical and finite modeling of fluid flow, heat transfer, and thermal/mechanical stress development, and texture simulations to predict the effect of SEN surface conditions on nozzle accretion, (4)Detailed wetting behavior of nozzle materials by molten steel as a function of steel chemistry and temperature, and (5)Development of a simulation that accurately reproduces the thermal shock conditions that are present during use of nozzles. These aspects, when combined, should provide the data necessary to define the mechanism(s) controlling nozzle accretion, providing the basis for developing new technologies for reduction or elimination of clogging.

3.0 Progress Toward Achieving Specified Tasks

A number of tasks were identified during the initial kick-off meeting for the program and are included in the following paragraphs.

Task 1 - Survey of Steelplants Sponsoring Research (08/98 - 12/98) - Survey information will include data from a recent AISI sponsored survey as well as information about techniques and equipment being used currently, successes and failures in recent trials, and identification of materials that sponsors wish to submit for post-mortem characterization.

Task 2 - Identification of Post-Mortem Samples (08/98 - 10/98) - A standard nozzle specimen will be selected based on the most common material used by sponsors and this material will be used in subsequent studies. Other types of nozzles will be selected for characterization based upon variations in refractory composition, metallurgical practice, observed performance, and type/location of accretion.

Task 3 - Literature Survey (08/98 - 06/99) - The initial objectives of the literature review will be three-fold; (1) highlight refractories that have been shown to be useful in reducing clogging of nozzles, (2) identify steel conditions that influence accretion especially those that yield consistent clogging or anti-clogging behavior, (3) critique all previous nozzle accretion experimentation. During the literature review, research groups conducting studies in this area will be identified. Where appropriate and with sponsorship approval, these groups will be contacted to determine possible interactions.

Task 4 - Design and Construct Accretion Simulation (09/98 - 09/99) - A furnace to simulate nozzle accretion will be designed and constructed. The equipment will be modeled after the concept indicated in the proposal, although appropriate modifications will be made if the literature review yields promising information.

Task 5 - Post-Mortem of Nozzle Specimens (10/98 - 06/00) - The standard nozzle specimen identified in the survey portion of the research will be subjected to the first post-mortem characterization effort. This post-characterization will be used not only to examine the specimens but also to determine which characterization techniques are the most useful for evaluating used nozzles.

Task 6 - Accretion Simulation on Standard Nozzle Specimen (05/99 - 12/99) - Unused examples of the standard nozzle specimen will be obtained and used in the simulated accretion test. Multiple iterations based on variations in temperature, steel composition, oxygen partial pressure, etc., will be conducted until the resulting accretion is similar to that observed in the post-characterization portion of the research program.

Task 7 - Accretion Simulation - Metallurgical Effects (01/00 - 12/00) - The initial accretion studies will provide baseline conditions for the design of experiments study to determine the effects of key metallurgical variables. Small variations in steel composition, super heat, liquid steel velocity, etc., will be included in the design.

Task 8 - Contact Angle Measurements (10/98 - 12/00) - Contact angle studies will be used to identify refractory oxides that are not wet by the steel compositions of interest in this research. Refractory composition, temperature, steel composition, and oxygen partial pressure will be varied to determine how each affect the wetting behavior.

Task 9 - Accretion Simulation - Refractory Composition (11/00 - 04/01) - The last phase of the accretion simulation will include evaluating promising refractory aggregates as well as new nozzle materials from vendors. Initially specimens of new refractory aggregates will be fabricated at UMR, however at some point venders will have to be contacted to fabricate actual nozzles to allow comparative evaluations to be conducted.

Task 10 - Thermal Shock Validation (01/00 - 04/01) - The thermal shock simulation will be used to insure that candidate nozzles for field trials can withstand the thermal shock encountered during service.

Task 11 - Field Trials (07/00 - 06/01) - Field trials will be initiated at sponsor steelplants after sponsor representatives have reviewed results from the research and agree that the recommended modifications have the potential to be successful. Although nozzle performance will be the best measure of success, the corresponding post-mortem characterization will provide critical information concerning further improvements.

4.0 Results of Work

A study of the use of cathodoluminescence microscopy on accretion of steelmaking nozzles was initiated and the resulting manuscript is included as appendix A. The goal of the manuscript was to review previous nozzle clogging studies, focussing on post-mortem microscopy techniques, and to present microtexture results of nozzle clogging that were obtained using cathodoluminescence microscopy. The cathodoluminescence microscopy technique was found to be uniquely suited to study the nozzle clogging phenomenon. When CL was used in conjunction with reflected light microscopy and scanning electron microscopy, an extensive amount of information was generated.

The purpose of the industrial surveys (included as appendix B) was to determine the most difficult casting situations with respect to nozzle clogging and to gain background information on the operations of the supporting companies. The operating background information was used during examination of the post-mortem samples to assist in understanding the formations that were observed. The surveys were also used to gauge the direction in which the sponsoring companies wanted the research to progress. Information on caster types, factors influencing clogging, nozzle materials and corresponding use duration, tundish preparation and campaign duration, ladles and flow control devices was acquired from most of the sponsors.

A literature review entitled "Nozzle Accretion Formation in the Continuous Casting of Aluminum-Killed Steel" is included as Appendix C. Presented was a review of the nozzle clogging literature through 1998 including accretion morphology, proposed mechanisms of accretion formation, countermeasures utilized and experiments used to study or simulate nozzle clogging.

Appendix D is a manuscript reviewing the wetting behavior results. The sessile drop method, modified by use of a doser tube rather than *in situ* drop formation, was used to study commercial steel compositions in contact with idealized refractory substrates. Steels containing varying amounts of carbon, aluminum, and titanium were tested in hydrogen and forming gas atmospheres at 1600°C.

Thermochemical reactions that could effect nozzle clogging were investigated (see appendix E) using an alumina-graphite refractory crucible containing molten steel. This paper presents preliminary results of a study directed towards performing this characterization. The strategy used in the study was to perform static experiments with molten steel of various compositions in refractory crucibles made of typical nozzle materials, followed by a post mortem characterization using cathodoluminescence (CL) microscopy, scanning electron microscopy (SEM) and reflected light (RL) microscopy. From these static experiments a number of observations were made. The

predominant oxide inclusion in aluminum-killed steel was alumina with some magnesium aluminate ($MgO \bullet Al_2O_3$) and calcium hexa-aluminate ($CaO \bullet 6Al_2O_3$) also present.

A manuscript reviewing the casting simulation apparatus that was built to measure the effect of metallurgical and refractory factors on nozzle clogging is included as appendix F. Measurements taken with the apparatus were used to calculate a clogging factor (CF). The CF provided a quantitative method of evaluating different factors on the rate of accretion formation. Cathodoluminescence microscopy of nozzles used in the simulation has shown the accretions in the simulation nozzles to be reasonably similar both chemically and morphologically to those found in spent industrial nozzles.

Appendix G is a manuscript reviewing the study of inclusions in continuously cast. Non-metallic inclusions are inherent to wrought steel and are undesirable because they adversely affect the quality and fabrication of the formed steel. A microscopic technique called "Cathodoluminescence Microscopy" was used for rapid recognition and identification of macro- as well as micro- inclusions. This technique provided direct assessment of defects with little of the sample preparation required with other techniques. The CL images provided clear contrast among different inclusions that otherwise could not have been obtained by optical and electron microscopy techniques.

Accretions on the inner wall of submerged entry nozzles (SENs) are affected by interactions between molten steel and refractory materials. Thermochemical reactions that qualitatively explain these interactions were modeled using FACT thermodynamic software and the results are presented as Appendix H. Predictions were compared to results from high temperature static experiments. Steels were melted in refractory crucibles to understand the interactions and establish the effect of refractory and steel composition on accretion formation. Steels, with and without aluminum, and various oxide refractories, with and without graphite, were evaluated. Samples were characterized using cathodoluminescence (CL) microscopy, reflected light (RL) microscopy and scanning electron microscopy (SEM).

Appendix I is a manuscript presenting the results of experiments conducted to establish the effect of refractory composition on accretion formation. The experiments were conducted with various refractories, fabricated with controlled additives, which were then tested for their interactions with molten steel. The interactions between commonly used refractory materials and molten steel were explained. The strategy used in the study was to perform static experiments with molten steel of different compositions in crucibles made of various refractories, followed by a post characterization using cathodoluminescence microscopy (CLM), reflected light microscopy (RLM) and scanning electron microscopy (SEM).

The final results from the nozzle clogging simulation design of experiments are included as Appendix J. The approach was used to determine the effects of carbon, aluminum, titanium, and superheat of low carbon steels as well as the graphite and silica content of alumina nozzles on clogging. Although the experimental work is complete, the final interpretation of the results has not been completed. Casting curves and the associated clogging factors will be interpreted along with nozzle post-mortem analysis.

Appendix K is a manuscript reviewing a case study of an eight heat casting sequence on a two-strand continuous casting slab machine. Two SENs were used on each strand during the casting sequence. All four nozzles were provided to UMR for post-characterization. The summary includes macroscopic images of the SENs as well as microstructural analysis along the thickness and the height of each SEN.

5.0 Facts Impacting Performance

The greatest difficulty encountered during the program related to fabricating nozzles that could be used during industrial trials. UMR does not have the facilities necessary for fabrication of tundish nozzles, let alone the much larger submerged entry nozzles. Instead the assumption was that refractory supplier(s) could be included in the later stages of the program so that the results could be applied to industrial scale nozzles. Contacts were made and meetings were initiated, but no suitable agreement was reached. Sample nozzles were provided but only when the compositions requested were consistent with products that were already produced by the supplier.

As such the final two tasks could not be completed. Another approach was required in order to provide nozzles for industrial trials. Although beyond the scope of this study, thermal spray coating of industrial nozzles was one such approach. In that case existing nozzles could be coated with materials that have been engineered to be resistant to nozzle accretion. This approach is not intended to be the economically viable long-term solution but instead allows these new materials to be evaluated in industrial trials. Once materials have been proven successful in industrial trials, the issue of how they will be fabricated and ultimately provided to the steel producers will have to be resolved.

6.0 References

See individual appendices for reference materials.

7.0 Appendix A: Study of Continuous Casting Nozzle Clogging using Cathodoluminescence Microscopy

J.D. Smith[1], L. Trueba Jr.[2], M. Karakus[1], and K.D. Peaslee[2]
[1]Department of Ceramic Engineering
[2]Department of Metallurgical Engineering
University of Missouri-Rolla

Abstract

Previous studies have addressed the issue of clogging in continuous casting nozzles as well as the mechanisms leading to accretion. Although techniques such as clogging simulations, flow modeling, chemical additives and gas injection have helped minimize catastrophic nozzle accretions they have not eliminated the problem. This paper reviews previous studies, focussing on refractory/metal interactions and proposed clogging countermeasures. Post-mortem analysis of nozzle accretions using cathodoluminescence microscopy will also be reviewed in order to demonstrate the utility of this characterization technique.

Introduction

Continuous casting nozzle accretions have been a problem for the steel industry for several decades. During that timeframe, extensive investigation has yielded improvements in both the refractory materials and the steelmaking process. However accretion problems persist, especially during casting of low and ultra-low carbon, aluminum-killed steels. The goal of this manuscript is to review the previous studies, focussing on post-mortem microscopy techniques, and to present microtexture results of nozzle clogging that were obtained using cathodoluminescence microscopy. This characterization technique is uniquely suited to study the nozzle clogging phenomenon.

Review of Accretions

Accretion Morphology

Most researchers have focused on accretions associated with low or ultra-low carbon aluminum-killed steels that have not been calcium treated. Therefore, accretion morphologies with these types of steels will be discussed first. Then, factors that have been reported to effect morphology will be presented.

The morphology of accretions reported by different researchers varies somewhat. Ogibayashi pointed out that the differences are likely due to variations in the cleanliness of steel and casting conditions.[1] However, in all cases, the accretions consist of powdery, friable alumina and/or metal nodules containing clusters of alumina inclusions. Many researchers have pointed out that the morphology of the alumina inclusions in the steel nodules are the same as the alumina built up on the refractory wall.[2,3] Most commonly, the alumina clusters consist of individual, round alumina particles sintered together. The clusters have a coral-like appearance.

Ogibayashi and Poirier et al., have separately described the accretion formations as consisting of two layers as shown in Figure 1.[1,4] The first layer, at the refractory-accretion interface, is densely packed alumina with small particles of metal contained within the alumina network. The metal particles in this layer are reported to contain relatively high concentrations of silicon.[1]

This layer has also been reported to contain a minor component consisting of a vitreous phase of Al_2O_3, SiO_2, Na_2O, and K_2O.[4] The maximum thickness of this layer is 300 μm. The next layer, the buildup layer, consists of either alumina clusters with metal nodules containing clusters of alumina or mostly metal nodules containing clusters of alumina inclusions. Poirier et al. have also reported observing traces of spinels ($MgO\text{-}Al_2O_3$ and $MgO\text{-}Fe_2O_3$) in the build-up layer.[4]

Many researchers have also reported the formation of a decarburized layer in refractory materials containing graphite. The decarburized layer is adjacent to the accretion and has been reported to have a depth of approximately 400 μm.[4]

There are many factors that have been reported in the literature to effect accretion morphology. Among these are: location of the buildup in the pouring system, steel chemistry, deoxidation method, ladle treatment, and composition of the refractory.

Location seems to play an important role in the morphology of accretions in submerged entry nozzles (SENs). Kasai et al. observed that with various grades of aluminum and aluminum-silicon-killed steel, deposits in the SEN above the meniscus are composed mainly of solidified metal and alumina, while below the meniscus, the deposits consisted of mainly alumina.[5] Poirier et al. similarly reported that the upper portion of the nozzle (above the meniscus) characteristically contains approximately 80% iron and iron oxide. The lower portion of the nozzle contains approximately 80 to 90% alumina (see Figure 2).[6]

Steel chemistry has an important effect on accretion morphology. In particular, calcium treatment and deoxidation method effect accretion morphology. For example, McKague et al. have shown that aluminum-killed grades that are calcium treated will form calcium aluminates and, if sulfur levels are high enough, calcium sulfide accretions.[7] These investigators have also shown that the composition of the accretions is determined by the ratio of Al_2O_3 to CaO when the metal stream reaches the nozzle. These observations are also true for non-calcium treated steel cast with nozzles containing lime-bearing materials.

Researchers studying titanium-killed or titanium-added steels have also noted differences in morphologies of inclusions in the steel and accretions on nozzles. In the case of titanium-added, aluminum-killed steels, coarsening of the steel and alumina nodules that make up the accretion have been reported. The individual particles making up the inclusions and accretions have a granular shape. The composition of the accretions consists of mostly alumina with titanium oxide rarely being observed.[2] Accretions with titanium-killed steels, on the other hand, consist of mostly titanium oxide with approximately 6 to 7% alumina. These accretions have an angular shape, in contrast to the round, coral shape typically reported for aluminum-killed steels.[8]

The ladle treatment of steel also seems to affect nozzle accretion morphology. Ogibayashi et al. observed that when a heat of steel was subjected to DH degassing, the accretion material consisted of mostly metal that contained clusters of alumina. Those heats that were subjected only to argon bubbling had accretion formations that consisted mostly of alumina.[8] The difference in morphology is thought to be due to the difference in the cleanliness of the steel. The DH degassed steel is cleaner than steel that only receives argon stirring. Therefore, its accompanying accretions contain more solidified steel and less alumina.

Mechanisms of Formation

The most prominent theories of nozzle accretion formation are listed below.

1. The temperature drop that is inherent when steel flows through submerged entry nozzles causes a resulting decrease in the solubility of oxygen in steel. This drives the Al-O-Al_2O_3 equilibrium towards the alumina side, forming alumina accretions at the wall of the SEN nozzle.[9]

2. The flow of steel through the SEN causes low pressure to form inside the nozzle. This drives the diffusion of atmospheric oxygen through the nozzle wall. Aluminum in the melt is oxidized to form alumina at the nozzle wall either directly by the oxygen or indirectly from carbon monoxide formed by the reaction of oxygen with carbon in the refractory.[10]

3. Deoxidation and reoxidation products are driven to the nozzle wall due to fluid flow characteristics of the steel stream. Turbulence or separated flow around disturbances in the molten steel stream transports alumina to the nozzle where they attach due to a reduction in the overall surface energy of the system.[3]

4. Thermochemical reactions in the nozzle material transport oxygen either in the form of suboxides or carbon monoxide to the nozzle-steel interface where they react with aluminum in the steel to form alumina at the nozzle wall.[4]

It is possible that all of these mechanisms play a role in nozzle accretions. However, as Singh argued, theories 1 and 2 are not likely to play a significant role in nozzle clogging.[3] Severe clogging is often seen in areas that are submerged in molten steel such as the discharge of an SEN. This area is not likely to have a substantial temperature drop, and diffusion of air through the refractory is impossible because this area of the nozzle is surrounded by molten steel. One area where these conditions exist is the body of the SEN above the meniscus, and in that area, significant clogging rarely exists.

Singh also argued that theory 4 does not take place based on his observations in pilot-scale and bench-scale tests.[3] However, it should be noted that he used zirconia and alumina nozzles for his experiments. There is no indication as to whether or not the nozzles contained graphite, which Poirier et al., have indicated facilitates nozzle reactions.[4]

One likely theory presented by Ogibayashi indicates that the dense layer of alumina that is formed on the refractory surface is the result of thermochemical reactions between the refractory and the steel.[1] He goes on to say that the second, less-dense layer is the result of turbulent flow transporting the accretions to the nozzle wall. Once the alumina is transported to the nozzle wall, it adheres due to a reduction in interfacial energy of the system. Finally, the alumina accretion sinters to the dense alumina layer.

Post-Mortem Characterization of Nozzles

Sample Preparation

Multiple SENs and tundish nozzles were obtained from integrated US steel companies that typically experience nozzle clogging during the casting of aluminum-killed steel. Samples were photographed upon arrival and sectioned into sets of specimens for microstructural analysis.

Specimens were first impregnated with a low viscosity (60 cps) resin under vacuum and cured at 70°F overnight to ensure that the friable accretions would not be damaged during sample preparation. Impregnated specimens were then cut and mounted in plastic. Mounted specimens were ground to 600 grit with a rotating diamond disk and then polished with diamond paste and lapping oil to a 1 μm finish. Cleaned and dried specimens were then subjected to microstructural analysis.

CL Background

Refractory minerals, products, and slags produce characteristic colors when they interact with a high-energy electron beam. This optical emission phenomenon is called cathodoluminescence (CL). Alumina, Al_2O_3, for example, exhibits brilliant red CL (694 nm) due to the trace amounts of Cr^{3+} impurities in the corundum structure. Additionally, spinel, $MgAl_2O_4$, exhibits brilliant green CL (520 nm) due to tetrahedrally coordinated Mn^{2+} in the spinel structure. A large number of refractory minerals and products have been studied previously, and their CL characteristics cataloged.

A typical clogged nozzle accretion contains the following minerals and their associated CL responses:

1. Corundum (Al_2O_3): bright red CL
2. Spinel ($MgAl_2O_4$): bright green CL
3. Hibonite (CA_6 - $CaAl_{12}O_{19}$): green CL
4. Grossite (CA_2 - $CaAl_4O_7$): green-orange CL
5. Calcium-aluminate (CA - $CaAl_2O_4$): green-orange CL
6. Fe-oxides: (Fe_xO_y): non CL
7. Iron (Fe): non CL

The refractory nozzle materials and their characteristic emissions include:

1. Fused alumina grains: bright, dark red CL
2. Zirconia grains: intense blue-white CL
3. Fused alumina-zirconia (AZ) grains: intertwined bright, dark red and blue-white CL
4. Graphite: non-CL

Each mineral and component has a characteristic crystal habit and CL color, i.e. alumina in the clog as opposed to alumina in the refractory. The two different types of alumina are easily identified and characterized by CL microscopy.

Color photomicrographs of each of the samples were taken. The analytical advantages of the CL technique are demonstrated best with high-resolution color images. Due to publishing constraints, however, only select photos have been included in this report. Therefore, generalized sketches have been included to summarize observations made with the high-resolution color images. Color slides will be presented during the meetings to provide a complete record of the data. Upon completion of the analysis for each sample, a set of photos (color and black and white) along with the corresponding text will be available.

Microstructural Results

Photographs of the top and side views of a used submerged entry nozzle sample are shown in Figure 3 and Figure 4. This particular sample was the most severely clogged nozzle sample among the SENs studied. A sketch of the typical clog morphology is included as Figure 5. The

thickness of the clog material was approximately 20 mm in the area above the nozzle discharge ports and as much as 40 mm in the area below the discharge ports.

Figure 6 shows the characteristic structure of the "top" portion of the sample. It includes an approximately 15mm thick, loosely held (powdery) accretion and two refractory layers. The clog material appears light tan to yellowish-white in color and contains beads of metal. It consists predominantly of loosely held alumina (red to orange CL particles) and small amounts of CA_6 (green CL). Dark or black discoloration that was observed in the uppermost zone of the clog material was due to the oxidation of the metal phase to magnetite and hematite. A metal layer, as shown in Figure 6, separates the clog materials and the refractory materials. This metal layer has a typical gray iron microstructure with graphite flakes. Above this metal layer are the alumina deposits. Some refractory grains were also observed just above the metal layer. Below the metal layer is the first layer of the nozzle refractory. No decarburized zone was observed at the interface between the deposit and the refractories.

The nozzle refractory in the area of the meniscus line has a two-layer structure, an inner layer (approximately 13 mm thick) and an outer layer (approximately 19 mm thick). The outer layer consists of zirconia-graphite while the inner layer consists of alumina, fused alumina-zirconia, and graphite. The outer refractory layer is coated with a gray slag. This slag penetrated approximately 1-2 mm into the refractory and formed a dense zone. The slag deposit on the outer surface of the nozzle consists of spinel and CA_6 in a vitreous matrix.

Figure 7 shows the characteristic structure of the portion of the SEN sample below the meniscus. A very thick deposit (see Figure 5) is present in this area of the nozzle. The refractory in the bottom portion of the nozzle has a very different composition, compared to the rest of the nozzle, as a large concentration of cristobolite grains is present. It is likely that these grains were originally fused silica that crystallized during use.

The interface between the deposit and the nozzle is characterized by the presence of a steel layer. No decarburized zone was observed in this region. The clog was predominantly alumina that had a loose (friable) appearance but also contained spinel and CA_6. Areas of the accretion that contained increased amounts of spinel and CA_6 had a fused (glassy) appearance.

Figure 8 and Figure 9, included as an insert in this manuscript, are selected photographs from the nozzle characterization effort. RL images are on the left side of the Figures in the insert while CL images are on the right. Note the additional information that can be obtained by using RL and CL together.

Summary

A number of accretion formation mechanisms have been proposed in the literature and have been reviewed in this manuscript. Additionally, a considerable number of studies have used reflected light microscopy and scanning electron microscopy in an attempt to evaluate the various theories. Although these studies have been useful, none have provided definitive information regarding nozzle accretion formation.

This study has shown that CL microscopy is an effective technique for studying nozzle accretion. When CL is used in conjunction with RL and SEM, an extensive amount of information can be generated. Such detailed information is required to understand the mechanisms that lead to accretion formation.

Following is a summary of some of the relevant information obtained from the characterization effort.

1. The composition of the accretion seems to be independent of the type of refractory material and instead seems to relate directly to the chemistry of steel being cast. The powdery deposit sinters and forms a dense layer on the surface of the refractory. The amount of sintering is likely related to the casting time, temperature, and pressure at the location of the accretion.

2. 2. The composition of the inclusions (alumina, spinel, or Ca-aluminates) in the entrapped steel beads was similar to that of the accretion. This would imply that the accretion may be derived from inclusions within the steel.

3. 3. In a nozzle used to cast low carbon steel, the presence of gray iron on the surface of the nozzle was initially unexpected. This suggests that relatively high concentration of carbon and silicon must have been present. It is possible that both were derived from the nozzle through a carbothermal reduction of silica. Reduction of silica will generate carbon monoxide and silicon monoxide that can react with aluminum in the steel, leading to alumina formation with associated deposition of carbon and silicon.

4. 4. No chemical corrosion was observed in the interior of the nozzle and only limited mold flux corrosion was observed at the meniscus.

References

1. Ogibayashi, S. "Mechanism and Countermeasure of Alumina Buildup on Submerged Nozzle in Continuous Casting." *Taikabutsu Overseas*. Vol. 15, No. 1. pp. 3-14 (1994)

2. Hiraga, Y.; Yashima, Y.; Fujii, K. "Behavior of Alumina-deposition on Tundish Nozzles in Continuous Casting of Ti-Added Al Killed Steel". *Taikabutsu Overseas*. Vol. 15, No. 1. pp. 22-27 (1995)

3. Singh, S.N. "Mechanism of Alumina Buildup in Tundish Nozzles During Continuous Casting of Aluminum-Killed Steels". *Metallurgical Transactions*. Vol. 5. pp. 2165-2178 (1974)

4. Poirier, J.; Thillou, B.; Guiban, M.A.; Provost, G. "Mechanisms and Countermeasures of Alumina Clogging in Submerged Nozzles". *Steelmaking Conference Proceedings*. Vol. 78. pp. 451-456 (1995)

5. Kasai, N.; Kawasaki, M.; Hayashi, Y.; Kawai, H. "Explanation of Clogging Phenomena of CC Submerged Nozzle". *Taikabutsu Overseas*. Vol. 11, No. 1. pp. 22-33 (1990)

6. Poirier, J.; Verrelle, D.; Thillou, B.; Provost, G.; Taffin, C.; Tssot, P. "Study of Clogging Phenomena in Continuous Casting Submerged Nozzles". *UNITECR 1991*. pp. 226-229 (1991)

7. McKague, A.R.; Engel, R.; Suer, M.A.; Wolf, D.J.; Garbowsky, M.D.; Reed, L.F. "Resolution of Clogging at Armco's Mansfield Slab Caster". *Iron and Steelmaker*. Vol. 25, No. 11. pp. 35-41 (1998)

8. Ogibayashi, S.; Uchimura, M.; Maruki, Y.; Mizukoshi, D; Tanizawa, K. "Mechanism and Countermeasure of Alumina Buildup on Submerged Nozzle in Continuous Casting". *Steelmaking Conference Proceedings*. pp. 337-344 (1992)

9. Farrell, J.W.; Hilty, D.C. "Steel Flow Through Nozzles: Influence of Deoxidizers". *Electric Furnace Proceedings*. Vol. 29. pp. 31-45. (1971)

10. Benson, P.M.; Robinson, Q.K.; Dumazeau, C. "New Technique for the Prevention of Alumina Build-Up in Submerged Entry Nozzles for Continuous Casting". *UNITECR 1993*. pp. 1087-1096 (1993)

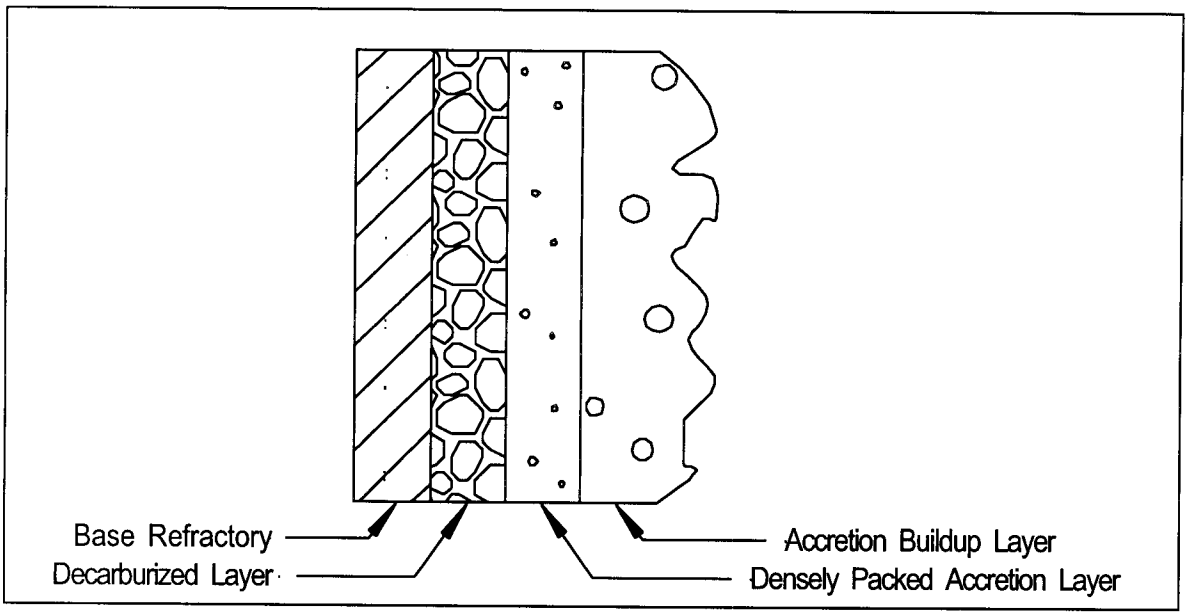

Figure 1. Schematic diagram of accretion morphology.

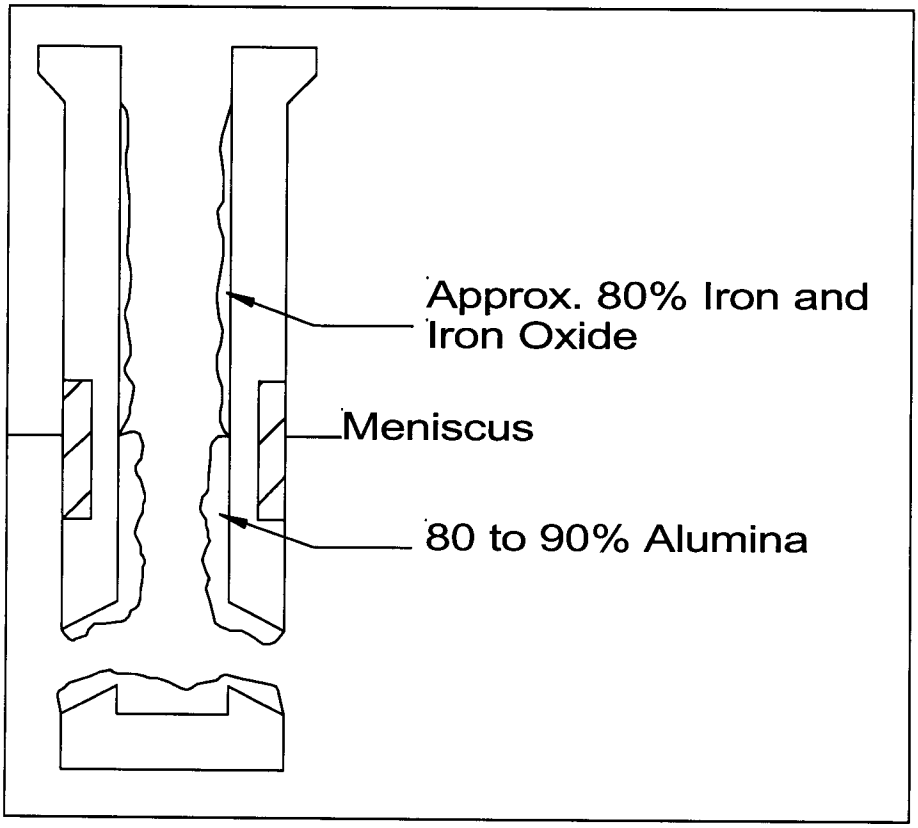

Figure 2. Schematic diagram of accretions in a submerged entry nozzle.

Figure 3. Appearance of a used submerged entry nozzle sample (top view).

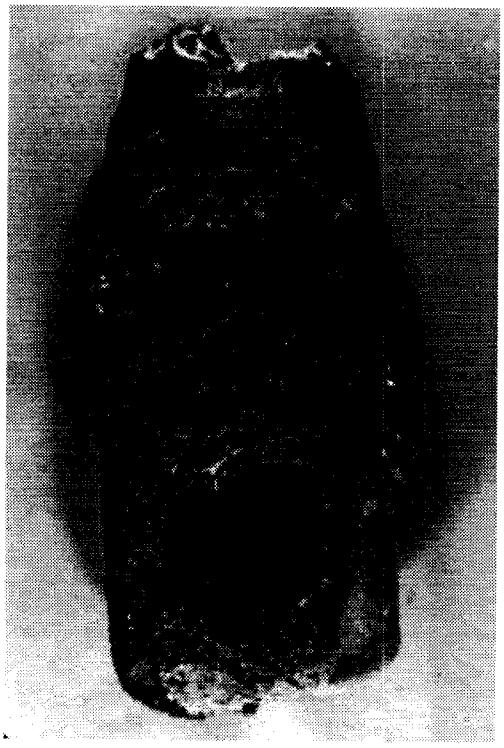

Figure 4. Photograph of the same nozzle sample showing corrosion of powder line and slag coating of refractory surface.

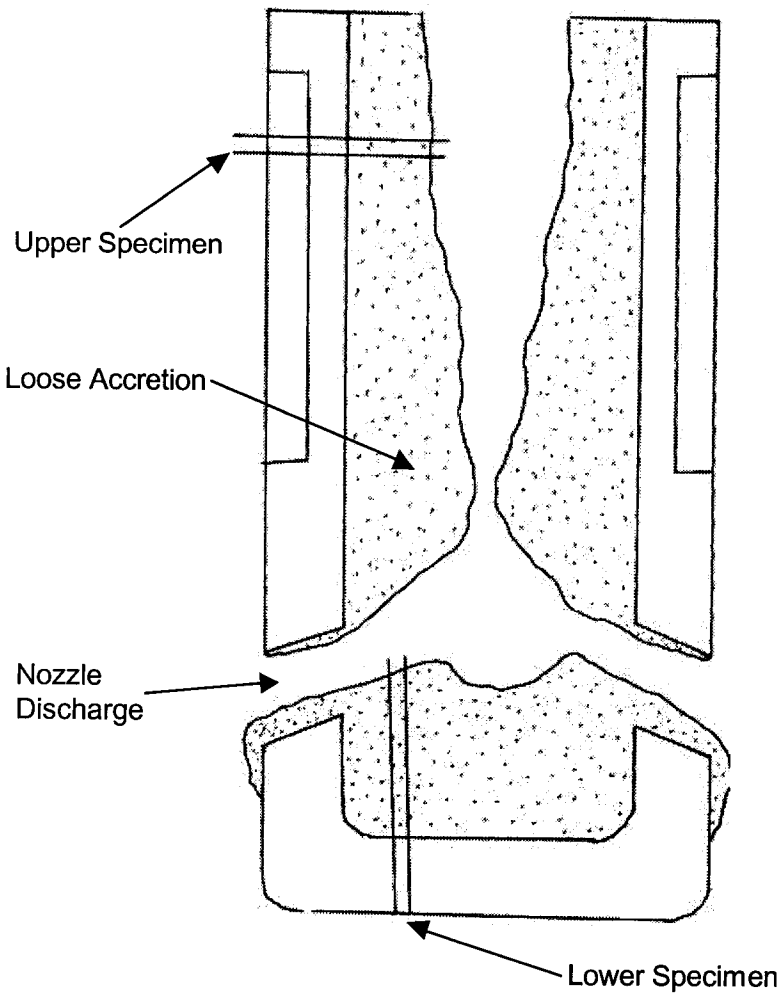

Figure 5. Schematic of a SEN showing accretion morphology and specimen locations.

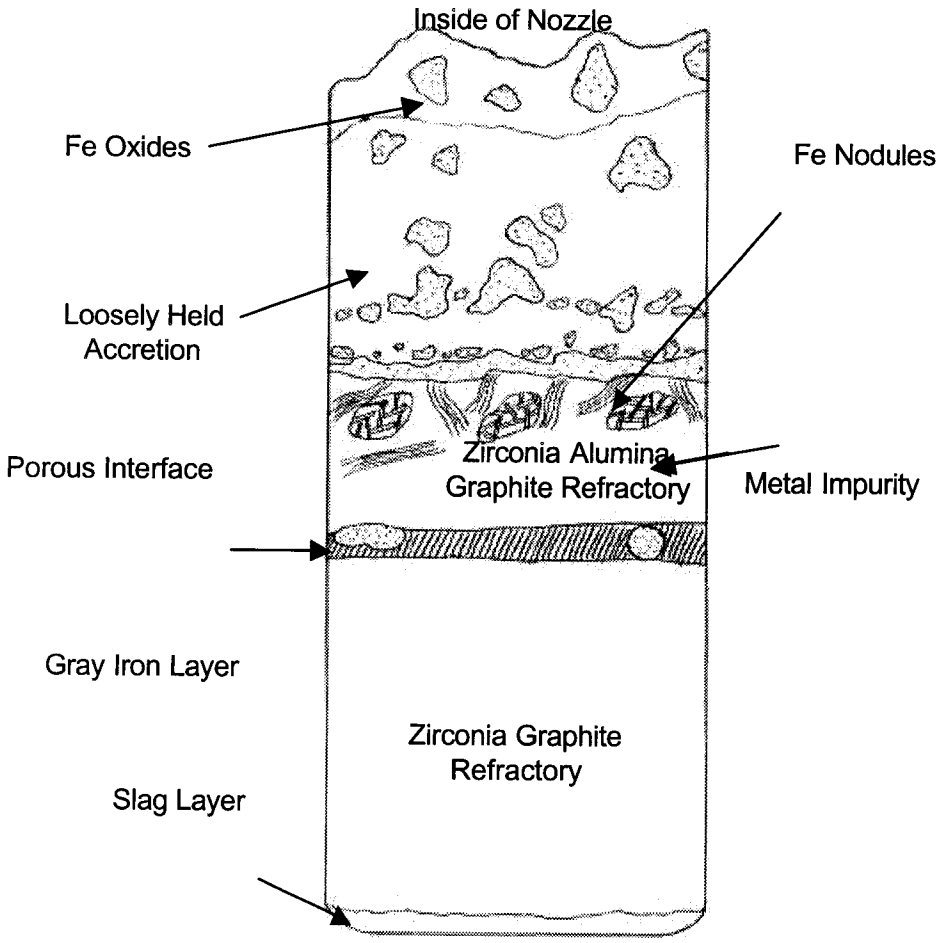

Figure 6. Sketch of the "top" portion of the SEN showing characteristic structures.

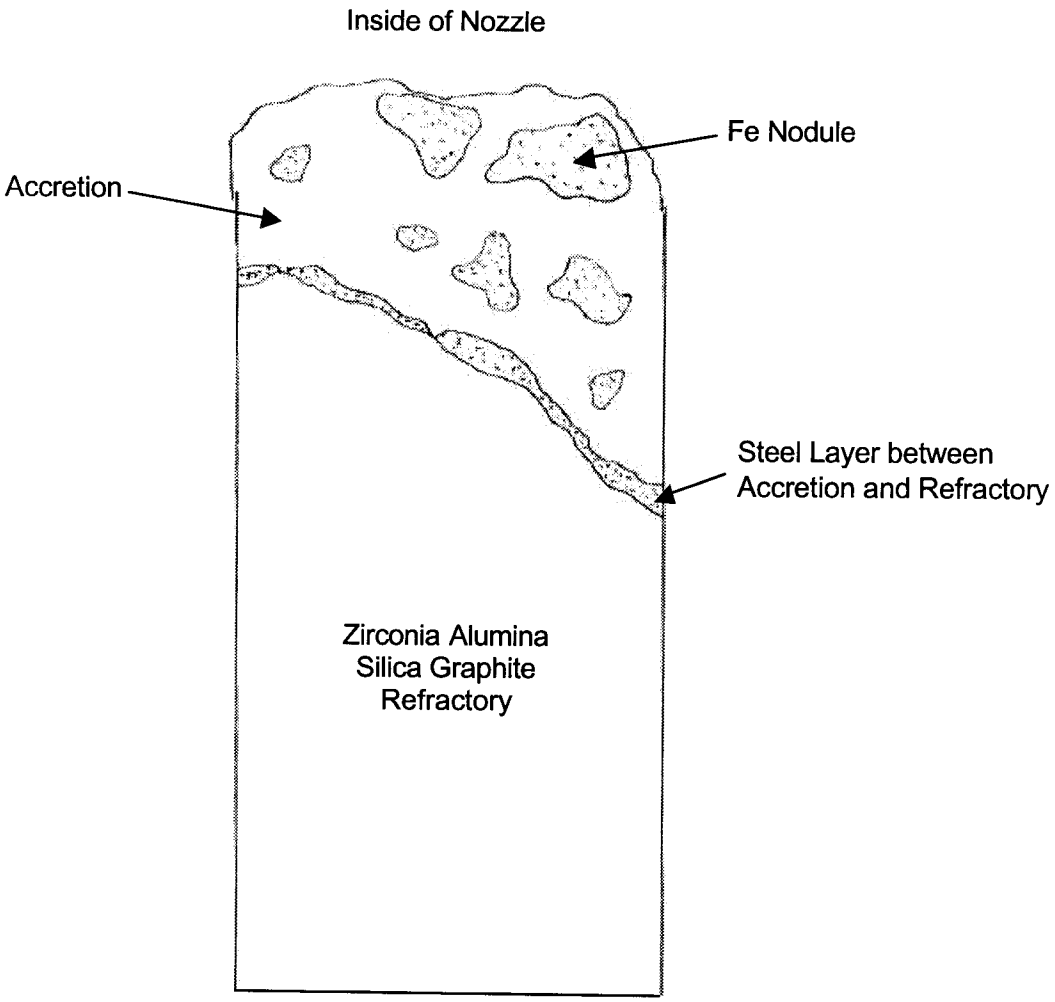

Figure 7. Schematic of the bottom portion of the SEN showing characteristic structure.

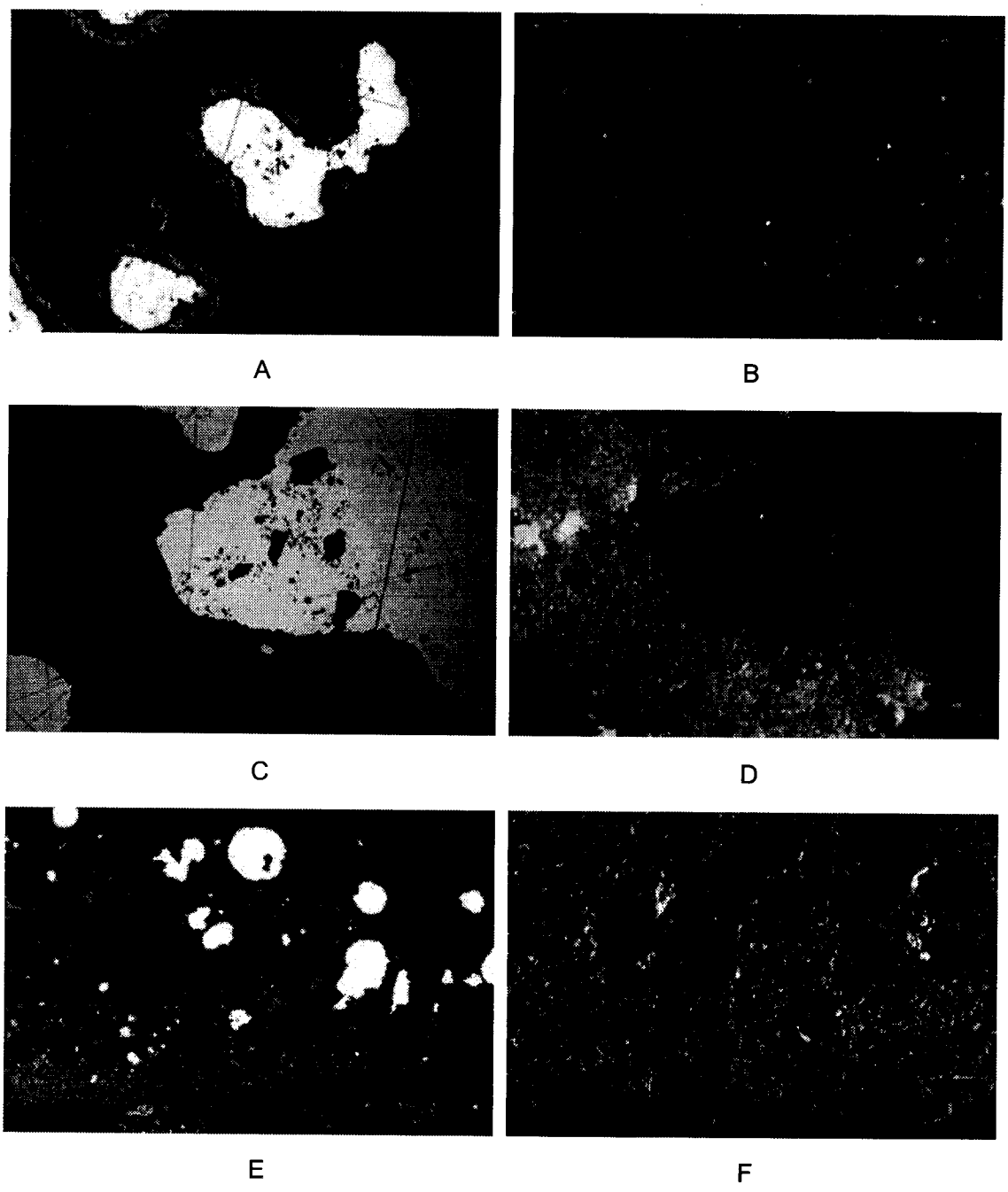

Figure 8. RL and CL microstructures of submerged entry nozzle sample as shown in Figure 1 and Figure 2. (A) and (B) RL and CL micrographs of loosely held alumina build-up (bright red CL), (C) and (D) RL and CL micrographs showing spinel+CA_6 build-up (bright green and intense green CL), and (E) and (F) RL and CL micrographs of refractory-build-up interface showing relatively well-sintered alumina deposits(red to brown CL) and minor amounts of green CL CA_6.

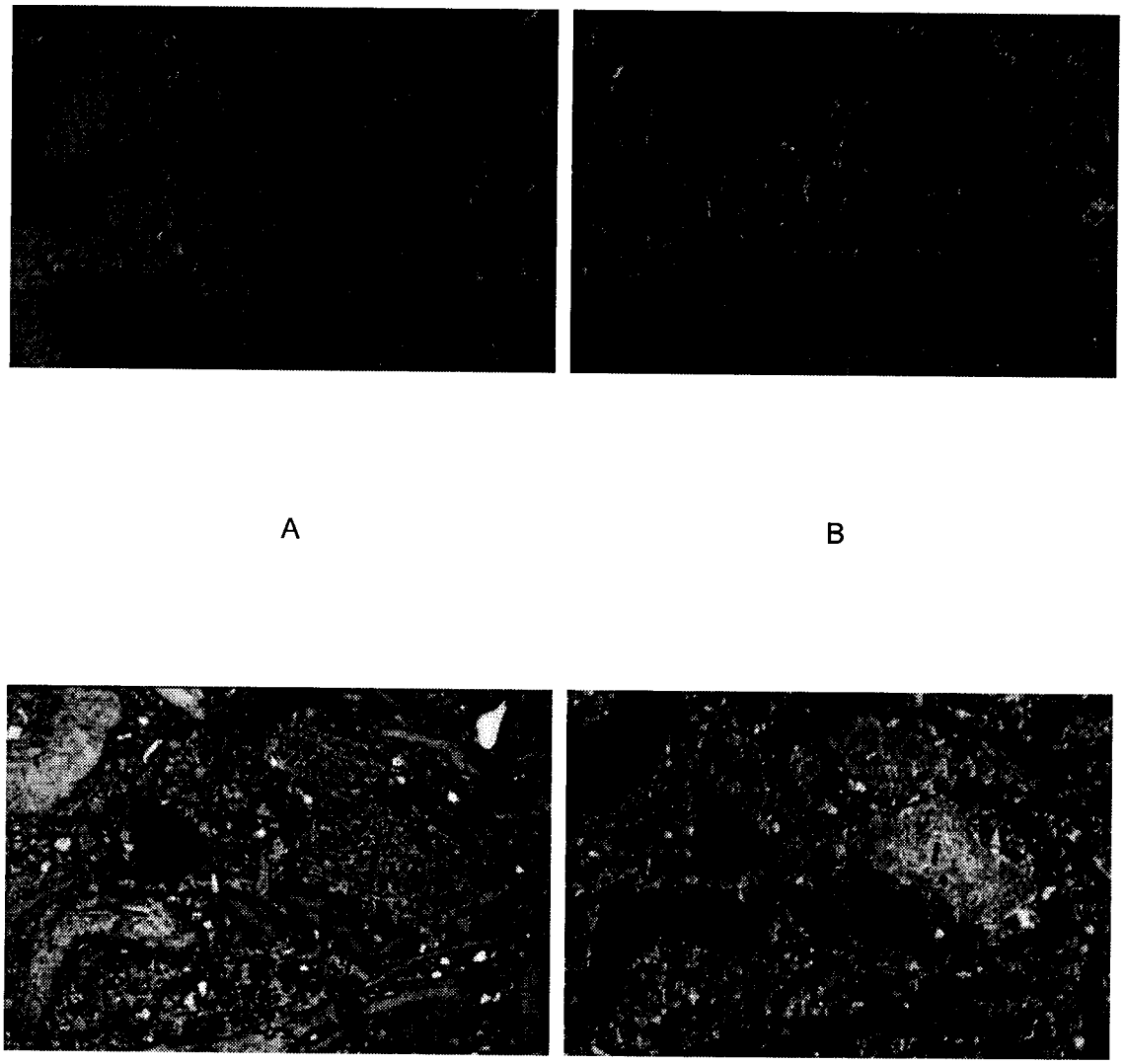

Figure 9. (A) CL microstructure of loosely held spinel + CA_6 deposits, (B) CL microstructure of dense alumina layer on the top of refractories, (C) and (D) RL and CL microstructures of alumina-graphite refractories.

8.0 Appendix B: Industrial Survey Results

1.0 Introduction

A survey was distributed in the early summer of 1998, to the companies supporting the nozzle clogging research project. The purpose of the surveys was to determine the most difficult casting situations with respect to nozzle clogging and to gain background information on the operations of the supporting companies. The operating background information is being used while examining the post-mortem samples to assist in understanding the formations that are observed. The surveys are also being used to gauge the direction in which the sponsoring companies would like the research to progress.

Completed surveys have been received from the following: Acme Steel, AK Steel's Ashland and Middletown Works, Bethlehem Steel, Ispat Inland, LTV Steel, National Steel's Great Lakes and Granite City Divisions, Rouge Steel, Stelco, Timken.

While reviewing the surveys, it became apparent that some of the questions were ambiguous. In addition, the depth of information provided in the surveys varied greatly from company to company. While some companies provided extensive amounts of information, many did not answer some of the questions or gave very brief answers. Because of this, it was often difficult to draw conclusions based on the surveys.

One area that seems to cause confusion is the different terminology used by each of the companies to refer to the various parts of their casting flow control systems. To minimize this confusion, Figures 1 and 2 illustrate the locations of the various nozzles and the standardized terminology that was used when referring to nozzles.

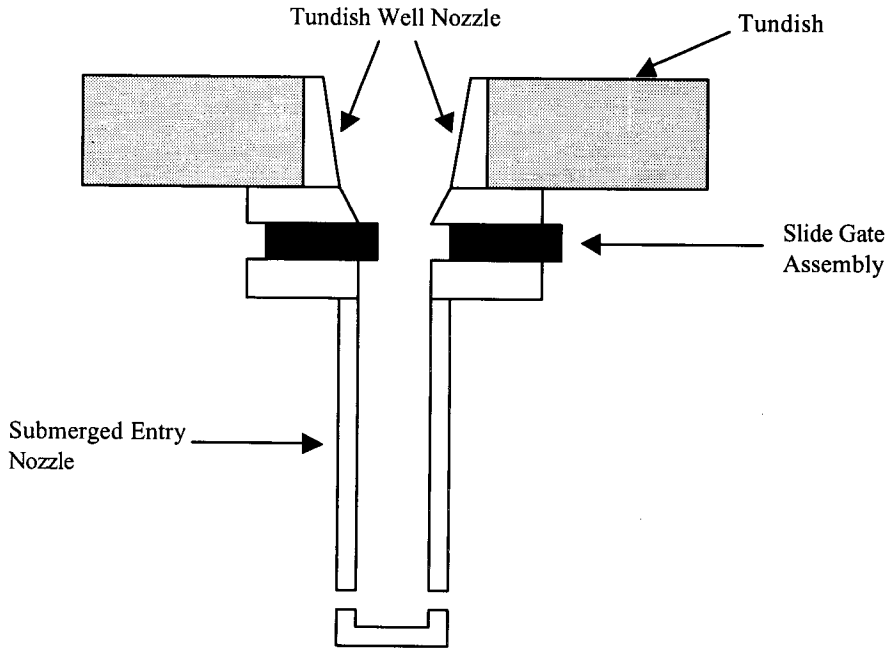

Figure 1. Tundish-to-mold flow control system showing tundish and submerged entry nozzle.

It is also very important to specify the nozzle being referred to in the discussion. For instance, we have found that many companies do not have a submerged entry nozzle clogging problem, but rather a tundish nozzle clogging problem. If these companies refer to a nozzle clogging problem without specifying which nozzle, the problem could be assumed to be in the SEN rather than in the tundish

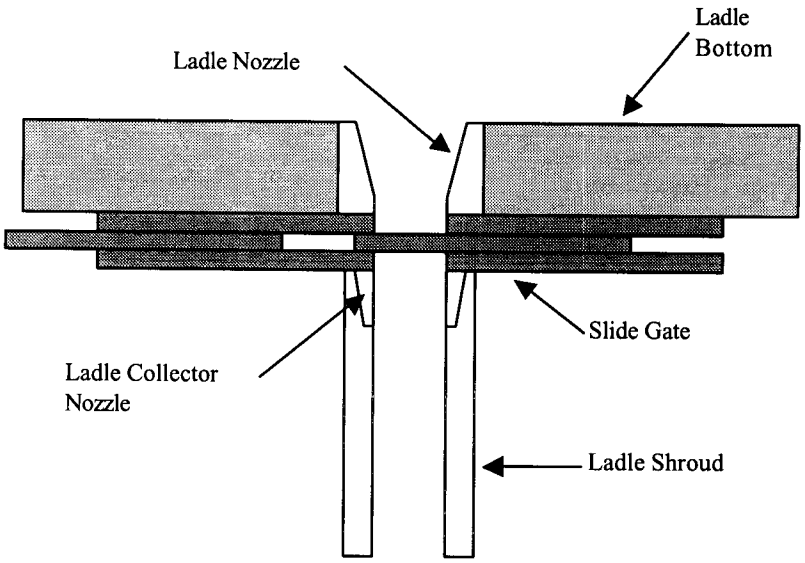

nozzle.

2.0 Caster Types

Different types of casters produce different grades of steel and use different SEN designs. Most slab casters produce predominantly low or ultra-low carbon, aluminum-killed steels. The other casters typically produce a wider range of chemistries. The SEN designs are somewhat similar with the slab casters, but differ substantially with the other caster types.

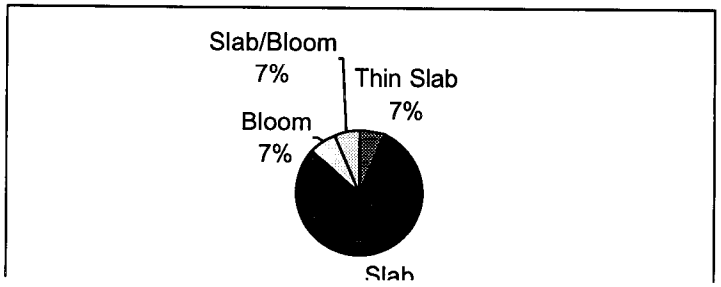

Figure 2. Ladle flow control system illustrating location and terminology of nozzles.

Figure 3. Caster types indicated in surveys.

Figure 3 illustrates the relative percentage of the different types of casters in the survey. The overwhelming majority of casters are curved mold slab casters. Only four of the casters are straight mold casters.

3.0 Clogging Factors

Not all grades of steel are expected to be prone to clogging. For example, grades with higher carbon contents and little to no aluminum have been thought to clog less than grades with greater aluminum concentrations and low carbon contents. As expected, most companies in our survey reported that low carbon aluminum-killed steels and ultra-low carbon aluminum-killed steels are the most difficult grades to cast with respect to clogging. Three companies reported ultra low carbon grades with titanium additions to be prone to clogging. Re-phosphorized grades cause particularly difficult clogging problems for one of the companies.

In our survey, we found that the greatest percentage of respondents, 36%, reported that nozzle clogging is a problem with specific grades of steel while 27% of the surveys reported clogging with all grades of steel. For the 27% of the respondents that report clogging for all grades of steel, it is possible that they only cast low carbon aluminum-killed grades. The overall product mix for each company was not asked. For 18% of the casters, clogging is sometimes a problem with specific grades of steel, and 18% of the casters reported that clogging is not a problem.

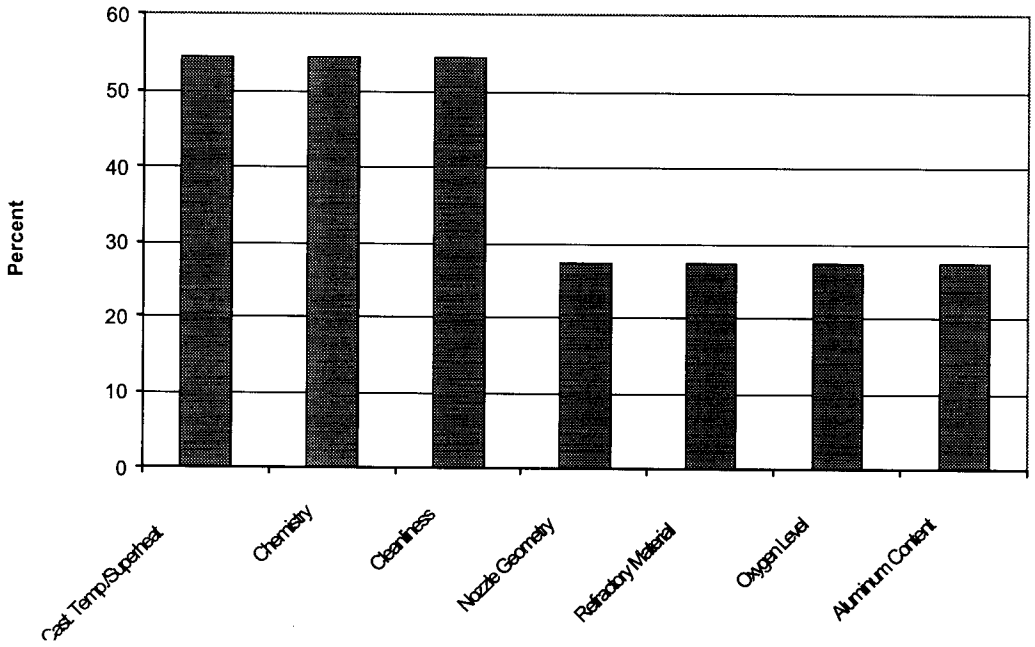

Figure 4. Histogram showing the most frequently cited nozzle clogging factors.

The most commonly cited nozzle clogging factors were casting temperature/superheat, steel chemistry, and steel cleanliness (Figure 4). In addition, three companies reported that argon flow and/or distribution were a factor in nozzle clogging. One company reports seeing a difference in the type of clogging based on whether or not the heat is degassed. The company reports that "open" heats processed through the degasser produce more skulling in SEN's while heats processed through the CAS-OB station usually have accretions composed of mostly alumina.

4.0 Nozzle Materials

Tundish nozzle materials varied with the most common material being alumina-graphite followed by magnesia and finally porous alumina tundish nozzle. All companies use alumina graphite submerged entry nozzles with a slag line insert. Although the compositions of the inserts were not always given in the survey, the majority of those reported were zirconia-based inserts.

Only three companies in our survey have tried alternate materials. Among the materials evaluated for nozzle clogging resistance by the surveyed companies are alumina, various compositions of alumina graphite, magnesia, silica, and boron nitride and lime bearing liners. None of the companies reported positive results with any of these materials.

5.0 Nozzle Life

It should be noted here that when referring to nozzle life, it was not specified in the survey which nozzle was being referred to. Therefore, some companies responded by referring to tundish nozzles and others referred to SEN's. However, many companies did not specify whether they were referring to either one. Therefore, nozzle life is merely generalized here. Typical nozzle life varies from company to company with approximately one heat being the lowest to a maximum of twelve heats. There was significant variation in the life of nozzles even among each company.

For most companies, nozzles are removed from service because of clogging about ten to twenty percent of the time. The reason for this is that many companies schedule nozzle changes based on a known life for the nozzle prior to clogging. In addition, some companies make frequent grade changes that dictate that the nozzle is changed before it becomes clogged. Only one company reported that it changes nozzles approximately 80% of the time due to clogging.

The most common method used to gauge the degree of clogging is by simultaneously measuring the gate or stopper rod opening and casting speed. This is then converted to a nozzle clogging factor which is the percentage of the theoretical steel flow that is actually flowing through the nozzle system. Other companies observe gate opening and mold level fluctuation to gauge the degree of nozzle clogging. Some companies monitor nozzle clogging by monitoring argon back pressure and the mold level.

6.0 Tundish Preparation and Life

Seven respondents indicated using a hot tundish practice; five companies indicated using a cold tundish practice. Most companies prepare their tundishes by replacing slidegates, SEN's, and flow modifiers. Then a refractory lining in sprayed on. The working refractory lining is usually magnesia. Two

respondents reported using a magnesia-silica refractory while one company uses a chrome oxide-magnesia refractory. All flow modifiers and pour pads utilize an alumina-based refractory.

The typical life of a tundish was reported as approximately ten heats. Three respondents reported tundish lives of approximately twenty heats. For most companies, the reason for replacing the tundish is a scheduled change, while approximately four out of ten companies report changing the tundish for nozzle clogging or nozzle erosion.

7.0 Ladle

All of the companies in our survey, with the exception of one, report use a high alumina (70% to 80% alumina) refractory in the ladle. The other company uses dolomite. All companies report using alumina-graphite ladle shroud. Only two companies use a high-wear insert at the slag line of the ladle shroud.

The life of ladle shrouds varies widely, from one heat for those using bayonet style nozzles, to several heats for the others. For those that do not use bayonet style nozzles, the reasons for changing were for breakage and wear. Four companies reported that ladle nozzles occasionally clog. Either tundish or submerged entry nozzle clogging usually accompanies ladle nozzle clogging.

8.0 Flow Control Devices

Approximately half of the companies in this survey use slide gates. Four companies use a Delta-T system, and two companies use a stopper rod system. The materials used in the flow control devices all consist of alumina or alumina-graphite. One company uses a magnesia coating at the tip of the stopper rod to prevent the stopper rod from adhering to the inlet of the SEN. All companies with the exception of one use a high wear zirconia insert. Four of the respondents use a porous insert, while two use a grooved insert for argon purging.

9.0 Research Focus

Seven of eleven responses indicated that research should focus on keeping inclusions in the steel and preventing their attachment to the refractory surface. Four respondents felt that research should be conducted on several grades of steel in an attempt to provide commonalties that might provide insight into a root cause for clogging. Only one respondent indicated that the research should concentrate on a specific grade of steel and reduce associated clogging with that grade.

Based on the survey, it appears that most companies are having clogging problems with low carbon aluminum-killed grades. Our research will initially focus on these grades. After we have gained some experience and knowledge with low carbon aluminum killed accretions, we plan to look at other grades such as titanium-stabilized aluminum-killed steel.

9.0 Appendix C

NOZZLE ACCRETION FORMATION IN THE CONTINUOUS CASTING OF ALUMINUM-KILLED STEEL

Literature Review

Luis Trueba
Center for Pyrometallurgy
Department of Metallurgical Engineering
University of Missouri-Rolla

March 9, 1999

INTRODUCTION

The following is a review of the literature pertaining to nozzle clogging in the continuous casting of aluminum-killed steel. The review includes most of the literature that was available as of June 1998. This work in progress will continually be updated over the course of this research.

Background

Nozzle clogging is a build-up of accretions on the internal bore of refractory nozzles used in the continuous casting of steel. The purpose of the refractory nozzles is to protect the steel stream from reoxidation and control its flow as the steel moves from the tundish to the mold of a continuous caster. The accretions eventually build up to a level that either completely blocks the flow of steel or disrupts the flow of steel to the extent that casting must be aborted.

Nozzle clogging in the continuous casting of aluminum-killed steels has been a problem for nearly 30 years. Snow and Shea first reported observing alumina and steel nodule accretion formations on the walls of ladle nozzles associated with the teeming of fine grained aluminum-killed steels in 1949.[1] This observation was made while studying ladle nozzle erosion. No effort was made to understand the problem because at that time, steel was teemed into ingot molds and clogging was not considered a serious problem. Ladle nozzles could easily be changed or opened with an oxygen lance after casting a heat of steel. It was not until the advent of continuous casting that nozzle clogging would be recognized as a major hindrance to productivity.

Continuous billet casters in the late 1960's and early 1970's utilized metered nozzles. Nozzle blockage with these casters caused the casting speed to be reduced to keep the mold level constant, which hindered production. Eventually, oversized nozzles were introduced with stopper rods to control the flow of steel to the mold. The oversized nozzles were a means to counter clogging by allowing more time before clogging became so severe that the casting rate

would have to be slowed. Shrouding is particularly important with the use of stopper rods because the steel stream is considerably disturbed so that reoxidation becomes a serious problem.[2]

Clogging continues to be a problem with modern slab and thin slab casters. Several methods to counter clogging have been introduced such as calcium treatment and argon injection, however clogging often continues to limit productivity in the steel industry.

MORPHOLOGY

Most researchers have focused on accretions associated with low or ultra-low-carbon, aluminum-killed steels that have not been calcium treated. Therefore, accretion morphologies with these types of steels will be discussed first. Then, key factors that have been reported to effect morphology will be presented.

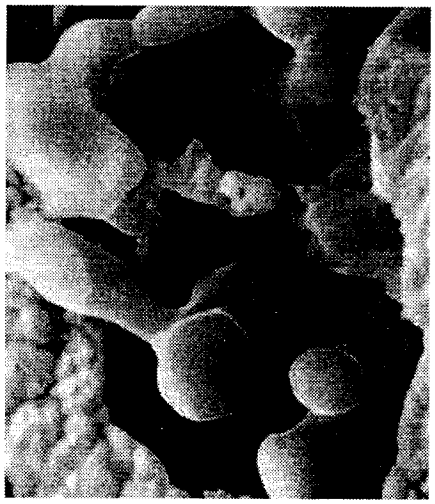

Figure 1 Typical structure of alumina accretion. 5000X [5]

The morphology of accretions reported by different researchers varies somewhat. Ogibayashi pointed out that the differences are likely due to variations in the cleanliness of steel and casting conditions.[3] However, in all cases, the accretions consist of powdery, friable alumina and/or metal nodules containing clusters of alumina inclusions. Many researchers have pointed out that the morphology of the alumina inclusions in the steel nodules are the same as the alumina built up on the refractory wall.[4,5] Most commonly, the alumina clusters consist of individual, round alumina particles sintered together as shown in Figure 1. The clusters have a coral-like appearance.

Ogibayashi and Poirier et al., have separately described the accretion formations as consisting of two layers as shown in Figure 2.[3,6] The first layer, at the refractory-accretion interface, is densely packed alumina with small particles of metal contained within the alumina network. The metal particles in this layer are reported to contain relatively high concentrations of silicon.[3] This layer has also been reported to contain a small amount of a vitreous phase consisting of Al_2O_3, SiO_2, Na_2O, and K_2O.[6] The maximum thickness of this layer was reported as 300 μm. The next layer, the buildup layer, consists of either alumina clusters with metal nodules containing clusters of alumina or mostly metal nodules containing clusters of alumina

inclusions. Poirier et al. have also reported observing traces of spinels ($MgO-Al_2O_3$ and $MgO-Fe_2O_3$) in build-up layer.[6]

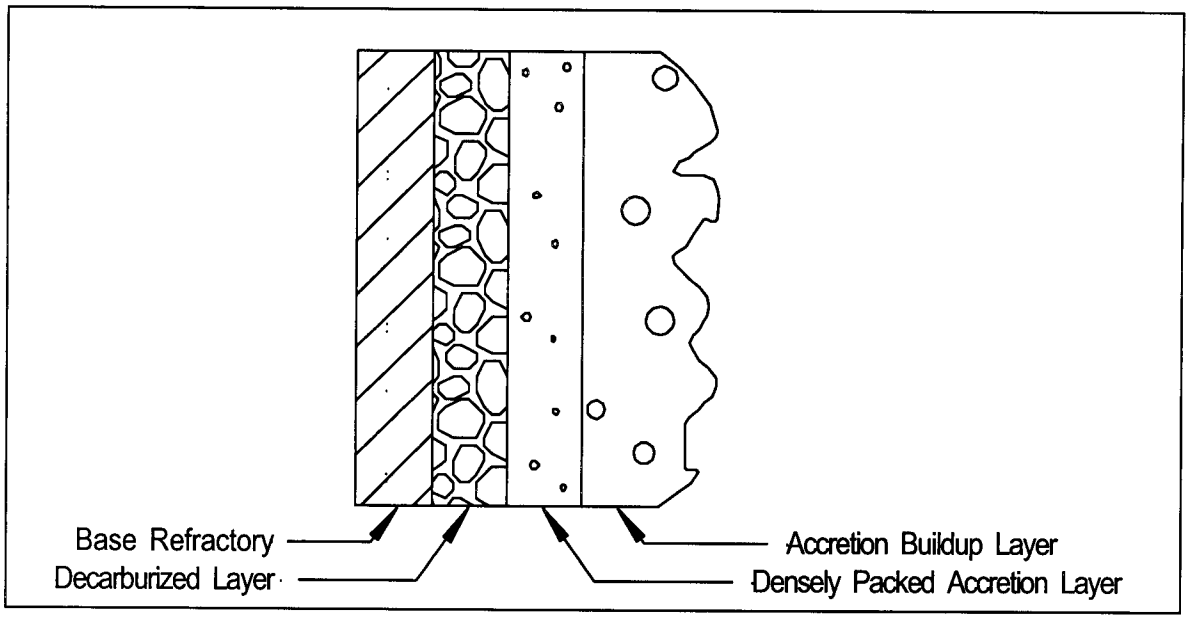

Figure 2 Schematic diagram of accretion morphology.

Many researchers have also reported the formation of a decarburized layer in refractory materials containing graphite. The decarburized layer is adjacent to the accretion and has been reported to have a depth of approximately 400 μm.[6]

Many factors have been reported to effect accretion morphology. Among these are: location of the buildup in the pouring system, steel chemistry, deoxidation method, ladle treatment, and composition of the refractory.

Location seems to play an important role in the morphology of accretions in submerged entry nozzles (SENs). Kasai et al. observed that with various grades of aluminum and aluminum-silicon-killed steel, deposits in the SEN above the meniscus were composed mainly of solidified metal and alumina, while below the meniscus, the deposits consisted of mainly alumina.[7] Poirier et al. similarly reported that the upper portion of the nozzle (above the

meniscus) characteristically contains approximately 80% iron and iron oxide.[8] The lower portion of the nozzle contains approximately 80 to 90% alumina (see Figure 3).

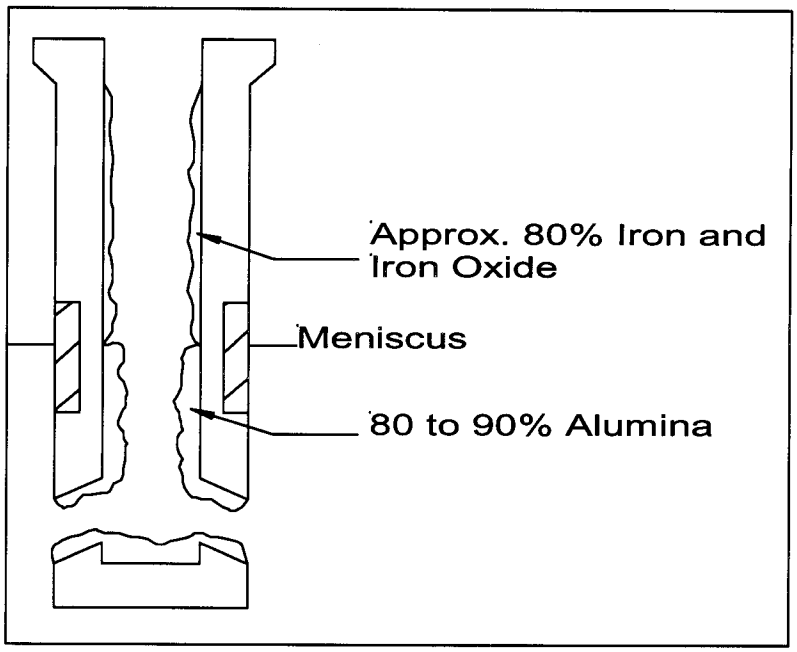

Figure 3 Schematic diagram of accretions in a submerged entry nozzle.

Steel chemistry has an important effect on accretion morphology. In particular, calcium treatment and deoxidation method effect accretion morphology. For example, McKague et al. have shown that aluminum-killed grades that are calcium treated will form calcium aluminates and, if sulfur levels are high enough, calcium sulfide accretions.[9] These investigators have also shown that the composition of the accretions is determined by the ratio of Al_2O_3 to CaO when the metal stream reaches the nozzle. These observations are also true for non-calcium treated steel cast with nozzles containing lime-bearing materials.

Researchers studying titanium-killed or titanium-added steels have also noted differences in morphologies of inclusions in the steel and accretions on nozzles. In the case of titanium-added, aluminum-killed steels, coarsening of the steel and alumina nodules that make up the accretions, have been reported. The individual particles making up the inclusions and accretions have a granular shape. The composition of the accretions consists predominantly of

alumina with titanium oxide rarely being observed.[4] Accretions with titanium-killed steels, on the other hand, typically consist of titanium oxide with approximately 6 to 7% alumina. These accretions have an angular shape, in contrast to the round, coral shape typically reported for aluminum-killed steels.[10]

The ladle treatment of steel also seems to affect nozzle accretion morphology. Ogibayashi et al. observed that when a heat of steel was subjected to DH degassing, the accretion material consisted mostly of metal that contained clusters of alumina. Those heats that were only subjected to argon bubbling had accretion formations that consisted mainly of alumina.[10] The difference in morphology was reported to be due to the difference in the cleanliness of the steel. The DH degassed steel is cleaner than steel that only receives argon stirring. Therefore, its accompanying accretions contain more solidified steel and less alumina.

MECHANISMS OF ACCRETION FORMATION

The most prominent theories of nozzle accretion formation are listed below and are discussed in more detail in the following sections.

1. The temperature drop that is inherent when steel flows through submerged entry nozzles causes a resulting decrease in the solubility of oxygen in steel. This drives the Al-O-Al_2O_3 equilibrium towards the alumina side, forming alumina accretions at the wall of the SEN nozzle.[2,11]
2. The flow of steel through the SEN causes low pressure to form inside the nozzle. This drives the diffusion of atmospheric oxygen through the nozzle wall. Aluminum in the melt is oxidized to form alumina at the nozzle wall either directly by the oxygen or indirectly from carbon monoxide formed by the reaction of oxygen with carbon in the refractory.[12]
3. Indigenous alumina particles are driven to the nozzle wall due to fuid flow characteristics of the steel stream. Turbulence or separated flow around disturbances in the molten steel stream transports alumina to the nozzle where they attach due to a reduction in the overall surface energy of the system.[5,13,14]
4. Thermochemical reactions in the nozzle material transport oxygen either in the form of suboxides or carbon monoxide to the nozzle-steel interface where they react with aluminum in the steel to form alumina at the nozzle wall.[6]

Thermally Induced Accretions

Duderstadt et al. observed that in clogged tundish nozzles, steel froze in a directional, dendritic structure, which indicated that heat was being extracted from the steel stream by the nozzle refractory material.[2] The accretion within tundish nozzles was found to contain alumina suspended within a MnAlSi-oxide matrix. It should be noted that the steel cast in these experiments was killed with ferrosilicon and aluminum. Duderstadt et al. concluded that the

mechanism of accretion formation was the precipitation of aluminum within a MnAlSi-oxide matrix that was further strengthened by solidifying steel.

Farrell and Hilty further proposed that nozzle accretion is due to a reduction in temperature of steel as it passes through a nozzle.[11] It was reasoned that any deoxidation product that is solid and refractory at steel making temperatures has the potential to precipitate onto the nozzle wall. The precipitation of solid oxides is due to the temperature decrease in the steel as it enters the nozzle; even though a nozzle may be preheated, its temperature is still much lower than steel. This cooling of the steel causes a decrease in the solubility of the oxide (more likely the solubility of oxygen) in the steel and causes the oxide to precipitate onto the nozzle wall. At some point, the rate of precipitation will begin to accelerate as the flow of steel decreases due to the accretion formation, which results in a decrease in the flow of steel through the nozzle and a resulting temperature drop.

With a set of casting simulation experiments, Andersson and Wijk showed that except for the solidification of steel within the nozzle, temperature is not a significant factor in accretion formation within nozzles.[14] The nozzle used in the casting experiments was heated to temperatures at or above the casting temperature of the molten steel. There was a noticeable increase in the teeming rate of steel when the temperature of the nozzle was equal to or up to 50°C greater than the steel temperature. The explanation given for the increased teeming rate was that steel was prevented from solidifying because of the high nozzle temperature. This conclusion was reached because up to 90% of the clog matrix in the nozzles was composed of steel. It was also observed that the alumina accretion within the nozzle was not substantial enough to be the sole cause of nozzle blockage. As the flow of metal decreases through the nozzle, the rate of heat influx into the nozzle decreases and the transfer of heat out of the steel becomes large enough to cause solidification within the nozzle. Therefore, it was concluded that both alumina accumulation and steel solidification affect nozzle clogging.

Dawson also pointed out that with a temperature drop of 10°C in the steel as it passes through a nozzle, the resultant decrease in solubility of oxygen is less than 1ppm with aluminum-killed steels.[13] That is because approximately 99% of the oxygen has already been consumed in the deoxidation process, leaving only a very small amount of oxygen to further react.

Diffusion of Oxygen through Nozzle Refractory

While the diffusion of oxygen through refractories is commonly mentioned in the literature as one of the possible mechanisms of nozzle accretion, no papers specifically addressing the problem were located. Poirier et al. mentioned that increased permeability of SEN refractories has been noticed when the refractory glaze contained defects.[8] They then reported that when the permeability of the refractory increases, not only is aluminum in the steel oxidized but the steel itself and then the carbon in the refractory are also oxidized. When the carbon becomes oxidized, corrosion of the refractory takes place more rapidly because of a breakdown in the structure of the refractory.

Flow Transported Accretions

Singh proposed that nozzle accretion formations are produced by deoxidation products already present in the steel passing through the nozzle.[5] A boundary layer exists adjacent to the nozzle wall in which the flow of steel is essentially zero. Any inclusions present in this boundary layer will adhere to the nozzle wall because the total surface area of the particles in contact with the steel decreases, resulting in an overall reduction of surface energy. Singh reports that conditions are favorable for a particle to adhere to the nozzle wall when:

$$⑨_{pr} \blacktriangle\sigma_{pr} > ⑨_{pm} \blacktriangle\sigma_{pm} + ⑨_{mr} \blacktriangle\sigma_{mr} \qquad (1)$$

where:

⑨ = specific energy
▲σ = change in surface energy
p = particle
r = refractory
m = metal

The work of adhesion of a particle is given by:

$$W = ⑨_{pm}(1 - \text{Cos } ⌒) \quad (2)$$

where:

⌒ = contact angle between the particle and the metal

The contact angle between steel and alumina is reported as being between 134 to 136 degrees. Therefore, there is a significant force acting to adhere a particle of alumina to another substance with a similar surface energy such as another alumina particle or a refractory surface.

Singh reported that inclusions are transported to the boundary layer by eddy currents, which throw the inclusions toward the boundary layer where they attach to accretions that have already begun to form on the nozzle wall.[5] Once the accretions attach themselves together and to the nozzle wall, the particles quickly begin sintering. Singh calculated that for 2 μm diameter alumina particles, a significant neck forms within one minute.[5]

Dawson demonstrated through a series of water modeling experiments that areas of separated flow occur adjacent to nozzle surfaces whenever the flow of steel is disrupted.[13] The flow patterns within the separated flow region were demonstrated to be random. The direction of flow in these regions changes constantly and at times is directed at the nozzle wall. Areas that were demonstrated to have separated flow included the inlet of tundish nozzles and the SEN, downstream of tundish slide gates. These areas of separated flow correspond well with the areas of preferential accretion formation observed in industrial nozzles. It was postulated that nozzle clogging occurred because of the separated flow in these areas.

Dawson went on to test this theory by using a nozzle that was angled at 60° from horizontal in an a casting simulation.[13] Within an angled nozzle such as this, steel flows in a streamlined pattern against one side of the nozzle while the other side of the nozzle has a separated flow region adjacent to the wall. Analysis of the tundish nozzle revealed that no

accretion formation occurred on the side of streamlined flow while an accretion layer formed on the side of the nozzle that experienced separated flow.

Dawson therefore concluded that separated flow within a nozzle acts to transport inclusions to the nozzle wall.[13] Once the inclusion is deposited on the nozzle wall, it is protected from the bulk flow of steel because it lies within the area of separated flow. It was shown that within the separated flow region, the shear stress adjacent to the wall is zero. A particle deposited on the nozzle wall in the separated flow region will not be subject to shear stress and therefore will not be removed from the wall.

Andersson and Wijk concluded after a set of casting experiments that the rate of nozzle accretion formation is dependent on the amount of alumina present in the steel.[14] In these experiments, the amount of aluminum in the melt was varied. The total oxygen was assumed to be constant. The equilibrium oxygen in solution in the steel was then calculated using:

$$Al_2O_3 = 2\,\underline{Al} + 3\,\underline{O} \qquad (3)$$

$$\log K = \frac{64000}{T} + 20.57 \qquad (4)$$

The amount of alumina precipitated in the melt was then calculated from:

$$m_{Al_2O_3} = \frac{[\%O_{tot}] - [\%O]_j}{100 \cdot 3 \cdot M_O} \cdot m_{Fe} \cdot M_{Al_2O_3} \qquad (5)$$

where:

m_{Al2O3} = mass of alumina (g)
$[\%O_{tot}]$ = percent of total oxygen by weight
$[\%O]_j$ = percent dissolved oxygen by weight in experiment j
M_O = molecular weight of oxygen
M_{Al2O3} = molecular weight of alumina
m_{Fe} = weight of steel melt (g)

It was observed that the rate of clogging was directly proportional to the amount of alumina precipitated in the melt. It was postulated that a break down of the viscous sublayer below a critical value allowed the transport of alumina particles to the nozzle wall. However, it was

acknowledged that a region of separated flow within the nozzle might be the rate limiting mechanism of accretion formation.

Thermochemically Formed Accretions

Several researchers have proposed various accretion formation mechanisms involving thermochemical reactions between the steel and the nozzle refractory. Some theories of accretion formation as a result of these thermochemical reactions are presented below.

Poirier et al. have proposed a thermochemical mechanism for accretion formation in nozzles during the continuous casting of aluminum killed steel.[6,8] Their proposal for the mechanism of accretion formation involves three steps: the dissolution of graphite into the steel, the formation of a first layer deposit that consists of alumina and a vitreous phase formed by the volatilization and oxidation of some of the refractory species, and finally alumina formation by the oxidation of aluminum in the melt by carbon monoxide.

In the first step, carbon dissolves into the molten steel from the refractory material.[4,6] The increased carbon concentration near the nozzle wall increases the activity of aluminum in the melt. This increase in activity of aluminum causes alumina to form and deposit as a thin film on the nozzle refractory.

The second step involves a series of volatilization/oxidation reactions.[6,8] Through a set of volatilization/condensation experiments (See the section entitled Experimental Procedures: Thermochemical Reactions) it was demonstrated that SiO_2, Na_2O, and K_2O can be volatilized at steel making temperatures. The mechanism proposed to volatilize these species is the carbothermal reduction by graphite in the refractory according to the following reactions:

$$SiO_2\,(s) + C\,(s) \rightarrow SiO\,(g) + CO\,(g) \qquad (6)$$

$$Na_2O\,(s) + C\,(s) \rightarrow Na\,(g) + CO\,(g) \qquad (7)$$

$$K_2O\,(s) + C\,(s) \rightarrow 2K\,(g) + CO\,(g) \qquad (8)$$

A negative pressure caused by the flow of steel through the nozzle drives the gasses toward the refractory-steel interface.[6,8] At the refractory steel interface, the gaseous species react with oxygen in the steel, which is reported to have a partial pressure of 10^{-11} atmospheres. This produces a low melting temperature liquid phase that dissolves alumina from the steel or refractory to produce albite according to the following reactions:

$$2\,Na\,(g) + 6SiO\,(g) + Al_2O_3 + 7[O]_{Fe} \rightarrow Na_2O\text{-}Al_2O_3\text{-}6SiO_2\ (albite) \qquad (9)$$

$$2Na\,(g) + 6SiO\,(g) + 2[Al]_{Fe} + 10[O]_{Fe} \rightarrow Na_2O\text{-}Al_2O_3\text{-}6SiO_2\ (albite) \qquad (10)$$

Lastly, carbon monoxide oxidizes aluminum in the melt to form Al_2O_3, which is precipitated at the nozzle wall.

Sasai and Mizukami performed a set of experiments to investigate thermochemical reactions as an accretion formation mechanism (See section entitled Experimental Procedures: Thermochemical Reactions).[15] These researchers concluded that the following reaction occurs when alumina graphite refractories are in contact with aluminum-killed steels at steelmaking temperatures:

$$3SiO_2\,(s) + 3C\,(s) + 4[Al]_{Fe} \rightarrow 2Al_2O_3\,(s) + 3[Si]_{Fe} + 3C \qquad (11)$$

As an intermediate step to the above reaction, silica and alumina are reduced to suboxide gasses by carbon in the refractory. The Al_2O gas reacts with additional silica and reforms solid alumina. This last assumption was drawn after calculating the equilibrium partial pressures of the suboxide gasses versus temperature. SiO is the most stable suboxide gas at steelmaking temperatures.

Fukuda et al. proposed an accretion formation mechanism whereby alumina in the refractory is carbothermally reduced to a suboxide gas.[16] This gas then diffuses to the refractory-steel interface where it is oxidized to alumina as a precipitate on the nozzle wall. This mechanism was proposed after observing alumina accretion formation on an alumina graphite

specimen submersed in iron in the absence of aluminum. This mechanism occurs by the following reactions:

$$SiO_2 + C \rightarrow SiO\ (g) + CO\ (g) \qquad (12)$$

$$Al_2O_3 + 2\ C \rightarrow Al_2O\ (g) + 2\ CO\ (g) \qquad (13)$$

The following reactions were proposed to occur when the gasses are transported to the refractory-steel interface.

$$SiO\ (g) \rightarrow [Si]_{Fe} + [O]_{Fe} \qquad (14)$$

$$Al_2O\ (g) \rightarrow 2\ [Al]_{Fe} + [O]_{Fe} \qquad (15)$$

$$3\ Al_2O\ (g) \rightarrow 4\ [Al]_{Fe} + Al_2O_3 \qquad (16)$$

The dissolved aluminum metal from the above reaction then reacts with oxygen in the steel to form alumina at the nozzle wall.

Discussion of Accretion Mechanisms

It is possible that all of these mechanisms play a role in nozzle accretions. However, as Singh argued, theories 1 (thermally induced accretions) and 2 (diffusion of oxygen through refractory) are not likely to play a significant role in nozzle clogging.[5] Severe clogging is often present in areas of the nozzle that are submerged in molten steel such as the discharge area of an SEN. This area of the nozzle is not likely to have a substantial temperature drop, and diffusion of air through the refractory is impossible because it is surrounded by molten steel. One area where these conditions exist is the body of the SEN above the meniscus, and in that area significant clogging rarely exists.

Singh also argued that theory 4 (thermochemically formed accretions) does not occur based on his observations of clogged nozzles in pilot-scale and bench-scale tests.[5] However, it should be noted that he used zirconia and alumina nozzles for his experiments. There is no indication as to whether or not the nozzles contained graphite and silica, which Poirier et al., have indicated facilitate nozzle reactions.[6]

One likely theory presented by Ogibayashi indicates that the dense layer of alumina that is formed on the refractory surface is the result of thermochemical nozzle refractory reactions.[3] He added that the second, less-dense layer is the result of turbulent flow transporting the accretions to the nozzle wall. The particles then adhere to the nozzle wall due to a reduction in interfacial energy of the system. Finally, the alumina accretion sinters to the dense alumina layer.

COUNTERMEASURES

Several countermeasures have been proposed to eliminate nozzle clogging such as oversized nozzles, argon injection, calcium treatment, and lime additions to nozzle refractories. These countermeasures are discussed individually in the following sections.

Oversized Nozzles

Duderstadt et al. proposed one of the first strategies to counter nozzle clogging in the continuous casting of billet.[2] The proposed strategy was the use of an oversized nozzle along with a stopper rod mechanism to control the flow of steel through the tundish nozzle. The oversized nozzle provides longer casting times before accretion formation becomes significant enough to slow the casting rate. Duderstadt et al. found that the use of a stopper rod disturbed the flow of steel from the tundish to the mold. Therefore, to make the oversized nozzle/stopper rod system functional, a shrouding system was necessary to prevent reoxidation of the steel due to the inherently turbulent stream.

Argon Injection

Argon injection is used extensively in the steel industry. Depending on each company's operating practice, argon may be injected into the tundish well nozzle, top plate, tube holder, and submerged entry nozzle. Argon is bubbled either through pores in the refractory itself or through pierced holes in the refractory. The injected argon forms a protective gas layer that prevents the adherence or precipitation of accretions and provides turbulent flow to dislodge accretions from the refractory wall.

It should be noted that improvements to ladle nozzle argon systems have been made that are similar to tundish well nozzle and SEN improvements. The primary focus of this research is on tundish to mold systems, therefore improvements to ladle nozzles are not specifically considered.

Several researchers have made improvements to argon injection that have resulted in a reduction of nozzle clogging.[17-22] Many of the improvements in argon injection have focused on preventing cracking of refractory materials, gas leakage, and obtaining better argon bubble distribution.

Cameron and Alavanja et al. have reported cracking of the tundish well nozzle refractory, which leads to non-uniform argon distribution.[17,18] When refractories crack, argon is bubbled from one or several concentrated areas rather than in a fine, evenly dispersed pattern. Steel can also infiltrate the cracks and fill the argon delivery system. Under these conditions, clogging occurs quickly. Nozzle cracking problems have been reduced by carefully selecting refractory materials and effectively preheating nozzles.

Tundish well nozzle pore size and distribution has been shown to be a very important factor in the effectiveness of argon injection. Alavanja et al. have reported that variability in the size of pierced holes in nozzles affects clogging.[18] It was established that when pierced holes are too large, steel can penetrate into the holes, reducing the effectiveness of argon injection. Schmidt, et al. found that using two argon injection ports and refractory with smaller and more evenly distributed pores resulted in significant decreases in the occurrence of tundish well nozzle clogging.[21]

Likewise, Takasugi, et al., found that the pore size and distribution of porous nozzles could be better controlled by incorporating spherical grains in the refractory material.[9] Changes in argon back pressure using these nozzles were very small from the first to the last heats cast through the nozzles, indicating better clogging prevention performance. This was confirmed by measuring deposits on spent nozzles. Through water modeling experiments, it was determined that the optimum pore size for low throughput casting ([2 tons/min.) is 40 μm from the standpoint of slab quality and nozzle clogging. Larger gas bubbles are produced with this pore size, which have less opportunity to become entrapped in the slab and cause pinholes.

Leaks from the steel canisters which encase tundish well nozzles have been reported to decrease the effectiveness of argon injection.[17,19] Gas leakage from the steel canisters has been corrected by designing a better seal between the canister and the nozzle refractory material.

Dofasco has designed tundish well nozzles to form accretions at specific locations of the tundish well nozzle.[17] Argon is injected in these areas of highest deposition. This strategy has worked well, with a 26% reduction in the thickness of deposits for the same length of casting time. Dofasco has also experimented with argon-purged stopper rods.[17] However, these were found to be ineffective, and when the argon purging system in the tundish well nozzle performed properly, there was no need for the added argon shielding.

Ando, et al. have found that the performance of argon-injected submerged entry nozzles can be improved by reducing the amount of SiO_2 in the refractory.[20] It was reported that SiO_2 in the refractory is reduced by carbon to form SiO gas. This changes the size and distribution of pores in the refractory, which leads to an increase in argon back pressure over time and increased clogging. By reducing the amount of SiO_2 in the refractory, the reduction in argon back pressure during operation is reduced, therefore giving greater resistance to clogging.

Calcium Treatment

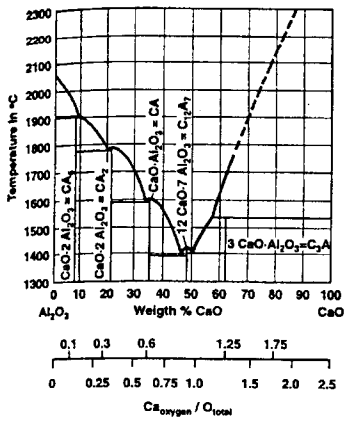

Figure 4 Lime-alumina phase diagram. [25]

Calcium treatment is a common method utilized to prevent nozzle clogging.[23] Calcium is added to steel melts to react with the alumina present in the melt so that liquid calcium aluminate compounds can be formed. The ratio of CaO/Al_2O_3 must be such that the calcium aluminate is liquid at steelmaking temperatures. This is achieved by approaching the composition of $12CaO{\cdot}7Al_2O_3$ (see Figure 4). While casting, the liquid calcium

aluminates pass through the nozzles and do not attach to the refractory wall, preventing accretion formation.

Several problems can occur when calcium treating steels. To be effective, the total oxygen of the steel should be known in order to make the correct amount of calcium additions. Faulring et al. have shown that with small calcium additions, the occurrence of clogging increases up to a threshold amount.[24] McKague et al. have also demonstrated that too much calcium can also cause nozzle clogging.[9] In either case, the calcium aluminates that form are solid at steel making temperatures and promote clogging.

If sulfur levels in the steel are too high, solid CaS particles will form with calcium treatment, which will promote clogging. Bannenberg has shown that there is a small compositional "window" of calcium additions that will produce liquid inclusions at steel making temperatures.[25] This "window" is related to the total oxygen and sulfur content of the steel. For constant total oxygen content and increasing sulfur contents, the amount of calcium needed to precipitate calcium sulfide particles decreases. Therefore, to be successful, the sulfur content of the steel should be low before calcium treatment. McKague et al. report that calcium treatment is not attempted with steels containing greater than 0.012% sulfur to avoid the formation of CaS.[9]

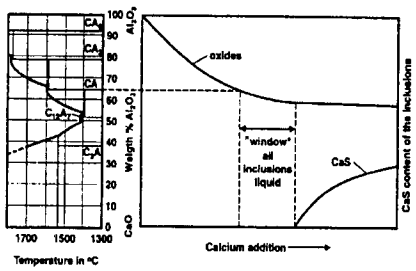

Figure 5 Compositional window in which inclusions are liquid. [25]

Another problem that can occur with calcium treatment is the reoxidation of steel. If steel reoxidizes before it is cast, the excess alumina formed can change the composition of calcium aluminates to be alumina rich, which are solid at steel making temperatures. McKague et al. reported problems with reoxidation of steel when filling the tundish.[9] After changes were made to use less aluminum at the ladle metallurgy station and to reduce reoxidation during

tundish fill, the practice of adding calcium wire to the tundish during start-ups was employed. This practice has reduced the occurrence of clogging, but has not eliminated it.

Lime Bearing Nozzle Materials

Lime additions to nozzle refractory materials have also been used to prevent nozzle plugging. Typically, the refractory material consists of lime stabilized zirconia. Lime in the nozzle reacts to form low melting temperature calcium aluminates. As reported by Ogibayashi et al., the liquid calcium aluminates then provide a low energy interface so that subsequent attachment of alumina particles is avoided.[10]

Ogibayashi et al. have also reported that nozzle replacements due to clogging have dropped to 14% of the previous frequency with lime bearing nozzles as compared to alumina graphite nozzles. A decrease of approximately 50% in the number of inclusions greater than 30 μm in the slab, as measured under the microscope, has also been reported.

It should be noted that Benson et al. have made the observation that good results with lime bearing refractories are typically observed in steel plants that have only marginal clogging problems while those that have major problems with clogging do not find any benefit.[26] In the case of plants that have significant clogging problems, the transport of lime to the steel refractory interface is considered to be the limiting step because when analyzing spent lime bearing refractories, lime is still available in the refractory while the alumina build-up on the nozzle surface has not reacted to form calcium aluminates. Tsujino and colleagues also reported that in laboratory trials, dirty steel formed greater accretions on zirconia-lime-graphite refractories than standard alumina graphite.[27]

Attempts have been made by researchers to provide greater amounts of lime at the refractory surface to react with alumina in order to avoid these problems. In 1990, TYK reported the development of a nozzle material with SiO_2 additions that were intended to accelerate the reaction of lime with alumina.[28] Then in 1991, TYK reported the development of a nozzle containing additional non-hydrating CaO compounds that increase the transport of CaO to the

steel-refractory interface, thereby improving the clogging resistance of these nozzles.[29,30] Likewise, in 1993, Vesuvius reported that a nozzle material was developed that contains a destabilizer which increases the transport of lime to the nozzle wall, contributes to the formation of low melting point substances, and provides for controlled erosion of the nozzle wall so that new refractory material becomes exposed to steel over time.[26]

Despite the success that some researchers have reported with lime bearing nozzles, several problems that have also been reported. Problems similar to those experienced with calcium treatment are also often encountered with lime bearing nozzles. For example, Ramacciotti and Marino reported that clogging occurs with CaS accretions with lime bearing nozzles if the sulfur level of the steel is above 0.020%.[31]

Another problem that is mentioned with lime bearing refractories is the hydration of lime in the nozzle material. Pure lime cannot be added to refractory materials because of this hydration. Instead, the lime is added in the form of lime stabilized zirconia.[26] However, even in stabilized materials, hydration has been observed. In tests performed by Oguri et al., nozzles that were thought to contain non-hydrating lime also showed weight increases over time.[29] The weight gain was thought to be caused by the presence of hydrating lime in the refractory material.

If the concentration of CaO in lime bearing nozzles is too high, erosion can become a problem. Oguri et al. reported such problems with nozzles containing 29% non-hydrating CaO compound.[29] Aoki and colleagues reported similar results with increasing erosion from 20% CaO to complete erosion with 30% CaO additions.[30]

Other Nozzle Materials

Boron nitride and zirconia boride have been investigated by Ishii et al. for potential use as nozzle materials.[32] In laboratory simulations, it was found that BN and ZrB_2 materials exhibited excellent resistance to alumina deposition. Industrial trials with nozzles composed of BN based materials showed no alumina adhesion. The clogging resistance performance of the

BN and ZrB_2 materials is reported to be due to their non-wetting characteristics with steel. In addition, it is reported that ZrB_2 materials react with oxygen in the steel to form B_2O_3 gas that forms a protective layer to prevent alumina deposition.

Vesuvius has patented SiAlON, a material that is reported to have good resistance to alumina adhesion.[33] SiAlON forms a vitreous layer at the surface of the nozzle which provides for controlled erosion of the nozzle refractory. This controlled erosion prevents the nucleation and adherence of alumina to the nozzle wall. The authors of the patent indicate that the material exhibits superior erosion resistance, similar to alumina graphite. However, Benson et al. reported that SiAlON exhibits uncertain erosion characteristics.[26]

Nozzle Modifications

Nozzle design modifications that have been proposed in the literature include annular step nozzles [34,35], an electrochemical cell nozzle [36], and a bubble curtain nozzle [37].

Annular Step Nozzles

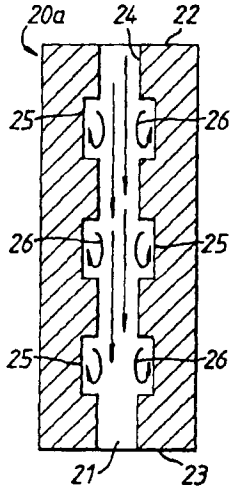

Figure 6 Annular Nozzle. [34]

Flogates Limited has a patent for an annular step nozzle as shown in Figure 6.[34] The annular nozzle uses a series of steps to produce eddies inside the nozzle. These eddies are used to preferentially deposit non-metallic inclusions within the step, where they will not hinder the flow of steel through the nozzle.

Using the same type of nozzle, Tsukamoto et al. have proposed that nozzle clogging can be reduced by preventing flow deviation downstream of the slide gate.[35] Using water modeling, it was shown that the flow of steel downstream of the slide gate is severely asymmetric. A separated flow pattern is generated in a standard SEN downstream from the slide gate, on the closing side of the gate. The purpose of the annular steps in this case is to redistribute the flow of steel so that a uniform stream is achieved within

the nozzle. In addition, the vortexes created around the annular steps uniformly redistribute argon gas bubbles within the steel stream. It was shown that in a traditional SEN, there is a significant difference in the flow rate of steel discharged from one port of the SEN to the other. The flow of steel leaving the SEN ports was reported as being equalized with the annular step nozzle. Use of a double annular step nozzle in an actual caster has given better performance against clogging as well as a 50% decrease in pinhole defects in the slab.

Electrochemical Cell Nozzle

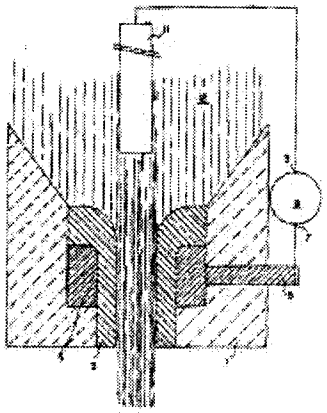

Figure 7
Electrochemical Nozzle.
[36]

Electro-Nite Co. holds a U.S. patent for an electrochemical cell that prevents the deposition of alumina on the nozzle wall (see Figure 7).[36] A zirconia "jet" or liner is used with this nozzle. An electric current is passed through the molten metal stream via a graphite electrode submersed in the molten metal bath and another electrode in contact with the zirconia liner. No details are given in the patent as to the actual mechanism employed to prevent the deposition of alumina on the nozzle wall.

Bubble Curtain Nozzle

Yokoya et al. have recently reported on a submerged entry nozzle that employs a bubble curtain to remove inclusions from the steel stream and prevent their deposition on the nozzle wall.[37] A vortex is created in the molten steel stream with "swirl blades" as it enters the SEN. Argon is injected just downstream of the entrance to the SEN through several holes in the nozzle wall. As the bubbles travel with the steel stream through the nozzle, the bubbles migrate to the center of the stream, creating a conical shaped "bubble curtain" as shown in Figure 8. Inclusions in the steel stream that might otherwise adhere to the nozzle wall are attached to the bubbles and transported to the center of the steel stream.

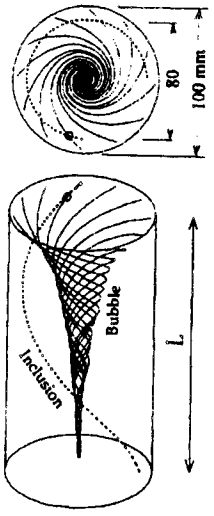

Figure 8 Schematic diagram of bubble curtain. [37]

Water modeling and computational fluid dynamic modeling were used to demonstrate the effectiveness of this nozzle.[37] No actual casting results are reported.

SEN Changing Systems

While the changing of spent submerged entry nozzles during casting does not actually improve nozzle clogging, productivity improvements can be achieved by using a quick change system as proposed by Nishio et al.[38] With such a system, the tundish does not have to be raised and lowered to change the nozzle, and the time it takes to change a nozzle is significantly reduced. This has also been reported to eliminate scrap generated during conventional SEN changes.

EXPERIMENTAL PROCEDURES

The two most common experimental procedures used to investigate accretion formation on nozzles are casting simulations and refractory immersion tests. These two methods will be discussed first, followed by less commonly employed techniques.

Casting Simulations

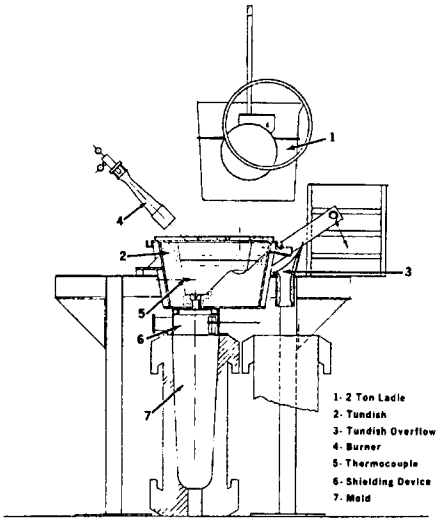

Figure 9 Experimental apparatus employed by Duderstadt et al. [2]

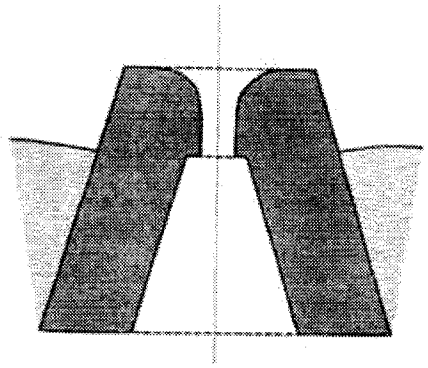

Figure 10 Schematic diagram of protruding nozzle. [2]

Casting simulations were the first methods used to study accretion formation. In 1968, Duderstadt et al. used a full-sized casting simulation to study nozzle accretions as shown in Figure 9.[2] In this study, 1020 steel was poured from a ladle into a 600 lb. tundish. The steel flowed through ½ in. and ¾ in. nozzles into an ingot mold below the tundish. The area between the tundish and mold was enclosed in a nitrogen atmosphere to shield the steel stream from oxidation. Aluminum concentrations were varied during the course of the experiments. Nitrogen shielding of the tundish was used to examine the effect of reoxidation on nozzle clogging. In order to evaluate the effects of nozzle temperature on clogging, two protruding tundish well nozzles were evaluated (see Figure 10). The first nozzle was composed of zirconia while the second nozzle was made of a thermally conductive material above the tundish and an insulating material below the tundish. The second nozzle was used to prevent heat loss to the tundish refractory.

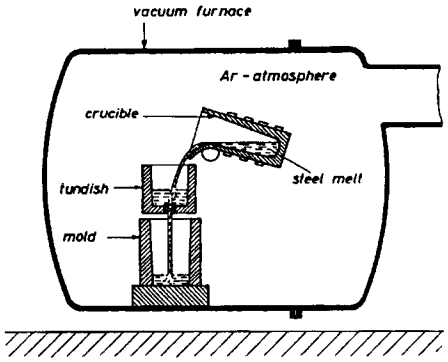

Figure 11 Casting simulation apparatus. [39]

In 1970, Schwerdtfeger and Schrewe melted 50 kg heats of steel in a vacuum induction furnace as shown in Figure 11.[39] The heats were poured into a model tundish with a fireclay nozzle having an 8 mm bore. The tundish emptied into a mold. The tundish and mold were also enclosed in the vacuum induction furnace. Vacuum deoxidation was carried out before the steel was aluminum-killed. Pouring from the furnace to the tundish was carried out in an argon atmosphere. The objective of the experiments was to evaluate the reoxidation of steel based on different refractory materials, therefore different tundish linings were utilized. These consisted of magnesite, alumina, and masrock.

Later, in 1971, Farrell and Hilty cast 90 lb. induction melted 1038 steel heats into a no. 10 clay-graphite crucible that served as a tundish.[11] The steel was cast from the tundish through a zirconia nozzle and into a cast iron ingot mold. The mold was suspended by four springs that were matched to have the same displacement under the same load. A differential transformer measured the displacement of the springs during casting, which was recorded on a strip chart. This served to record the weight of the steel cast as a function of time. During melting, the steel was kept under a protective argon atmosphere. Various deoxidizers were used to evaluate their effect on nozzle clogging.

Singh used essentially the same technique in 1974.[5] Three hundred pound heats of steel containing 0.05% carbon were induction melted in air or in a vacuum furnace. The heats were poured into a tundish containing a 3/8 inch I.D. zirconia nozzle. To test for the effect of reoxidation, some of the heats were poured inside a vacuum induction furnace, while all others were poured in air. Some of the runs were made using tapered, submerged nozzles. The

tundish emptied into a mold that was placed on load cells to measure the weight of the mold during the cast. The weight was recorded using a strip chart recorder.

Dawson[13] in 1990, and Anderson and Wijk[14] in 1992, employed the same basic casting simulation technique with some minor differences which will be discussed below. With this technique, a nozzle is inserted into a hole cut into the bottom of a crucible in a induction furnace. A stopper is used to keep the metal in the crucible during melting. The cast is started by removing the stopper, and the steel is cast into a mold beneath the induction furnace.

There are several advantages with this technique as pointed out by Dawson.[13] A tundish is not needed with this technique, and therefore preheating of a tundish is also unnecessary. Reoxidation is also avoided because the steel is not transferred from the furnace to a tundish. Because the steel is cast through the bottom of the crucible, the entrainment of slag in the steel stream can be avoided.

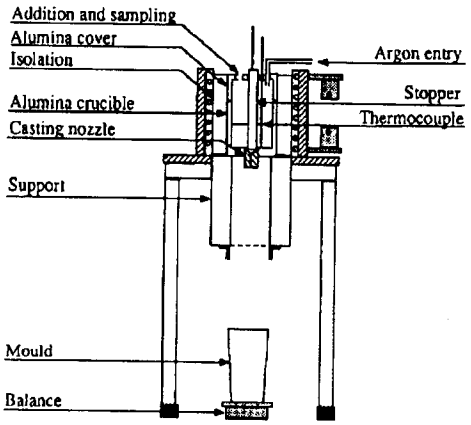

Figure 12 Schematic diagram of casting simulation. [14]

Dawson performed his experiments at two different scales.[13] The first set of experiments was performed using a 13 kg induction furnace; the second set of experiments was conducted in a 60 kg induction furnace. In all of the experiments, the steel was cast through 5/16 in. I.D. α alumina nozzle made from extruded tube. The crucibles for the experiments were clay-graphite that were coated with a paste consisting of 90% Al_2O_3 and 10% Cr_2O_3. Immediately after the cast was started, 0.1% aluminum was added to kill the melt. The furnace power was then shut off. The 13 kg experiments provided nozzle accretions in the early stages of formation, while the 60 kg experiments provided larger, macro scale accretions.

Andersson and Wijk employed an induction furnace with a 10 kg capacity (see Figure12).[14] The furnace had a cover so that an argon atmosphere could be maintained over the bath. The steel was cast into a mold that was placed on a balance. The weight of the mold as the cast progressed was used to infer the flow rate of steel through the nozzle. Two nozzle designs were tested, an angle entry nozzle and a radius entry nozzle. The materials used in the angle entry nozzles were alumina, magnesite, and zirconium silicate while the radius entry nozzles were made of zirconium silicate. A graphite susceptor and separate induction coil were used in some experiments to heat the angle entry nozzle. A thermocouple was placed in the nozzle near the steel-refractory interface to measure the nozzle temperature. Magnesite was added to the steel to increase the oxygen content before it was killed and cast.

Immersion Tests

Immersion tests are the most commonly encountered experimental procedure in the literature.[4,6-8,16,20] This is likely because it is simpler than the casting simulation procedures. Melting is carried out in an induction furnace with a protective argon atmosphere. After the steel is killed, samples of various composition are immersed in the molten steel bath for various lengths of time. Some researchers have chosen to rotate samples within the molten steel[6,7], while others have not.[8,16,40] Among those that had rotating samples, one specified a rotation speed that produces a tangential velocity similar to the velocity of steel in industrial nozzles.[27] Rotation is not likely to be important to the procedure because the induction furnace creates flow in the metal. All tests, rotating and not, yielded accretions on the refractory samples.

Two variations to the above procedure were found in the literature. Hiraga and colleagues injected argon gas into the center of their hollow refractory specimens for cooling.[4] Shikano et al. moved their refractory specimens up and down 1 cm at a rate if 30 Hz rather than rotating them in the bath.[41]

Molten Metal Pump

Asano et al. devised a molten metal pump that would allow steel to flow through a simulated nozzle.[42] A funnel-shaped alumina graphite piece was submerged within the steel bath. Argon was bubbled from the bottom of the funnel and carried molten steel into an alumina graphite crucible above the steel bath. The alumina graphite crucible had a simulated nozzle inserted with a 90° elbow. The simulated nozzle empties into the steel bath. In this way, steel can be circulated through the simulation nozzle indefinitely or until clogging occurs.

Ishii et al. used a molten metal pump of a different design.[32] A tubular section of the subject refractory was placed within a larger alumina graphite tube. The alumina graphite tube had a hole in it near the top. The tube was then reciprocated up and down within the furnace so that metal flowed in and out of the refractory sample.

Thermochemical Reaction Experiments

At least three different novel experiments have been reported in the literature to test for thermochemical reactions with refractory materials and deoxidized steel. These experiments are discussed below.

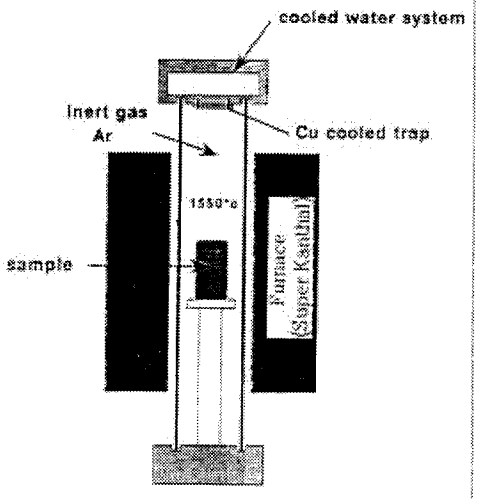

Figure 13 Volatilization-condensation furnace. [8]

Poirier et al. performed a set of volatilization/condensation experiments on alumina graphite material to test for thermochemical reactions within the refractory.[8] The alumina graphite was heated in a furnace with a controlled argon atmosphere to 1550°C as shown in Figure 13. A water-cooled copper top was used in the furnace to condense any volatilized species within the furnace. Deposits consisting of SiO_2, Na_2O, and K_2O were found on the copper chill after the experiments.

Sasai and Mizukami also performed an experiment to test for thermochemical reactions in alumina graphite materials and silicon carbide materials.[15] In these experiments, 40 grams of refractory were ground into a powder and placed into the bottom of an alumina crucible. A porous alumina refractory barrier was placed over the powder in the crucible. The porous barrier had a pore size of 86 μm so that gasses could pass through the barrier but steel could not. The barrier was cemented in place with an alumina solvent. Electrolytic iron (500 g) was melted in the crucible above the porous alumina barrier and heated to 1600°C before 0.1% Ti or Al was added to the melt. Chemical samples were taken from the melt using quartz tubes to detect the products of any thermochemical reactions that might occur. It was found that carbon and silicon levels increased over time while aluminum or titanium levels decreased.

Nakamura et al. used refractory crucibles filled with molten steel to test for thermochemical reactions between the steel and refractory.[40] In this set of experiments, 50 grams of steel with 1.075% aluminum was placed in alumina-silica-graphite crucibles of two different compositions. A protective coating was placed over the steel to prevent oxidation. The exact composition of the crucibles was not provided. The crucibles were heated in an electric furnace to 1580°C, and after 30 minutes, the steel was tapped from the crucibles. The crucibles were then air cooled and examined for accretion formation.

REFERENCES

1. Snow, R.B.; Shea, J.A. "Mechanism of Erosion of Nozzles in Open-Hearth Ladles". *The Journal of the American Ceramic Society*. Vol. 32 No. 6. pp. 187-194 (1949)

2. Duderstadt, G.C.; Iyengar, R.K.; Matesa, J.M. "Tundish Nozzle Blockage in Continuous Casting". *Journal of Metals*. Vol. 20 No.4. pp. 89-94 (1968)

3. Ogibayashi, S. "Mechanism and Countermeasure of Alumina Buildup on Submerged Nozzle in Continuous Casting." *Taikabutsu Overseas*. Vol. 15, No. 1. pp. 3-14 (1994)

4. Hiraga, Y.; Yashima, Y.; Fujii, K. "Behavior of Alumina-Deposition on Tundish Nozzles in Continuous Casting of Ti-Added Al Killed Steel". *Taikabutsu Overseas*. Vol. 15, No. 1. pp. 22-27 (1995)

5. Singh, S.N. "Mechanism of Alumina Buildup in Tundish Nozzles During Continuous Casting of Aluminum-Killed Steels". *Metallurgical Transactions*. Vol. 5. pp. 2165-2178 (1974)

6. Poirier, J.; Thillou, B.; Guiban, M.A.; Provost, G. "Mechanisms and Countermeasures of Alumina Clogging in Submerged Nozzles". *Steelmaking Conference Proceedings*. Vol. 78. pp. 451-456 (1995)

7. Kasai, N.; Kawasaki, M.; Hayashi, Y.; Kawai, H. "Explanation of Clogging Phenomena of CC Submerged Nozzle". *Taikabutsu Overseas*. Vol. 11, No. 1. pp. 22-33 (1990)

8. Poirier, J.; Verrelle, D.; Thillou, B.; Provost, G.; Taffin, C.; Tssot, P. "Study of Clogging Phenomena in Continuous Casting Submerged Nozzles". *UNITECR 1991*. pp. 226-229 (1991)

9. McKague, A.R.; Engel, R.; Suer, M.A.; Wolf, D.J.; Garbowsky, M.D.; Reed, L.F. "Resolution of Clogging at Armco's Mansfield Slab Caster". *Iron and Steelmaker*. Vol. 25, No. 11. pp. 35-41 (1998)

10. Ogibayashi, S.; Uchimura, M.; Maruki, Y.; Mizukoshi, D; Tanizawa, K. "Mechanism and Countermeasure of Alumina Buildup on Submerged Nozzle in Continuous Casting". *Steelmaking Conference Proceedings*. pp. 337-344 (1992)

11. Farrell, J.W.; Hilty, D.C. "Steel Flow Through Nozzles: Influence of Deoxidizers". *Electric Furnace Proceedings*. Vol. 29. pp. 31-45. (1971)

12. Benson, P.M.; Robinson, Q.K.; Dumazeau, C. "New Technique for the Prevention of Alumina Build-Up in Submerged Entry Nozzles for Continuous Casting". UNITECR 1993. pp. 1087-1096 (1993)

13. Dawson, S. "Tundish Nozzle Blockage During the Continuous Casting of Aluminum-Killed Steel." *Steelmaking Conference Proceedings*. pp. 15-31 (1990)

14. Andersson, M.; Wijk, O. "A study on Tundish Nozzle Blockage During Casting of Aluminum Deoxidized Steel". *Sixth International Conference on Refining Process*. pp. 175-209 (1992)

15. Sasai, K.; Mizukami, Y. "Reaction Mechanism Between Alumina Graphite Immersion Nozzle and Low Carbon Steel". *ISIJ International.* pp. 802-809 (1994)

16. Fukuda, Y.; Ueshima, Y.; Mizoguchi, S. "Mechanism of Alumina Deposition on Alumina Graphite Immersion Nozzle in Continuous Caster". *ISIJ International.* pp. 164-168 (1992)

17. Cameron, S.R. "The Reduction of Tundish Nozzle Clogging During Continuous Casting at Dofasco". *Steelmaking Conference Proceedings*. Vol. 75. pp. 327-332 (1992)

18. Alavanja, M.; Gass, R.T.; Kittridge, R.W.; Tsai, H.T. "Continuous Improvement of Practices to Reduce Tundish Nozzle Clogging". *Steelmaking Conference Proceedings*. Vol. 78. pp. 415-426 (1995)

19. Takasugi, H.; Masaoka, T.; Shirayama, A.; Mori, T.; Hiroshi, M. "Prevention of Alumina Build-Up in Submerged Entry Nozzles for Continuous Casting of Low Carbon Aluminum-Killed Steel". *The International Iron and Steel Congress.* Vol. 3. pp. 462-469 (1990)

20. Ando, M.; Takahashi, S.; Okumura, H.; Yamaguchi, K. "Slit Type Immersion Nozzle of Alumina-Graphite Material". *UNITECR 1995.* Vol. 2. pp. 73-78 (1995)

21. Schmidt, M.; Russo, T.J.; Bederka, D.J. "Steel Shrouding and Tundish Flow Control to Improve Cleanliness and Reduce Plugging". *Steelmaking Conference Proceedings*. pp. 451-460 (1990)

22. Kobayashi, S.; Ishige, T.; Ogata, M. "Prevention for Nozzle Clogging of SLCC at NKK Keihin Works". *Taikabutsu Overseas*. Vol. 15, No.1. pp. 33-37 (1994)

23. Fruehan, R.J. *The Making, Shaping and Treating of Steel.* 11th Ed. The AISE Steel Foundation. Pittsburgh, PA. pp. 687-693 (1998)

24. Faulring, G.M.; Farrell, J.W.; Hilty, D.C. "Steel Flow Through Nozzles: Influence of Calcium". *Continuous Casting, Vol. 1, Chemical and Physical Interactions During Transfer Operations*. Iron and Steel Society. Warrendale, PA. pp. 57-66. (1985)

25. Bannenberg, N. "Inclusion Modification to Prevent Nozzle Clogging." *Steelmaking Conference Proceedings*. Vol. 78. pp. 456-463 (1995)

26. Benson, P.M.; Robinson, Q.K.; Park, H.K. "Evaluation of Lime-Containing Sub-Entry Shroud Liners to Prevent Alumina Clogging." *Steelmaking Conference Proceedings*. pp. 533-539 (1993)

27. Tsujino, R.; Tanaka, A.; Imamura, A.; Takahashi, D.; Mizoguchi, S. "Mechanism of Deposition of Inclusion and Metal in ZrO_2-CaO-C Immersion Nozzle of Continuous Casting". *ISIJ International.* pp. 853-858 (1994)

28. Nakamura, T.; Aoki, T.; Okumura, H.; Kondo, Y. "Immersion Nozzle for Prevention of Alumina Clogging". *Taikabutsu Overseas*, Vol. 11, No. 1. pp. 39-39 (1990)

29. Oguri, K.; Ando, M.; Muroi, T.; Aoki, T.; Okumura, H. "Alumina Clogging Resistant Materials for Immersion Nozzle". *UNITECR 1993.* pp. 1119-1127 (1993)

30. Aoki, T.; Nakamura, T.; Ozeki, H.; Elksnitis, A. "Alumina Clogging Resistant Materials for Tundish Shrouds". *Steelmaking Conference Proceedings*. Vol. 78. pp. 357-360 (1991)

31. Ramacciotti, A.; Marino, E. "Use of Sintered Calcium Oxide Nozzles in the Continuous Casting of Aluminum-Killed Steel". *EAF Conference Proceedings*. Vol. 42. pp. 293-298 (1984)

32. Ishii, A.; Ishikawa, A.; Nakamura, Y. "Prevention of Nozzle Clogging During Continuous Casting of Al-Si Killed Steel". *Interceram*. Special Issue. pp. 70-74 (1987)

33. Hoggard, D.B.; Park, H.K. "Prevention of Al_2O_3 Formation in Pouring Nozzles and the Like". European Patent #EP0309225. (1989)

34. Hill, P.L.; Griffiths, W.A. "Controlling Deposition of Particles from Molten Metals". English Patent #GB2230719. (1990)

35. Tsukamoto, N.; Kurashina, Y.; Yanagawa, K. "Optimum Shape Obtained by Hydraulic Model Study on Annular Step Submerged Entry Nozzle and Its Performance". *Taikabutsu Overseas*. Vol. 15, No. 1. pp. 43-49 (1994)

36. Cure, O.P. "Process Intended to Prevent Deposition on the Walls of Metallurgical Containers and Metallurgical Containers Suitable for Carrying out This Process". U.S. Patent No. 4,850,572. Electro-Nite Co. (1989)

37. Yokoya, S.; Takagi, S; Souma, H; Iguchi, M.; Asako, Y.; Hara, S "Removal of Inclusion through Bubble Curtain Created by Swirl Motion in Submerged Entry Nozzle". *ISIJ International*, Vol.38, No. 10. pp. 1086-1092 (1998)

38. Nishio, H.; Tsukamoto, N.; Yamamoto, K.; Taniguchi, T. "A Quick Change System for Submerged Entry Nozzles". *Taikabutsu Overseas.* Vol. 16, No. 1. pp. 13-15 (1995)

39. Schwerdtfeger, K.; Schrewe, H. "Reoxidation of Aluminum-Killed Steel by Contact with Refractory Materials". *Electric Furnace Proceedings*. Vol. 28. pp. 95-102 (1970)

40. Nakamura, M.; Kiwada, T.; Nomura, O.; Ichikawa, K. "Reactivity of Submerged Entry Nozzle to Molten Steel". *Taikabutsu Overseas*. Vol. 15, No. 1. pp. 28-32 (1994)

41. Shikano, H.; Tsutomu, H.; Iitsuka, S.; Shin-Ichirou, K. "Prevention of Alumina Deposition in Submerged Nozzles". *Taikabutsu Overseas*. Vol. 11, No. 1. pp. 10-21 (1990)

42. Asano, K.; Ishii, A.; Kasai, K. "Mechanism of Aluminum Buildup in Submerged Nozzle During Continuous Casting of Low Carbon Aluminum-Killed Steel." *UNITECR 1991*. pp. 229-232 (1991)

10.0 Appendix D
Contact Angle Of Molten Steel Applied To The Development Of Clog-resistant Submerged-Entry Nozzles

B. T. Eldred, P. D. Owney
Ceramic Engineering Dept., University of Missouri - Rolla

ABSTRACT

The sessile drop method, modified by use of a doser tube rather than *in situ* drop formation, was used to study commercial steel compositions in contact with idealized refractory substrates. Steels containing varying amounts of carbon, aluminum, and titanium were tested in hydrogen and forming gas atmospheres at 1600°C. All of the compositions investigated had significantly different equilibrium contact angles than pure iron, but steel chemistry overall had a limited effect on wetting. A reaction of the high titanium steels with hydrogen is still under investigation.

INTRODUCTION

Many investigations have been conducted involving iron or one of its alloys in contact with an alumina substrate. In 1988, B.J. Keene published an extensive review [1] of the research conducted to that point. Nearly all of the published work has been of a scientific nature with very little emphasis given to practical application of the data. The goal of this continuing investigation is to determine what role the wetting properties of commercial steels play in the clogging mechanisms of submerged-entry nozzles used in continuous casting. Once the effect of wetting on the mechanisms of clogging is understood, it may be possible to tailor the properties of the refractory or of the steel itself to minimize the chances of initiating a clog.

Aluminum and titanium content were chosen as the experimental variables of the steel itself since these elements are commonly added to kill or partially deoxidize commercial steel. Ayushina *et al.* [2] and Popel *et al.* [3], among others, have studied the iron-aluminum system, but in general the emphasis has been on large additions of aluminum, especially around 55 at% where Ayushina *et al* reported a large inflection in the surface energy. Although there is some variation between sources, it is agreed that any addition of aluminum to pure iron will lower its surface tension and therefore produce a lower equilibrium contact angle. The present study focuses on low aluminum steels, 0.12wt% or less, containing 0.03wt% or less carbon. Keene quotes Kishimoto's [4] and Smirnov's [5] results for low concentrations of titanium in iron. In helium, titanium had little effect on surface tension, whereas it was very surface active under a hydrogen atmosphere. The present study includes concentrations from 0% to 0.12wt% titanium and finds similar effects. The third experimental variable in the present study is oxygen partial pressure. Experiments were carried out in pure hydrogen and in forming gas, a mixture of 10vol% hydrogen and 90vol% nitrogen. Oxygen partial pressures measured exiting the sessile drop furnace were typically 10^{-16} atm in hydrogen and 10^{-10} atm in forming gas. Table 1 lists the compositions of the steel samples.

Table 1 - Steel Compositions

Label	wt% C	wt% Al	wt% Ti
LC-AD,med	<0.02	.004	.001
LC-AD,low	<0.03	.002	.002
ULC-AK,low	.0060	.0069	.0005
ULC-AK,high	.0055	.1235	.0006
ULC-AK,Ti	.0061	.1162	.1169

EXPERIMENTAL

The typical sessile drop apparatus was modified in this study by the introduction of a doser tube, a 99.8% Al_2O_3 closed-on-one-end tube with a small hole drilled at the end. The iron or steel sample was melted in the doser tube then dropped at the desired temperature by momentarily stopping gas flow through the main furnace tube, creating a pressure differential. This procedure ensures that the area of the substrate directly below the drop is in equilibrium with the furnace atmosphere at the time of drop formation. The doser tube technique has been used previously by Ownby and Li [6] and shown to be a superior method of drop formation for samples that are highly sensitive to oxygen partial pressure. Figure 1 shows a schematic of the sessile drop furnace.

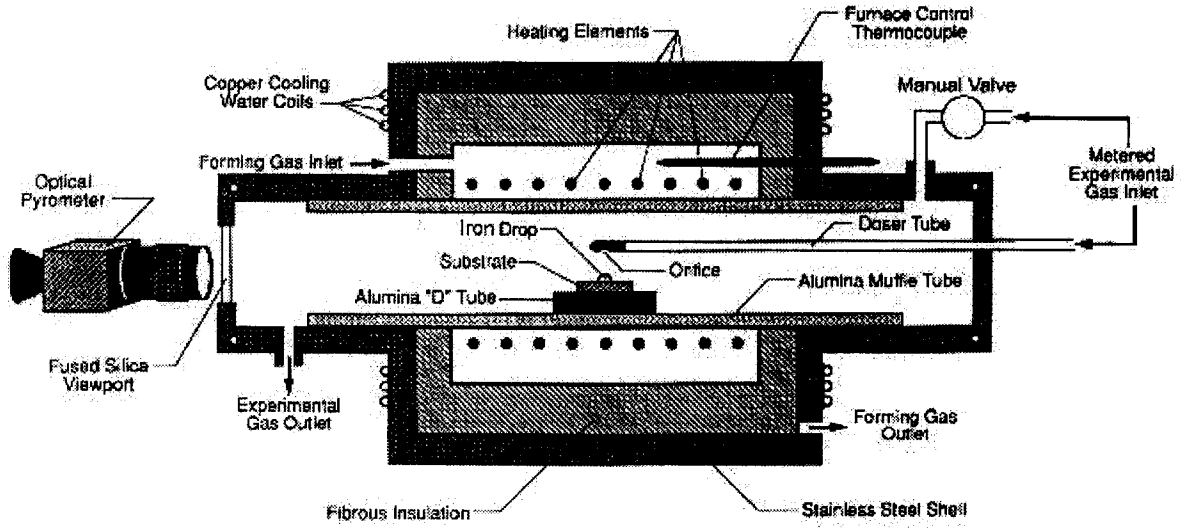

Figure 1 - Sessile Drop Furnace

The sessile drop furnace was connected by a series of solenoids to a smaller furnace containing a thoria oxygen sensor that was maintained at a constant temperature of 1000°C. The solenoids allowed the gas flow to be switched so oxygen partial pressure could be measured entering or leaving the sessile drop furnace.

After a drop was formed, it was filmed continuously for 45 minutes, then once every half-hour for eight hours using a digital video camera. The film was then transferred onto computer and still images were extracted each five minutes for the first 45 minutes, then each half-hour thereafter. Finally, the contact angle was measured from the still images using commercial image processing software.

RESULTS AND DISCUSSION

A significant difference in contact angle was observed between 99.97+% pure iron and the various steel compositions; however, with one exception, all of the steels had similar equilibrium contact angles. All of the steels except ULC-AK-Ti in hydrogen fell between approximately 100° and 105°. The case of ULC-AK-Ti in hydrogen will be discussed separately later. Repeated measurements of a single still image produced an error (three standard deviations) of ±2.1°, which is assumed to remain constant. Figure 2 below summarizes the data for steel samples at 1600°C on sapphire, along with pure iron for comparison. Error bars are shown as a gray band around the uppermost and lowermost steel curves only for the sake of clarity. These bands nearly overlap over the entire length of the curves, implying that all of the steels shown here had almost the same equilibrium contact angle within the limits of error.

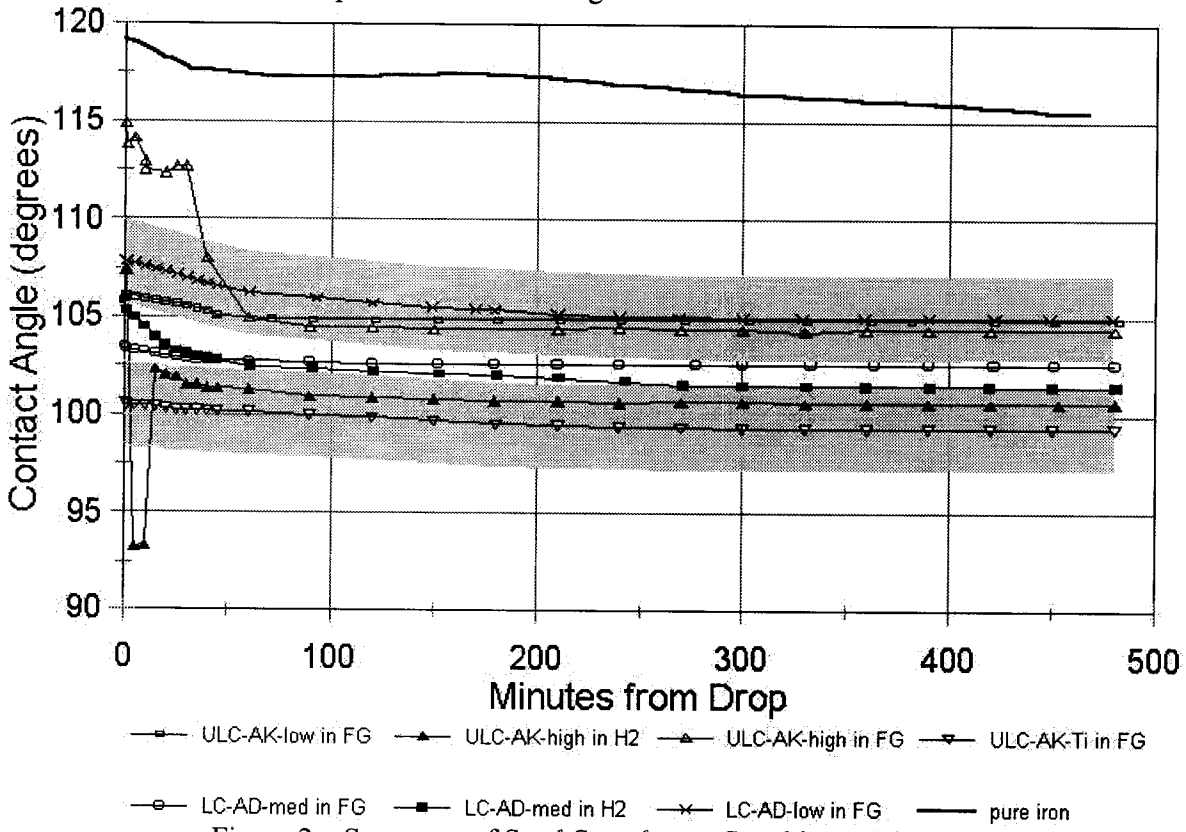

Figure 2 – Summary of Steel Samples on Sapphire at 1600°C

The most probable explanation for this behavior is the issue of concentration. Adding even a small amount of a second element to a pure system greatly increases the entropy of the interfacial

region, causing a decrease in δ_{SL}, the solid-liquid interfacial energy. The contact angle is related to the solid-liquid, solid-vapor, and liquid-vapor interfacial energies by the Young-Dupre Equation: $\cos\theta = (\delta_{SV} - \delta_{SL})\delta_{LV}$. If δ_{SV} and δ_{LV} remain constant, a decrease in δ_{SL} causes an increase in $\cos\theta$, which causes a decrease in δ for $90°<\theta<180°$. In short, adding a second element to a pure, non-wetting system causes it to become more wetting. However, most of the studies in the literature were conducted on alloys with extremely high concentrations of the second phase, 30 to 50% or more. Some studies included the entire range from pure iron to the other pure end member. The present study was conducted on samples reasonably close to commercial steel compositions – a few hundredths or tenths of a percent of each alloying phase. While this is enough to produce a significant change from pure iron, it is not sufficient to produce large differences between real steel compositions.

The one steel composition whose contact angle did not lie within the same 5° window (excluding error bars) as the others was ULC-AK-Ti. When this steel was tested in forming gas, it was the lowest of all of the others, but was within the 3? error bars; however, in hydrogen its equilibrium contact angle was significantly lower than any of the other compositions investigated, approximately 90°. In an effort to produce a contact angle between the hydrogen value of 90° and the forming gas value of 100°, the experiment was repeated using a mixture of the two gases. The hydrogen flow was set at 100 cm^3/min and the forming gas at 25 cm^3/min using mass flow controllers. The partial pressure of oxygen at the time of drop formation was measured to be $2x10^{-13}$ atm. Even with this 82% hydrogen atmosphere, the equilibrium contact angle was in the same 5° range as all of the other steels in forming gas. To see if the contact angle could be forced below 90°, the 99.99% pure hydrogen that is normally used in the furnace was passed through a Millipore filter, producing 99.99999% hydrogen. At the time of drop formation, the oxygen partial pressure was measured to be $7x10^{-16}$ atm. The equilibrium angle remained at 90°. When the sapphire substrate was replaced with a single crystal spinel ($MgO•Al_2O_3$) substrate, the contact angle remained at 90° in hydrogen, but increased to 109° in forming gas, four degrees above the average window of the sapphire substrates. These results are summarized in Figure 3.

When removed from the furnace, all of the ULC-AK-Ti samples run in hydrogen appeared clean (non-oxidized), had no distinguishing characteristics on the surface, and were adhered firmly to the substrate. Both samples run in forming gas, however, had a gold-colored layer on the surface and were not adhered to the substrate. These two samples were analyzed by Auger electron spectroscopy depth-profiling through the top surface of the drop. The sample on sapphire had a fairly uniform chemistry down to a depth of 360nm, with only a 2nm layer of carbon on the surface due to handling the sample during loading. A similar carbon layer was found on all samples and is a common artifact of this type of analysis. On spinel, Auger analysis detected titanium concentrations up to 45at% near the top surface of the drop that did not appear to be uniform around the entire liquid-vapor surface. At this time, the exact causes of the gold-colored surfaces and the nonuniform titanium layer are still under investigation.

Titanium is known to form a hydride that dissociates at approximately 405°C [7,8]. At the temperature of this study, 1600°C, the hydride should be completely dissociated. Apparently there is still interaction between the titanium and hydrogen at high temperatures, but the effects

are not visible to Auger analysis. At the time of this writing, the samples are being investigated by other methods to determine what causes the large drop in contact angle in hydrogen atmosphere. Also, ULC-AK-Ti is being investigated on other refractories such as TiO_2 and MgO to determine the relative importance of steel composition and substrate composition.

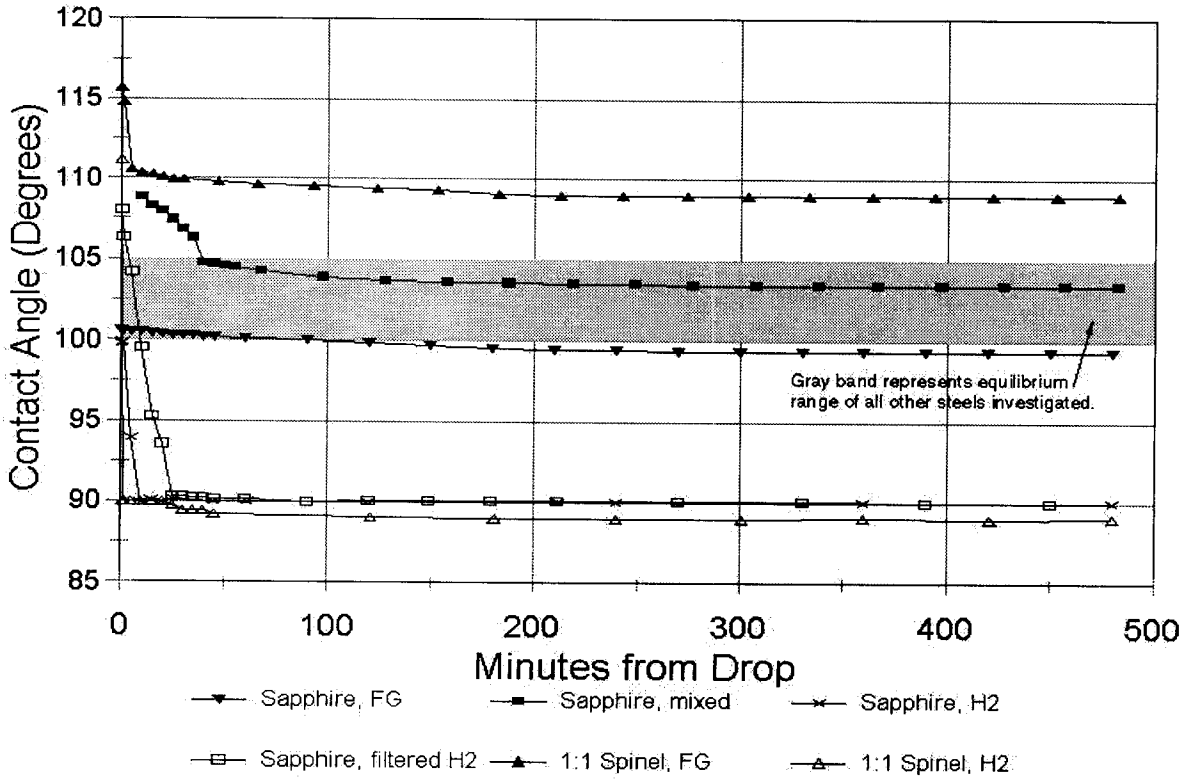

Figure 3 – Summary of ULC-AK-Ti Samples

CONCLUSIONS

1. Each of the steel compositions tested showed a significantly different equilibrium contact angle than pure iron. This is due to the very large decrease in surface energy that occurs when a pure system becomes impure.

2. Except for ULC-AK-Ti in hydrogen, all of the steels tested had similar equilibrium contact angles. While literature data shows significant changes in contact angle with large alloy additions, the very low concentrations of alloying agents found in commercial steels are insufficient to cause large changes. Consequently, wetting of the refractory by molten steel is not a controllable factor in clogging of submerged entry nozzles.

3. Steel composition ULC-AK-Ti displays a significantly lower contact angle in pure hydrogen than any of the other compositions studied. In forming gas, ULC-AK-Ti forms a gold-colored surface layer and does not adhere to sapphire or spinel substrates. Auger analysis shows a fairly uniform steel chemistry down to 360nm. Investigation into these phenomena is still underway.

REFERENCES

1. B. J. Keene, *International Materials Reviews*, 33, 1 (1988) 1.

2. G. D. Ayushina, E. S. Levin, and P. V. Geld, *Russian J. of Phys. Chem.*, 42, 11 (1968) 1489.

3. S. I, Popel, V. N. Kozhurkov, and A. A. Zhukov, *Russian Metallurgy*, 5 (1975) 56.

4. M. Kishimoto, K Mori, and Y. Kawai, *Nippon Kinzoku Gakkaishi (J. Jpn Inst. Met.)*, 48, 4 (1984) 413.

5. L. A. Smirnov, S. I. Popel, and B. V. Tsarevskii in *Surface Phenomena in Melts and Solid Phases Forming From Them*, (Nal'chik, Kabardino-Balkorskoye kn. izd. 1965) p320.

6. P. D. Ownby and K. W. K. Li, *Journal of the American Ceramics Society*, 74, 6 (1991) 1275.

7. H. Chatbi, M. Vergnat, and G. Marchal, *Applied Physics Letters*, 64, 10 (1994) 1210.

8. A. Efron, Y. Lifshitz, I. Lewkowicz, and M. H. Mintz, *Journal of the Less Common Metals*, 153 (1989) 23.

11.0 Appendix E: Static Nozzle Accretion Studies of Clogging during Continuous Casting

Sujatha Ramachandran †, Kent D. Peaslee †, Jeffrey D. Smith ‡

† Department of Metallurgical Engineering

‡ Department of Ceramic Engineering
University of Missouri-Rolla

ABSTRACT

Thermochemical reactions that could effect nozzle clogging were investigated using alumina-graphite refractory crucible containing molten steel. From these static experiments a number of observations were made. The predominant oxide inclusion in aluminum-killed steel was alumina. However, magnesium aluminate (MgO.Al2O3) and calcium hexa-aluminate (CaO.6Al2O3) was observed at the steel/refractory interface

Key Words
nozzle clogging, submerged entry nozzles, aluminum killed steel, refractory

INTRODUCTION

The clogging of submerged entry nozzles (SEN) and tundish well nozzles during continuous casting has been a problem facing the steel industry for years. Several attempts have been made in the past to understand this problem, most of which have been based on post mortem studies of spent refractories. However, a few fundamental studies have been initiated and still a number of questions regarding the basic interactions and the underlying mechanisms that effect clogging remain unanswered.

A few investigations that were completed have shown that nozzle clogging is affected by the interactions between liquid steel and the refractory material [1-4]. The nature of this interaction is affected by the compositions of both the steel and the refractory material. Therefore characterizing the underlying thermochemical reactions between steel and various refractory materials is essential to understanding the nozzle clogging process.

This paper presents preliminary results of a study directed towards performing this characterization. The strategy used in the study was to perform static experiments with molten steel of various compositions in refractory crucibles made of typical nozzle materials, followed by a post mortem characterization using cathodoluminescence (CL) microscopy, scanning electron microscopy (SEM) and reflected light (RL) microscopy.

EXPERIMENTAL PROCEDURE

To simulate nozzle-steel interactions small refractory pieces were cut from standard SEN refractories. Evenly spaced holes were machined into the refractory pieces. Each hole acts as a separate crucible to contain a given steel chemistry (see Figure 1). The experiments used alumina-graphite crucibles having composition as given in Table I.

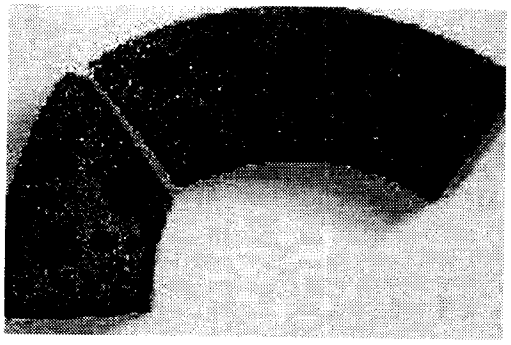

Figure1: Refractory Crucibles

Table I. Crucible Composition (wt. %)

Al_2O_3	C	CaO	MgO	SiO_2	Others
83.0	13.0	0.2	0.5	0.7	2.6

A design of experiments approach was used to establish steel compositions, to be used in the refractory crucibles. Two levels of carbon (ultra-low and medium), three levels of aluminum (unkilled, aluminum deoxidized and aluminum-killed) and two levels of titanium (none and high) defined the twelve "master" steel alloys to be used in all the experiments (See Table II). Each "master" steel alloy was melted using combination of electrolytic steel and low residual bar stock in an induction furnace in an argon atmosphere. Appropriate additions of carbon, aluminum and titanium were made to the melt and samples were extracted at suitable intervals by suction into quartz tubes (See Figure 2). Master steel composition was confirmed through chemical analysis.

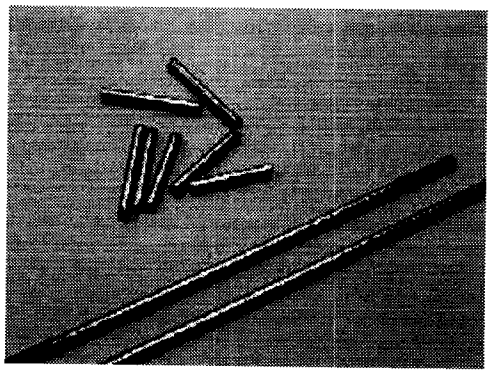

Figure 2: Steel Samples

Table II. Target Steel Chemistries

Factor	Factor Levels	Levels
Carbon	2	0.003 0.20
Aluminum	3	0.00 0.01 0.12
Titanium	2	0.00 0.10

A sample from each of the 12 steels was placed in refractory crucibles. The crucibles were placed in an alumina enclosure and graphite was packed around the sample to reduce the oxygen potential in the system. A thermocouple was inserted in one of the empty holes of the sample to monitor the refractory-steel temperature. The alumina enclosure was covered with an alumina lid and argon was fed into the alumina enclosure to provide an inert environment. The experimental apparatus was placed in a resistance furnace and heated at the rate of ~130°C/hour to 1585°C, held for a proper time and then furnace cooled for about 8 hours. A schematic of the experimental apparatus is given in Figure 3. Two sets of experiments were run one with holding period of 60 min and the second at 120 min. The samples were cut, mounted and polished for CL/SEM/RL characterization.

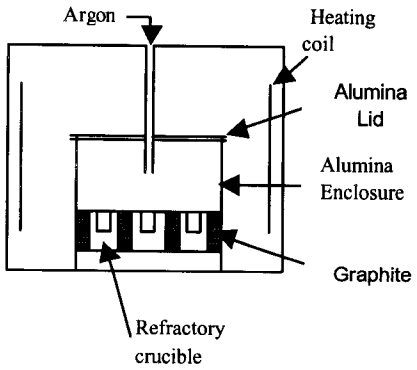

Figure 3: Schematic of the experimental setup

RESULTS AND DISCUSSION

Effect of Carbon

Results of the microscopic examination of the transverse cross-section of the alumina-graphite crucible/steel interface when steel (0.20C, no aluminum, no titanium) and steel (0.003C, no aluminum, no titanium) were held in the alumina-graphite crucible at 1585°C for 120 min are

shown in Figure 4. Alumina and CA_6 was found in both the samples even when though the melt did not contain any aluminum. This suggests that the alumina in the refractory be reduced by graphite to Al_2O, which diffuses to the interface where it is reoxidized into alumina and then further reacts with the calcia also extracted from the refractory by diffusion, to form CA_6.

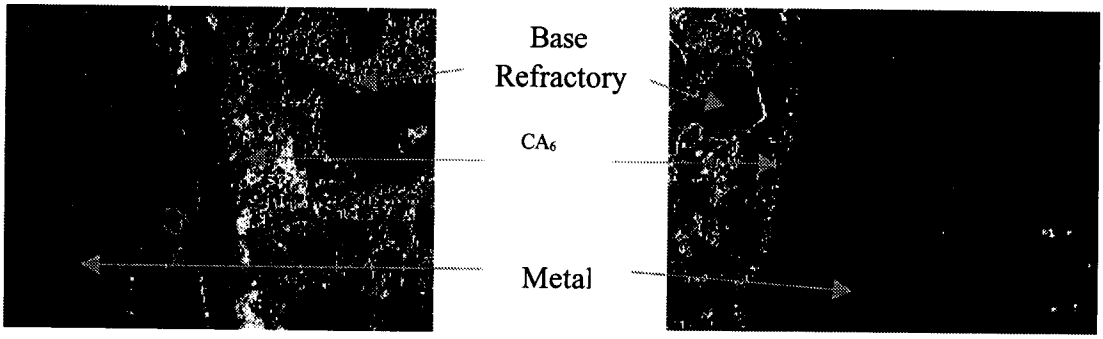

Figure 4: CL micrographs of steel (no additions)/refractory samples. (A) CL micrographs of 0.20C-steel/refractory sample, (B) CL micrographs of 0.003C-steel/refractory sample

Effect of Aluminum

Highly scattered alumina inclusions were found throughout the sample. The layer formed at the interface contains calcium aluminate (CA6) and spinel (MgO.Al2O3) along with alumina. This layer is greatly discontinuous in case of aluminum deoxidized-steel (0.01% Al) whereas it is continuous and is mostly on the metal side of the hot face in case of Al-killed steel (0.12% Al). See Figure 5.

Figure 5: CL micrographs of Al-killed steel/refractory crucible. (A) CL micrograph of aluminum deoxidized steel (0.01Al)/refractory crucible. (B) CL micrograph of aluminum killed steel (0.12Al)/ refractory crucible.

Effect of Holding Time

Holding time seems to have a significant effect on the nature of interfacial layer. Spinel, which is found in abundance in the samples held at temperature for 120 min was not found in samples

held for 60 min. It is also important note that the refractory is the only source of calcium and magnesium (0.2% calcia and 0.5% magnesia). See Figure 6.

Figure 6: CL micrograph of a sample held at a holding time of 60 min. CA_6 was found in the interface, no spinel was observed.

CONCLUSIONS

Preliminary experiments to understand the interaction between metal and refractory were conducted. The following are the current findings:
(1). Formation of CA_6 and alumina in the melt even when the steel sample did not have any aluminum suggests the formation of suboxide gases.
(2). Oxide inclusions in the metal were mainly alumina.
(3). CA_6 and spinel were found in the interface between metal and the refractory.
(4). Holding time seems to have a significant effect on the formation of spinels.

ACKNOWLEDGEMENTS

The authors wish to thank the American Iron and Steel Institute and the U.S. Department of Energy for their continual support for this research. We are also grateful to Mr. Jim Sanders, Rouge Steel and Dr. Penny Iwamasa, Timken Company for their help with the chemical analysis of the samples.

REFERENCES

1. Novozhilov, N.Yu; Khlynov, V.V; Kashcheev, I.D; Tsarevskii, B.V. " Selecting a Refractory Coating on the Basis of its Interaction with a Metal" *Refractories* Vol. 26. pp. 78-81 (1985)
2. Sasai; Mizukami. " Reaction Mechanism between Alumina Graphite Immersion Nozzle and Low Carbon Steel'. *ISIJ International* Vol. 34. pp. 802-809(1994)
3. Brabie Voicu. "A study on the mechanism of reaction between refractory materials and aluminum deoxidized molten steel" *Steel Research* Vol. 68 pp.54-60(1997)

4. Fukuda; Ueshima et al; " Mechanism of Alumina Deposition on Alumina Graphite Immersion Nozzle in Continuous Caster" *ISIJ International* Vol. 32 pp. 164-168 (1992).
5. Ogibayashi, S.; Uchimara,M et al. " Mechanism and Countermeasure of Alumina Buildup on Submerged Nozzle in Continuous Casting" *75th Steel Making Conference, Proceedings* pp. 304(1992)
6. Sasai; Mizukami; " Reoxidation Behavior of Molten Steel in Tundish" *ISIJ International* Vol. 40 pp. 40-47 (2000)
7. Smith, J.D; Peaslee, K.D et al. " Study of Continuous Casting Nozzle Clogging using Cathodoluminescence Microscopy". 38th Conference of Metallurgists and 29th Hydrometallurgical meeting of CIM, Quebec City, Quebec, Canada, August 23,1999
8. Yves; Bert et al." Prevention of Nozzle Clogging during the Continuous Casting of Al-killed Steels" *Steel Conference Proceedings (2000).*
9. Tsujino; Tanka et al. " Mechanism of Deposition of Inclusion and Metal in ZrO2- CaO-C Immersion Nozzle of Continuous Casting" *ISIJ International* (1994).
10. Gao; Sorimachi. " Formation of Clogging Materials in an Immersion Nozzle during Continuous Casting of Titanium Stabilized Stainless Steel" *ISIJ International* Vol. 33 pp. 291-297 (1993).

13.0 Appendix G: Study of Non-metallic Inclusions in Continuously Cast Steel Using Cathodoluminescence Microscopy

M. Karakus, J.D. Smith and K.D. Peaslee
University of Missouri-Rolla
Rolla, MO

Introduction

Non-metallic inclusions are inherent to wrought steel and are undesirable because they adversely affect the quality and fabrication of the formed steel. In this study, a microscopic technique called "Cathodoluminescence Microscopy" is used for rapid recognition and identification of macro- as well as micro-inclusions. This technique provides direct assessment of defects with little of the sample preparation required in other techniques.

Non-metallic Inclusions and Defects

An inclusion is defined as any solid non-metallic particle in the steel. The presence of these inclusions in formed steel is undesirable because they adversely affect not only the mechanical properties of the formed steel but also result in difficulties during manufacturing. Nonetheless, formation of inclusions is inherent to steel making processes and inclusions are present even in the cleanest, so-called inclusion free steel. In general, the amount and the type of non-metallic inclusions in steel has a direct impact on the following properties [1]:

1. Weldability
2. Fatigue
3. Finishing quality
4. Machinability
5. Fracture toughness
6. Corrosion

More specifically, the presence of non-metallic inclusion in final steel product can cause any of the following problems [2-11]:

1. Cracks and surface defects in automotive sheet steel
2. Reduced fatigue life of bearing steel products
3. Breakage in tire cord during drawing
4. Flange cracking in drawn and ironed cans
5. Corrosion pits and leakage in pipelines and storage vessel
6. Premature wear in tool steel
7. Hydrogen induced cracking and low temperature embrittlement
8. Nozzle clogging during casting

Careful control of inclusion composition, size, shape and distribution is of great importance during production of "clean steel." In clean steel, solute elements (P, S, N, O, and H) are kept at a minimum as they result in non-metallic inclusions. Desired level of solute element and non-metallic inclusion content as well as inclusion size for some steel applications are given in Table 1 [2].

Table 1. Solute elements (C, N, S) concentration, total oxygen content (T[O]), and inclusion size (D) for high purity and ultra clean steel application.

Product	Purity	Cleanliness
Automotive sheet steel	C<30 ppm N<100 ppm	T[O]<20 ppm D<100 μm
Drawn and ironed cans		T[O]<20 ppm D<20 μm
Lead frame for LSI	N<50 ppm	D<5 μm
Shadow mask for CRT		D<5 μm
Tire cord		D<20 μm
Ball bearings	[Ti]<15 ppm	T[O]<10 ppm D<15 μm
Line pipe	S<10 ppm	D<100 μm

Inclusion Nomenclature

Inclusions are commonly classified as either exogenous or indigenous. Exogenous inclusions are those derived from external sources such as entrained slag and dross particles, refractories and sand mold materials. They are commonly visible on the casting surface and they are easily identified. Indigenous inclusions are inherent in steel refining processes. They are formed within the system both from deoxidation and from reoxidation during casting. Originally, these inclusions are small (often sub-micron) but agglomeration results in inclusions larger than 10 microns. The most common indigenous inclusions include alumina (Al_2O_3), calcium aluminates, spinel ($MgAl_2O_4$), sulfides (MnS), phosphates (P_2O_5) and silicates. Nitrides (TiN) and are often observed in special steel grades.

Non-metallic inclusions are also divided into two general categories in formed steel: non-deformable and deformable inclusions. Deformable inclusions, for example MnS, are soft and deform into elongated inclusions in the direction of rolling. Most oxide inclusions are hard and non-deformable at rolling temperature. Wijk [1] has identified four types of inclusions in hot rolled steel:

1. Ductile inclusions: deform similar to steel matrix
2. Brittle inclusions: broken up into stringers during rolling
3. Brittle-ductile inclusions: consist of hard core and surrounded by deformable phase
4. Undeformed inclusions: forms fish-tail like cavities in steel matrix.

Alumina (Al_2O_3), calcium hexaluminate ($CaO \cdot 6Al_2O_3$) are brittle and undeformable at all working temperatures. Spinel ($MgAl_2O_4$) is known to be undeformable from room temperature to 1200°C. Silicate phases (silicates of Ca, Mn, Fe, and Al) are brittle at room temperature, but become deformable at higher temperatures. FeO (wustite), MnO and (FeMn)O exhibit plastic deformation at room temperature.

Origin and Sources of Inclusions

In general, sources for inclusion generation have been traced [2] to the following processes:

i) Deoxidation and reoxidation type inclusions
ii) slag entrainment inclusions
iii) erosion/corrosion of refractories

The main objective of inclusion identification is to determine the sources of inclusions so that countermeasures can be initiated. Microscopic analysis is an invaluable tool to trace the exact sources of inclusions in steel. Reflected light (RL), scanning electron microscopy with energy dispersive spectroscopy (SEM-EDS), electron microprobe (EPMA), transmission electron microscopy (TEM) as well as atomic force microscopy (AFM) and spectroscopic techniques such as optical emission spectroscopy (OES), x-ray fluorescence (XRF), low-energy electron induced x-ray spectroscopy (LEEIX), inductively coupled plasma (ICP) techniques, are used to characterize inclusions in steel. The intent of this paper is to introduce cathodoluminescence microscopy (CLM) for inclusion identification and attempt to trace the exact sources for inclusion generation.

Cathodoluminescence Microscopy

This technique combines the standard research grade petrographic Reflected Light (RL) microscope with Cathodoluminescence attachment. The latter consists of an electronic control unit, a cathode-ray type electron gun and a low vacuum chamber. An unfocused electron beam (flood) generated from the cold-cathode impinges on the surface of the polished/unpolished samples. As a result of reaction between electron beam and non-metallic inclusions, phases or minerals in inclusions produce characteristic cathode-luminescence colors. This physical phenomenon is known as cathodoluminescence (CL).

The CL process in minerals is mainly caused by trace amounts of impurities called activators. For example, transition metal ions, Mn^{2+}, Cr^{3+} and Fe^{3+} and practically all rare earth elements (REE), in particular, Eu^{2+}, Eu^{3+}, Sm^{3+}, Dy^{3+}, Tb^{3+}, are well known activators that results in CL colors in minerals under electron excitation. Few ions like Fe^{2+} produce poisoning affect in CL process. The CL color in minerals is also produced by crystal defects as well as by the intrinsic properties of crystals. The net outcome of CL color in minerals depends on the presence of activators, quenchers, and crystal defects. Cathodoluminescence spectroscopy is used to determine the type of activators as well as type of crystal defects.

The only serious disadvantage of this technique involves color separation (resolution) for complex inclusions (inclusions containing more than one phase), smaller than 20 μm. The

system uses objectives with long-working distances, required by the physical attributes of the vacuum, so the resulting resolution is low. In other words, only low magnification images can be obtained. Normally this is sufficient for identification of inclusions that are larger than about 10μm in diameter. Fortunately, micro-inclusions are very often single-phase inclusions that can be easily resolved.

This microscopic technique is a useful method of analysis before inclusions are subjected to SEM study. Many of the phases in these macro- and micro-inclusions produce similar back-scattered electron coefficients, for example alumina, spinel and CA_6. The steel back ground, on the other hand has extremely high back-scattered electron coefficient. This means that in relatively low magnification SEM images, compositional images would not result in differences between inclusions. Therefore, almost every inclusion has to be scanned and microprobed for positive identification. The CL images provide highly contrasted CL colors, for example red CL for alumina and green CL for spinel. Therefore, a CL study provides an excellent means for rapid phase recognition before, or in place of, an SEM study.

This technique has been successfully used to study undesirable oxide build-ups in channel induction furnaces [12], MgO-C slag line refractories in ladle, EAF and BOF [13], clogging in submerged entry nozzles for continuous casting [14], and refractories for EAFs in steel foundries [15].

In the following sections, the importance of the CLM technique for inclusion analysis is demonstrated in two case studies.

Case 1: Analysis of Surface Defects in Hot Rolled Strip

Two mounted and polished steel sections were studied by RL/CL microscopy to determine the nature of surface defects and to identify inclusions in the bulk of the steel specimens. Figure 1 shows the photograph of the surface defect. It shows an erupted lamination and blistering as well as brown rusting.

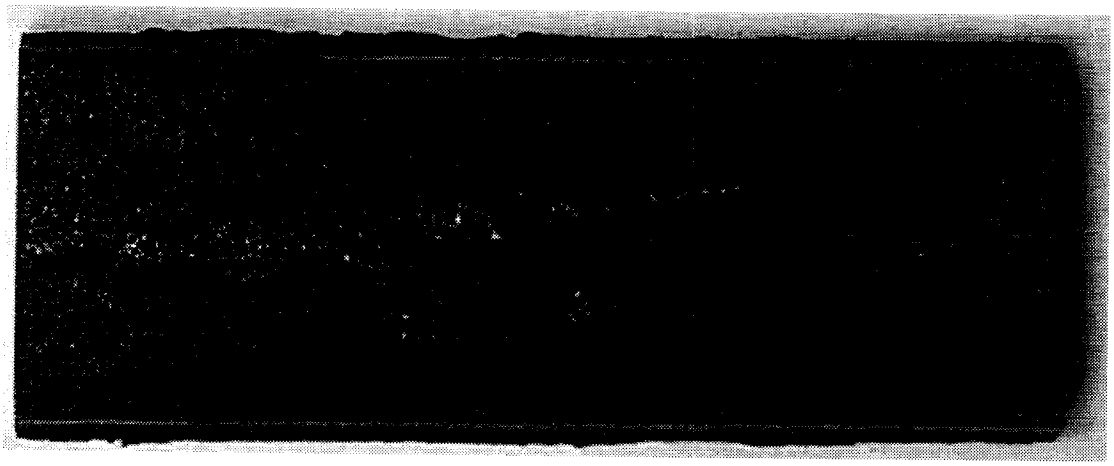

Figure 1. Surface defects showing white non-metallic inclusions, brown rust, laminations and blistering.

Figure 2 includes RL, CL and SEM micrographs for comparison at identical magnification. Under reflected light (Figure 2A) and scanning electron microscopy (Figure 2C), the surface defects appear as dark areas and little can be determined about the composition. The iron oxide scale observed on the surface in both images is dark but lighter than the embedded inclusion. Under cathodoluminescence, these dark areas or surface defects produced bright green color typical of spinel. These areas (defects) were confirmed to be spinel deposits based on chemistry using SEM-EDS analysis (see Figure 3A). The inclusions commonly showed spherical nature indicating that they were liquid during the steel solidification process. Intense green CL spherical inclusions in the bulk of the steel are identified as calcium aluminate based on their darker green color. SEM-EDS analysis of these inclusions verified the CL observation (see Figure 3B).

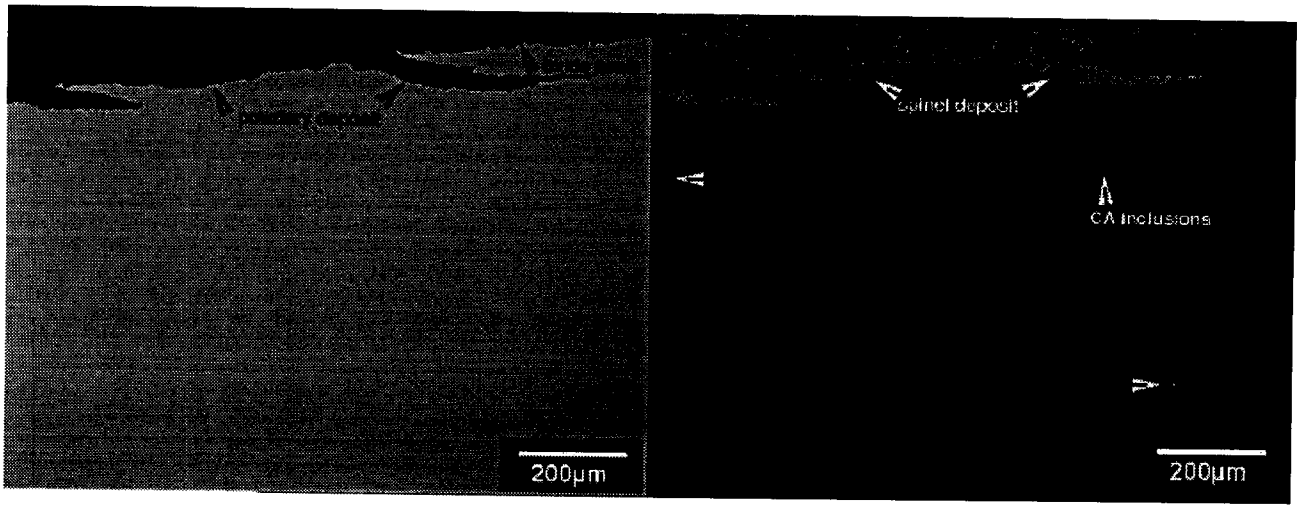

A) Reflected Light

B) Cathodoluminescence

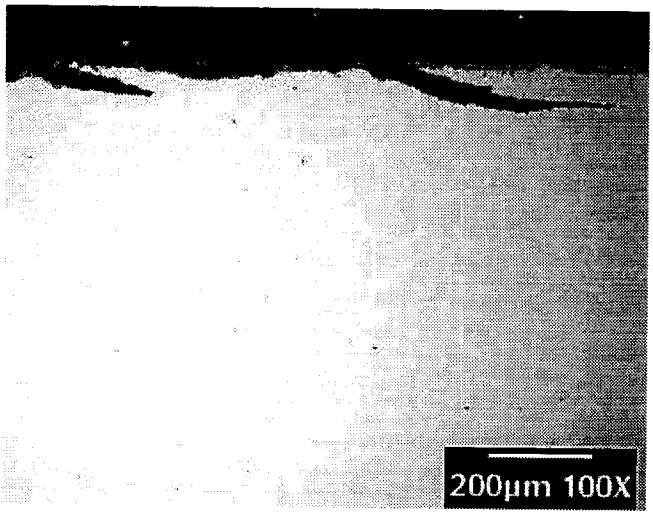

C) Scanning Electron

Figure 2. Spinel inclusions (deposit) associated with surface defect.

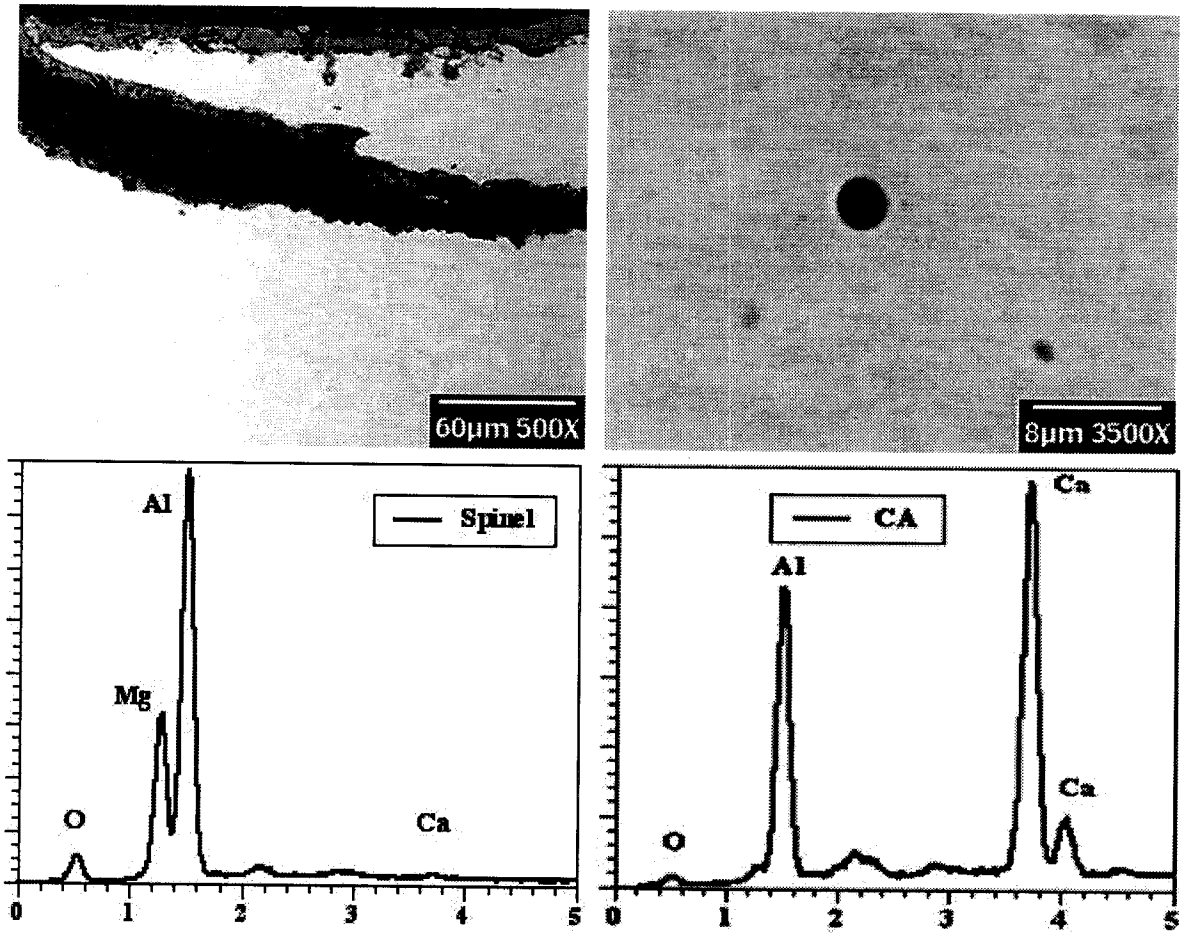

A) SEM/EDS for surface defect

B) SEM/EDS for internal inclusion

Figure 3. SEM-BSE images and EDS spectra for spinel surface deposit and spherical Ca-aluminate inclusion in the bulk steel.

Case 2: Analysis of Sub-surface Inclusions in Hot Rolled Strip

Two samples of zinc galvanized cold rolled strip containing "pencil pipe" type subsurface defects were analyzed to determine the mineralogy of the oxide inclusions. All photomicrographs for the samples are presented large to help resolve tiny inclusions. In these samples, the inclusions were predominantly alumina (red in CL, see Figure 4). A few spinel and calcium aluminate inclusions were observed. In the second sample, the inclusion was cuspidine, a calcium aluminum fluoro-silicate, most likely derived from mold flux (see Figure 5).

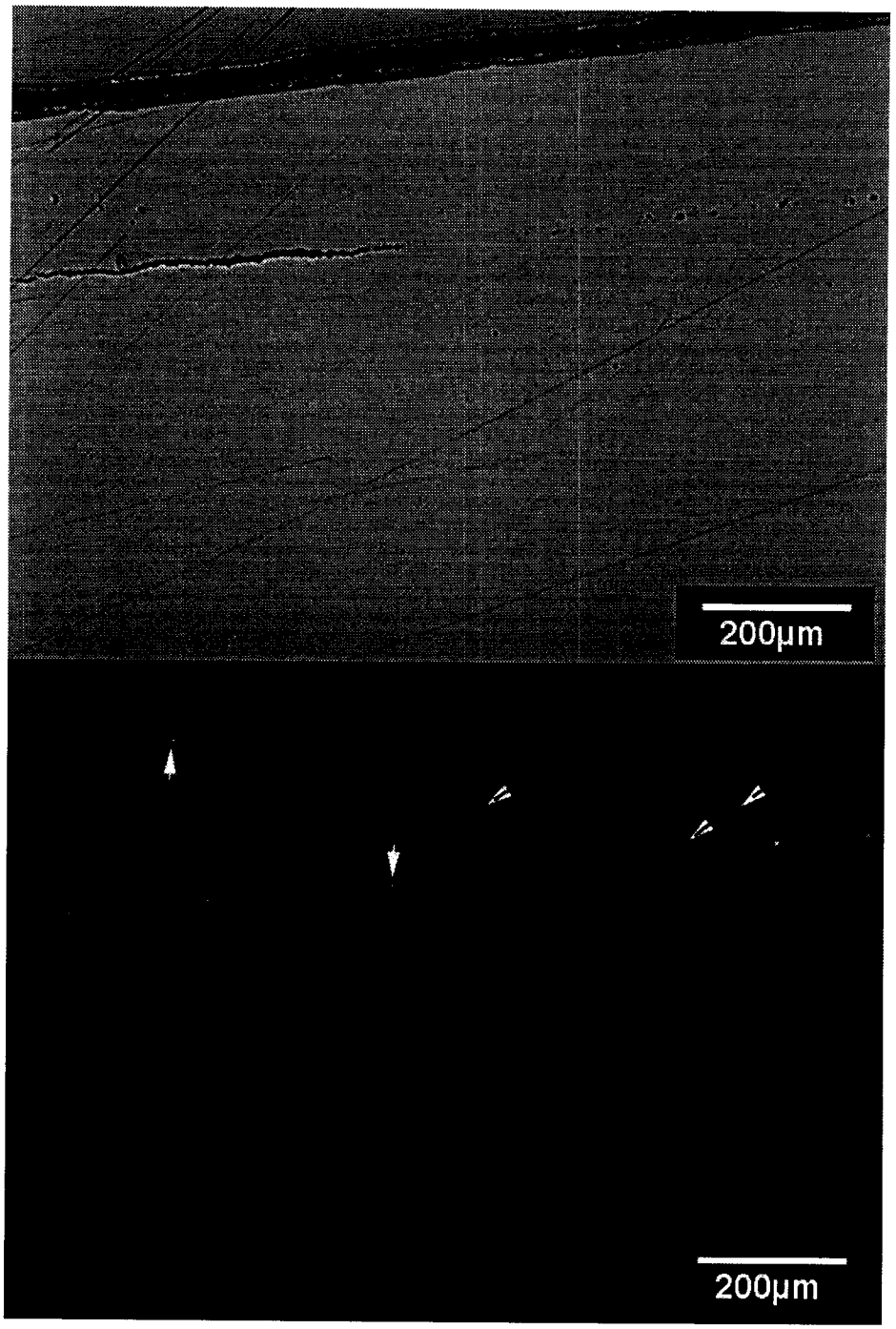

Figure 4. Alumina (red CL) is the main inclusion in the defect. However, there are a few calcium aluminate inclusions (green marked by arrow).

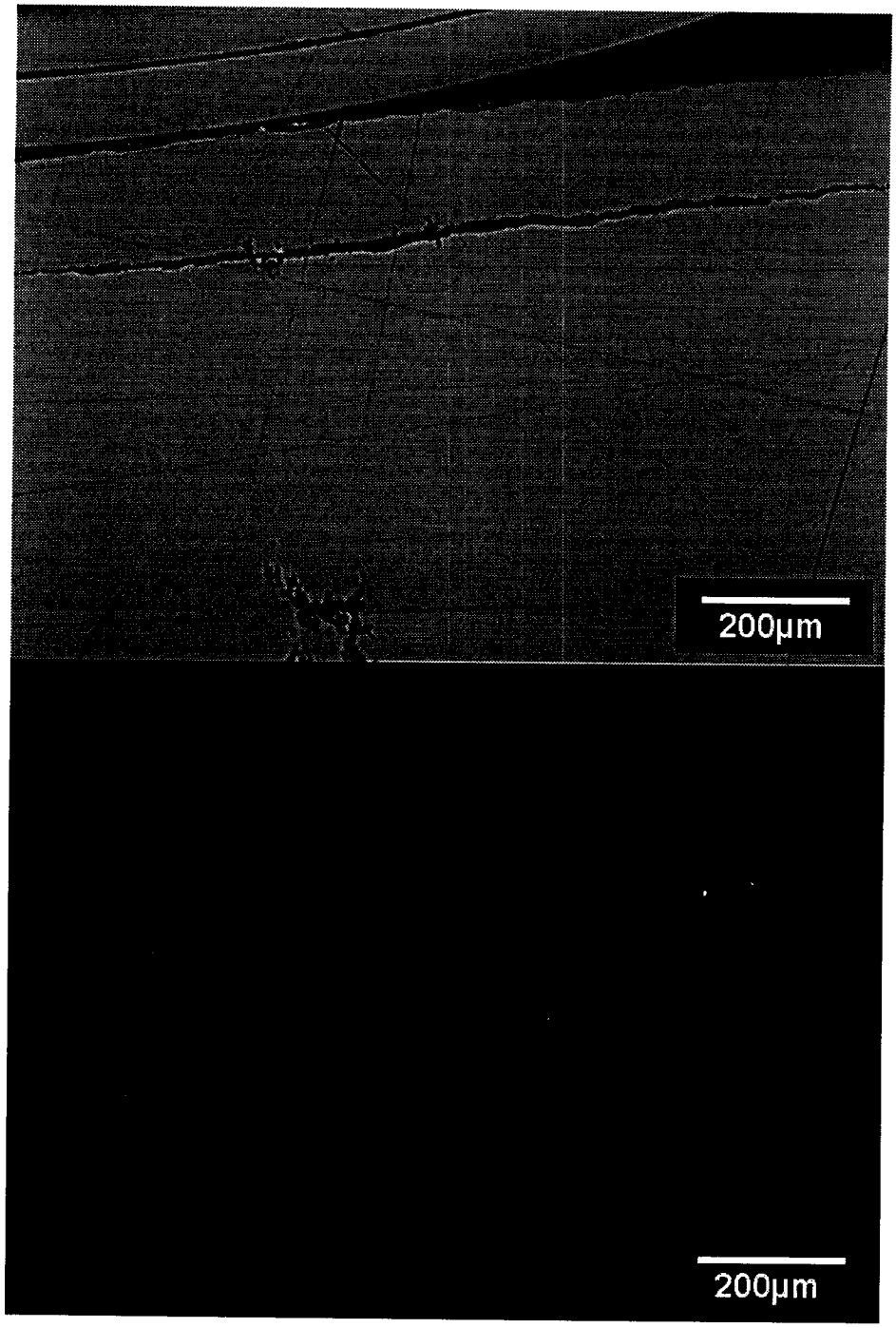

Figure 5. A mold flux defect, cuspidine: calcium aluminum flouro-silicate which appears dull pale yellow under CL.

Case 3: Analysis of Inclusions in Steel Samples from Degassing Ladle Treatment Operation

The images are of a steel chemistry sample taken at the degasser-ladle treatment facility. Large voids were visible on the surface of the sample. Microscopy indicated that the inclusions were alumina (red CL) with some spinel (bright green CL) or calcium magnesia-aluminates (more than 80 % alumina)as shown in Figures 6 and 7. These inclusions are closely associated with the voids suggesting gas (oxygen, argon and nitrogen) entrapment resulting in re-oxidation of the steel. Some inclusions revealed characteristic agglomeration to form complex and large inclusions. They always contain some TiO_2, MnO and FeO in their matrix also suggesting reoxidation.

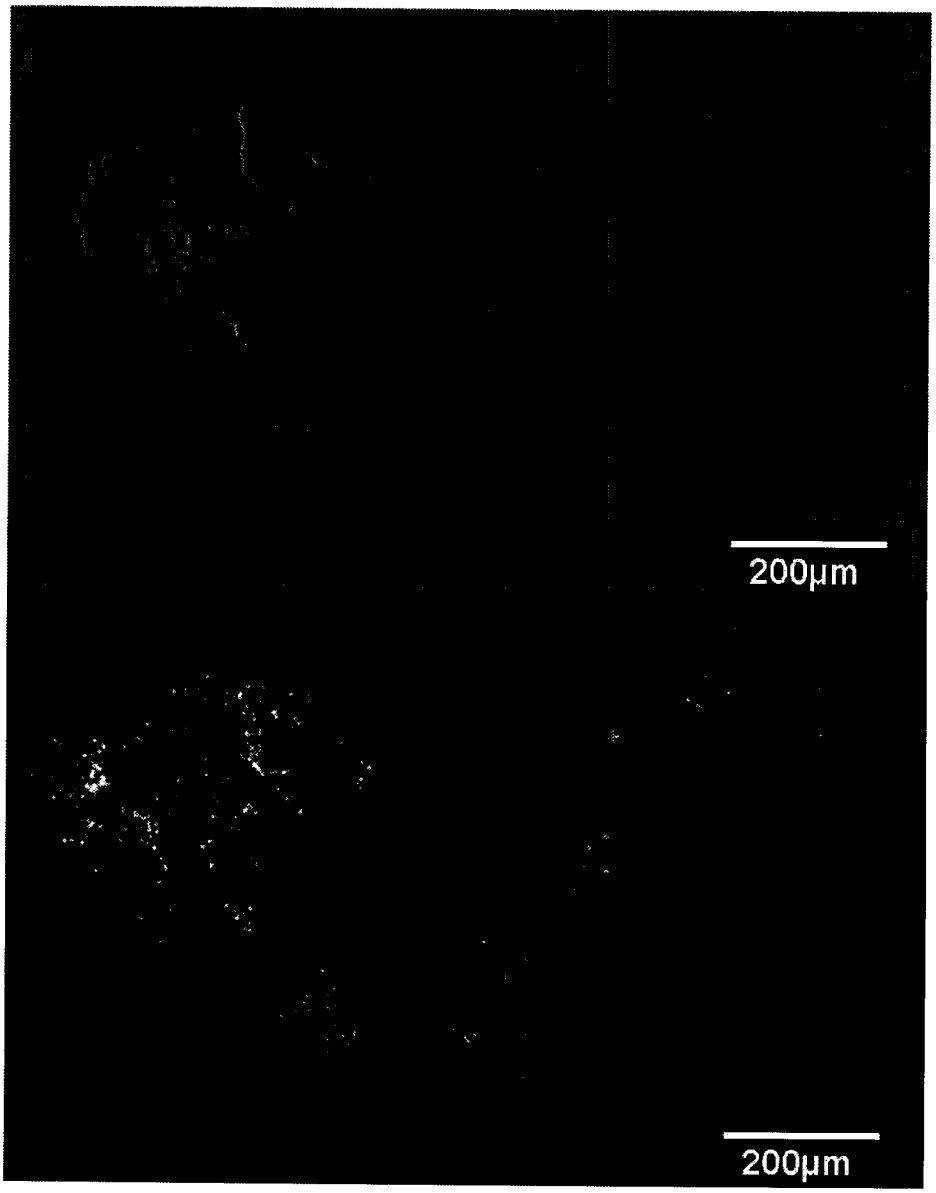

Figure 6. Oxide inclusions showing red CL alumina, bright green spinel and dark green calcium magnesia-aluminate inclusions.

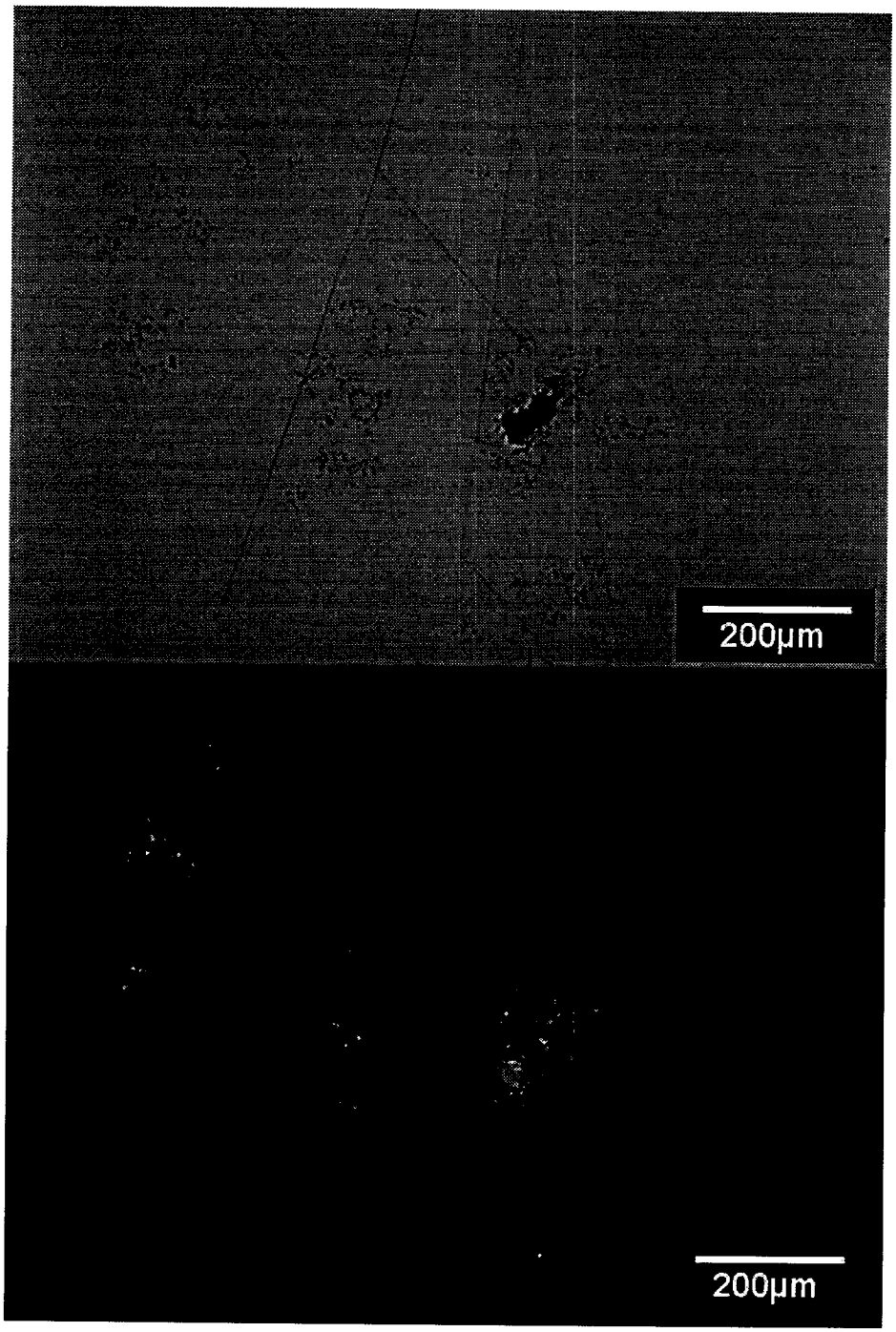

Figure 7. Inclusions in sample showing two bright green agglomerate of calcium aluminate or CA_6, red CL alumina and dark green, calcium magnesia-aluminate inclusions.

For comparison, SEM-SEIs and SEM-BSE microstructures of the same defects shown in the previous Figures are included as Figure 8. Although SEM provides superior spatial resolution of an inclusion, it is very difficult to see and determine the composition of inclusions in SEM images. Therefore almost every inclusion must be analyzed using EDS (see Figure 8E and 8F). The CL microstructures are clearly superior to SEM images in terms of rapid inclusion recognition and separation (alumina, spinel, Ca-aluminate, cuspidine or zirconia).

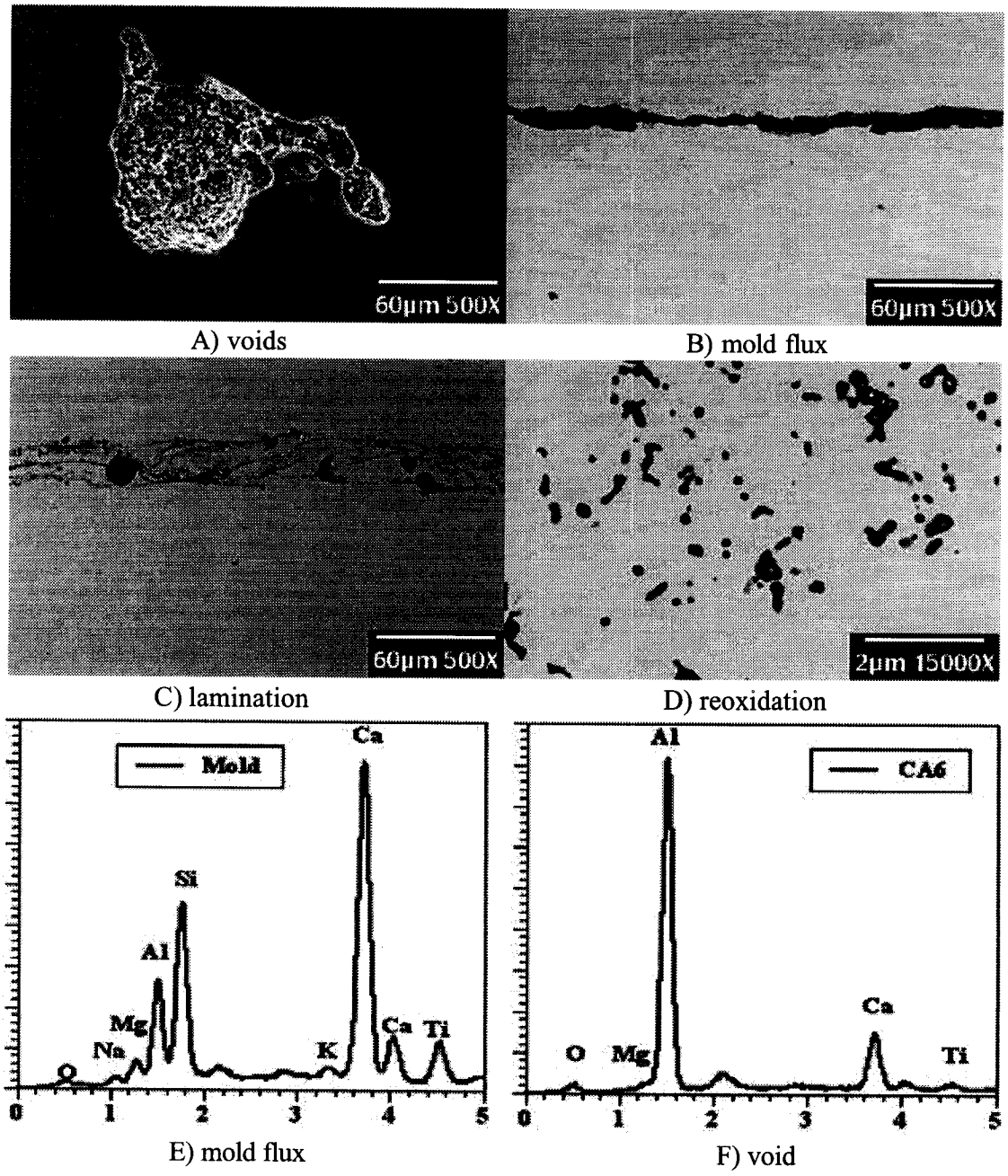

A) voids B) mold flux

C) lamination D) reoxidation

E) mold flux F) void

Figure 8. SEM photomicrographs (A-D) and EDS spectra (E-F) for selected inclusions.

Summary

The importance of the CL technique for defects and inclusion analysis in formed steel products was demonstrated for three case studies. The CL images have provided clear contrast among different inclusions that otherwise could not be obtained by optical and electron microscopy techniques. The CL technique is an invaluable method of inclusion and defect analysis not only for rapid recognition of inclusion but also trace the exact sources of these inclusions.

References

1. Wijk, O., Inclusion Engineering, pp. 35-67, (1995), Scanninject VII: 7th International Conference on Refining Processes 1995, Lulea, Sweeden.
2. Cramb, A.W., High Purity, Low Residual, and Clean Steels, pp. 49-89, (1998) in *Impurities in Engineering Materials,* C.L. Briant, editor, Marcel Dekker, New York.
3. McPherson, N. A. and McLean, A. (eds.), Continuous Casting, Volume 7: Non-Metallic Inclusions in Continuously Cast Steel, 313p, (1995), Iron and Steel Society, Warrendale, PA.
4. Tsai, H.T., Sammon, W.J., and Hazelton, D.E., Characterization and Countermeasures for Sliver Defects in Cold Rolled Products, Steelmaking Conference Proceedings, 1990, Vol. 73, pp. 49-59.
5. Emling, W.H., Waugaman, T.A., Feldbauer, S.L. and Cramb, A.W., Subsurface mold slag entrainment in ultra low carbon steels, Steelmaking Conference Proceedings, 1994, Vol. 77, pp. 371-379.
6. Knoepke, J., Hubbard, M., Kelly, J., Kittridge, R, and Lucas, J., Pencil blister reductions at Inland Steel Company, Steelmaking Conference Proceedings, 1994, Vol. 77, pp. 381-388.
7. Baker, H.D., Hallum, G.W., and Lawson, G.D., Reduction of pencil pipe defects at LTV Steels's Cleaveland works No. 1 continuous caster, Steelmaking Conference Proceedings, 1995, Vol. 78, pp. 613-618.
8. Su, J.L. and Lin, S.M., Surface defects improving of IF steel at China Steel Corporation, Steelmaking Conference Proceedings, 1997, Vol. 80, pp. 359-364.
9. Suito, H. and Inoue, R., Thermodynamics on control of inclusions composition in ultra clean steel, ISIJ International, 1996, **36** [5], pp. 528-536.
10. Fuchs, E. and Jonsson, P., Inclusion characteristics in bearing steel before and during ingot casting, High Temperature Materials and Processes, 2000, **19** [5], pp. 333-343.
11. vander Eijk, C. and Walmsley, J., Mechanisms of inclusion formation in low alloy steels deoxidized with titanium, Materials Science and Technology, 2000, **16** [2], pp. 55-64.
12. Karakus, M., Moore, R. E., and Hagni, R. D., Characterization of channel induction furnace build-ups, 1997, 26 p., in *Refractories for Foundries*, 33rd Annual Symposium on Refractories, St. Louis Section of The American Ceramic Society.
13. Karakus, M. Smith, J. D., and Moore, R. E., Cathodoluminescence mineralogy of used MgO-C bricks in basic oxygen furnaces, 2000, Veitsch-Radex Rundschau, No. 1, pp. 24-32.
14. Smith, J. D., Karakus, M., Peaslee, K. D., and Trueba, L., Study of continuous casting nozzle clogging using cathodoluminescence microscopy, 1999, pp. 187-200. in *Advances in Refractories for the Metallurgical Industries III*, C. Allaire and M. Rigoud (Eds).
15. Smith, J. D., Karakus, M. and Peaslee, K. D., "Post Mortem Analysis of Foundry EAF Refractories," Proc. of the 53rd Technical and Operating Conference, Steel Founders' Society of America, Chicago, IL, 1999.

14.0 Appendix H

Thermochemistry Of Steel-Refractory Interactions In Continuous Casting Nozzles

Sujatha Ramachandran

Kent D. Peaslee

Jeffrey D. Smith

Department of Metallurgical Engineering

University of Missouri-Rolla

ABSTRACT

Accretions on the inner wall of submerged entry nozzles (SENs) are affected by interactions between molten steel and refractory materials. Thermochemical reactions that qualitatively explain these interactions were modeled using FACT thermodynamic software. Predictions were compared to results from high temperature static experiments. Steels were melted in refractory crucibles to understand the interactions and establish the effect of refractory and steel composition on accretion formation. Steels, with and without aluminum, and various oxide refractories, with and without graphite, were evaluated. Samples were characterized using cathodoluminescence (CL) microscopy, reflected light (RL) microscopy and scanning electron microscopy (SEM). Both microscopy data and thermodynamic predictions indicated that graphite-containing refractories, especially magnesia-graphite and alumina-silica-graphite, resulted in the greatest degree of interaction with steels. All of the carbon-free and impurity-free materials resulted in significantly fewer interactions.

INTRODUCTION

Clogging of steelmaking nozzles has been a productivity and quality problem facing the steel industry for many years. Clogging is affected by a number of factors including oxide precipitation and deposition, steel chemistry, cleanliness, air aspiration through the refractory and refractory/steel interactions.

Several researchers[1-12] investigated clogging through characterization of used nozzles. These studies have provided a better understanding of clogging, but a number of fundamental questions regarding the basic steel/refractory interactions and underlying reaction mechanisms remain unanswered.

One of the earliest works by Hauck et al.[13] proposed that Al_2O gas evolving as a product during the reduction of alumina refractory by carbon in nozzle is the source of alumina deposits at the refractory/steel interface. Strelov et al.[14] emphasized the significance of oxygen transport between molten steel and the oxides within the refractories. The work also postulated the presence of a gas phase in equilibrium with the refractory due to the dissociation of the oxides at high temperature according to the general equation:

$$2MO_{(s)} = 2M_{(g)} + O_{2(g)} \quad \text{.....(1)}$$

Fukuda et al.[3] conducted an immersion test to understand the mechanism of network alumina formation. In the experiment, an alumina graphite rod was immersed in an aluminum-killed steel melt and held at 1873K for 4 hours. A thin layer of alumina formed and deposited on the surface of the alumina graphite rod in contact with the steel melt. They suggested that the alumina in the alumina graphite rod is reduced by graphite in the refractory to suboxide gas, and the suboxide gas diffuses to the contact interface with molten steel and is reoxidized to form alumina. They proposed that this reaction is accelerated by the presence of silica in the refractory and the dense network of alumina formed on the surface of the refractory served as a site for deposition of suspended inclusions in the steel melt. Sasai et al.[1,5] conducted experiments that also supported this hypothesis.

Ogibayashi and colleagues[4] examined used industrial SENs and observed network alumina on the nozzle side of the interface and cluster-containing metal and chalky alumina on the molten steel side, as shown in Figure 1. They believed that network alumina was formed when silica in the refractory was reduced to SiO gas by graphite in

the nozzle. The SiO gas formed would then react with aluminum in molten steel to form alumina and silicon as described in the following reactions:

$SiO_{2(s)} + C_{(s)} = SiO_{(g)} + CO_{(g)}$ [within refractory] .....(2)

$3SiO_{(g)} + 2\underline{Al} = Al_2O_{3(s)} + 3\underline{Si}$ [steel/refractory interface] .....(3)

$3CO_{(g)} + 2\underline{Al} = Al_2O_{3(s)} + 3\underline{C}$ [steel/refractory interface] .....(4)

$3SiO_{2(s)} + 3C_{(s)} + 4\underline{Al} = 2Al_2O_{3(s)} + 3\underline{Si} + 3\underline{C}$ [Overall] .....(5)

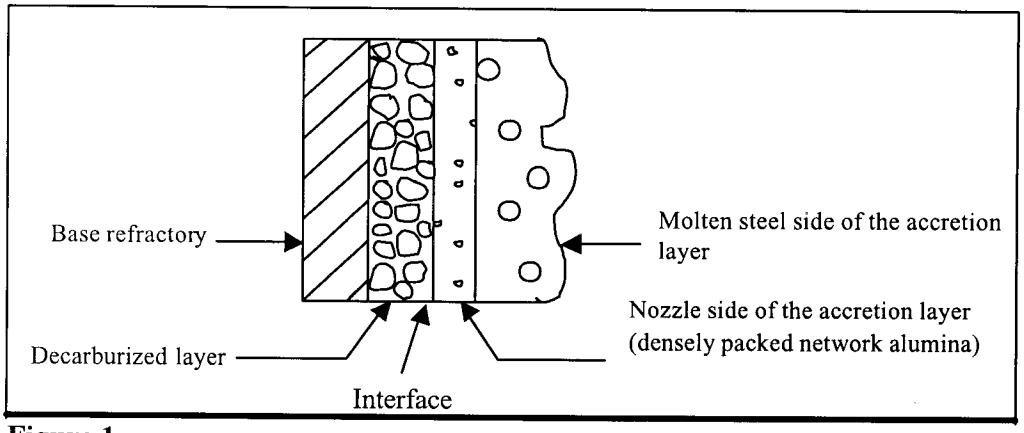

Figure 1
Schematic of accretion morphology on industrial SENs.

Tsujino et al.[11] investigated the conditions necessary for alumina deposition on a ZrO_2-CaO-C refractory and compared it to a similar deposition on a Al_2O_3-C refractory using rotating-immersion tests. In these tests, a refractory sample was immersed in a steel melt and rotated at 100 rpm for 15 sec to 30 min. They proposed that deposition on the nozzle proceeded in two steps. First, a fine oxide layer (the network alumina) was formed shortly after immersion at the hot face of the refractory due to reaction between molten steel and the refractory. Second, non-metallic inclusions were deposited onto the fine oxide layer.

Poirier et al.[12] focused on the influence of refractory composition on alumina accretions. This study described the mechanism of alumina accretion because of the

thermochemical reduction of nozzle constituents coupled with oxidation of aluminum in the steel. This study presented a three-step mechanism:

1) Formation of a decarburized zone within the refractory due to reaction of the refractory oxides with graphite.

2) Surface deposition of alumina and a vitreous phase due to reduction of the refractory alumina and impurities such as SiO_2, Na_2O, and K_2O by graphite. The reduction reactions generate gaseous species according to reaction (1), which migrate to the interface, reoxidize and condense to form the deposit.

3) Alumina accretion growth from oxidation of aluminum in steel by carbon monoxide.

This indicated that carbon in the refractory might be responsible for the deposition of alumina at the refractory/steel interface and that removal of carbon could eliminate the accretion.

Brabie[15] studied the possibility of carbon monoxide absorption and precipitation of inclusions in molten steel, when aluminum deoxidized molten steel was held in contact with a carbon monoxide atmosphere. Experiments were conducted in which droplets of aluminum-deoxidized steel were levitated in different CO-He atmospheres. The droplets were found to have a thin film of alumina after the experiments. At lower aluminum contents, the film formed a dense shell preventing further absorption of carbon monoxide. However, at higher aluminum contents the film was easily detached and entrapped into molten steel as oxide inclusions.

Brabie[2] also studied the mechanism of reaction between refractory materials and aluminum deoxidized molten steel by static experiments in which steel was melted in MgO-C crucibles cut from a commercial brick. The buildup at the refractory/steel interface consisted of MgO and/or $MgO{\cdot}Al_2O_3$, which was attributed to reaction between magnesium vapor and the carbon monoxide generated from the reduction of magnesia by carbon in the crucible walls. The oxide inclusions in the steel were mainly magnesia or alumina or a mixture of both. These studies showed that static experiments could produce accretions similar to those observed in industrial nozzles.

Recent works by Holler[7] and Yves et al.[10] also confirmed that the first reaction layer, depicted as the nozzle side of the accretion layer in Figure 1, formed due to the reduction reaction within the refractory. Holler's work explored the application of a ceramic (carbon-free) coatings and linings for submerged nozzles to reduce accretions. Yves et al. [10] attempted to plasma coat alumina onto an alumina-graphite refractory and showed that the technique has anti-clogging potential. This idea was proposed earlier by Benson et al.[16] who performed thermochemical analyses to calculate the limiting equilibrium that occur in carbon bonded refractories. Benson et al. proposed that carbon monoxide gas affects alumina formation in aluminum-killed steel and indicated that a carbon-free liner would help in the prevention of alumina buildup.

Although some fundamental studies were performed in the previous works cited, more needs to be done to understand the role of refractory components and the associated thermochemical reactions as well as the nature of refractory/steel interactions. This paper analyzes the effects of refractory and steel composition on accretion formation using results from thermodynamic modeling and static experiments. The thermodynamic

analysis utilized FACT (Facility for the Analysis of Chemical Thermodynamics) which is a fully integrated thermochemical database computing system. A program called *Equilib* that incorporates the thermochemical functions of *ChemSage* was used to perform Gibb's free energy minimization calculations. Static experiments were conducted using a variety of common refractories fabricated with controlled additives, which were then tested for their interactions with molten steel. Samples from the experiments were characterized using cathodoluminescence microscopy (CL), reflected light microscopy (RL) and scanning electron microscopy (SEM). Post-mortem results were compared to the thermodynamic model predictions.

THERMODYNAMIC ANALYSIS

Reviewing the thermodynamic aspects of molten steel/refractory nozzle interactions is an important step in understanding nozzle clogging. This study provides a comprehensive review of the prevailing thermodynamic predictions for standard nozzle systems used in the continuous casting of ultra-low carbon aluminum-killed (ULC-AK) steels. Oxide refractory systems in this study include graphite-free and graphite-containing alumina, magnesia and zirconia.

Each refractory system was studied with FACT using two modules, a refractory module and a steel module as illustrated in Figure 2. In the first module, one total mole of refractory components was combined with 0.1 moles of argon and allowed to reach thermodynamic equilibrium at the reaction temperature. The resulting gas phase was transported to the second module to react with ten moles of ultra-low carbon steel (either with or without aluminum). This ratio was based on the static accretion experiments in which the molar ratio between the steel and the refractory reaction layer at the interface was 10:1.

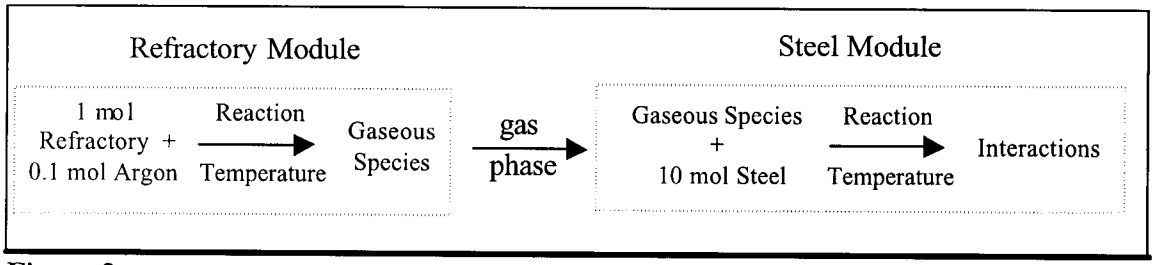

Figure 2
Overview of the general inputs for thermodynamic analysis using FACT.

It was assumed that the steel would not migrate into the refractory and would therefore not influence the prevailing internal reactions. This is a safe assumption based on results from post-mortem characterization of industrial nozzles[8] that showed essentially no penetration of steel or migration of steel components into the refractory. However, the static experiments showed some steel penetration due to isothermal conditions.

Internal Refractory Reactions

In the refractory systems studied, all possible species were considered in the calculations but many are not included in the figures when the resulting concentration was insignificant. This convention was included to prevent unnecessary confusion in the more complex systems. The cutoff for significant concentration was arbitrarily defined as 10^{-12} atm for the simple oxide systems and 10^{-6} atm for the more complex systems.

Carbon-free Systems

Al-O - The first system considered was alumina, historically the most widely used refractory oxide in the fabrication of steelmaking nozzles. One mole of pure alumina and 0.1 moles of argon (added to insure that there was always a gas phase) were allowed to come to equilibrium at 1550-1650°C (2882-3002°F). Gaseous species included in the equilibrium calculations were Al, AlO, Al_2O, Al_2O_2, AlO_2, Al_2, O, O_2, O_3, and Ar. Only

species present with partial pressures greater than 10^{-12} atm were considered significant and plotted. The data presented in Figure 3 indicate that an alumina refractory will dissociate to a minor degree at steelmaking temperatures and form a small amount of $AlO_{(g)}$ and $Al_{(g)}$ as described in the following reactions:

$$Al_2O_{3(s)} = 2Al_{(g)} + 3O_{(g)} \quad .....(6)$$

$$Al_2O_{3(s)} = 2AlO_{(g)} + O_{(g)} \quad .....(7)$$

Although thermodynamic calculations are independent of path (reaction sequence), the most likely reactions have been included to simplify further discussion.

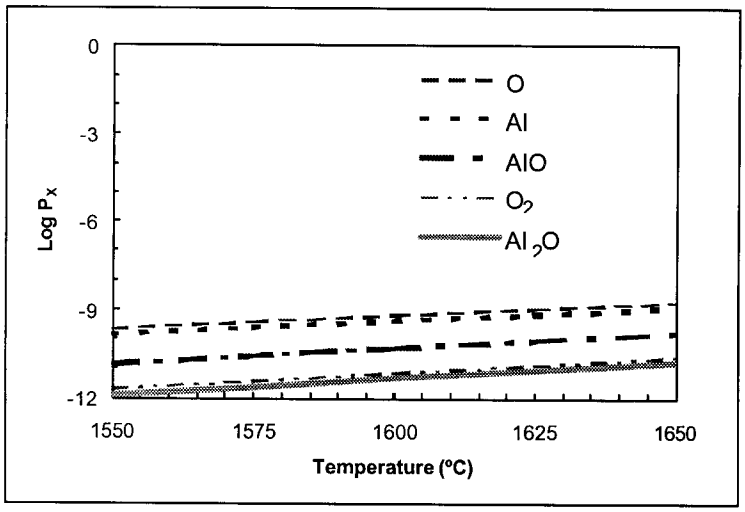

Figure 3
Generation of gaseous species in the Al-O system

Mg-O - In a similar way to the Al-O system, one mole of MgO was reacted with 0.1 mole of argon and allowed to reach equilibrium. Gaseous species considered were Mg, Mg_2, MgO, O, O_2, O_3, and Ar. The predominant gaseous species were found to be $Mg_{(g)}$ and $MgO_{(g)}$ as shown in Figure 4. Note that the partial pressures, although still

quite low, are considerably higher (nearly three orders of magnitude) than in the Al-O system. The reactions that describe the formation of these gaseous species are follows.

$MgO_{(s)} = Mg_{(g)} + 1/2O_{2(g)}$ .....(8)

$MgO_{(s)} = MgO_{(g)}$ .....(9)

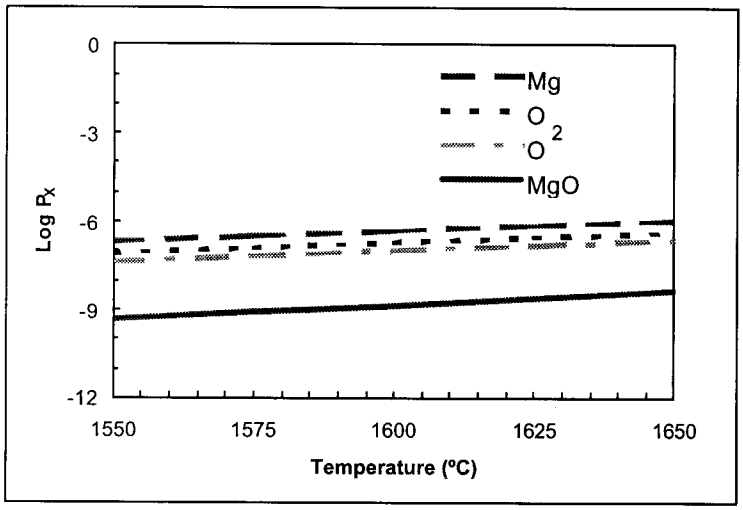

Figure 4
Evolution of gaseous species in the Mg-O system

Zr-O - In the zirconia system, the species considered were Zr, ZrO, ZrO_2, O, O_2, O_3, and Ar. The predominant vapor species were $ZrO_{(g)}$ and $ZrO_{2(g)}$ (see Figure 5), although neither is present in as high a concentration as the vapor species in either the Al-O or Mg-O system. Reactions that describe the formation of the Zr-containing gaseous species follow:

$ZrO_{2(s)} = ZrO_{(g)} + O_{(g)}$ .....(10)

$ZrO_{2(s)} = ZrO_{2(g)}$ .....(11)

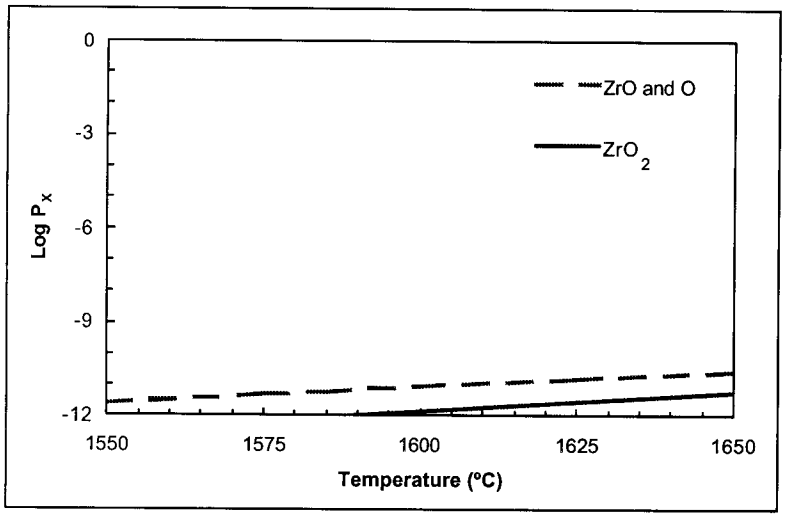

Figure 5
Evolution of gaseous species in the Zr-O system

Carbon-containing Systems

The addition of carbon to the oxide systems results in several carbon containing vapor species (C, C_2, C_3, C_4, C_5, C_2O, C_3O_2, CO, and CO_2) being considered with the gaseous species previously discussed for each refractory system. Only species present in significant concentrations ($P_x > 10^{-6}$ atm) were included in the Figures.

Al-O-C - The addition of carbon (20 wt.%) to the Al-O system yields considerably higher partial pressures of the gaseous species as shown in Figure 6. The two predominant Al-containing vapor species are $Al_2O_{(g)}$ and $Al_{(g)}$ as opposed to $AlO_{(g)}$ and $Al_{(g)}$ in the system without carbon (refer to Figure 3). The concentration of the species shown in Figure 6 are also considerably greater than was the case without carbon and a high concentration of $CO_{(g)}$ is also present. The reactions that would lead to the formation of the observed species are as follows:

$$Al_2O_{3(s)} + 2C_{(s)} = Al_2O_{(g)} + 2CO_{(g)} \quad .....(12)$$

$$Al_2O_{3(s)} + 3C_{(s)} = 2Al_{(g)} + 3CO_{(g)} \quad .....(13)$$

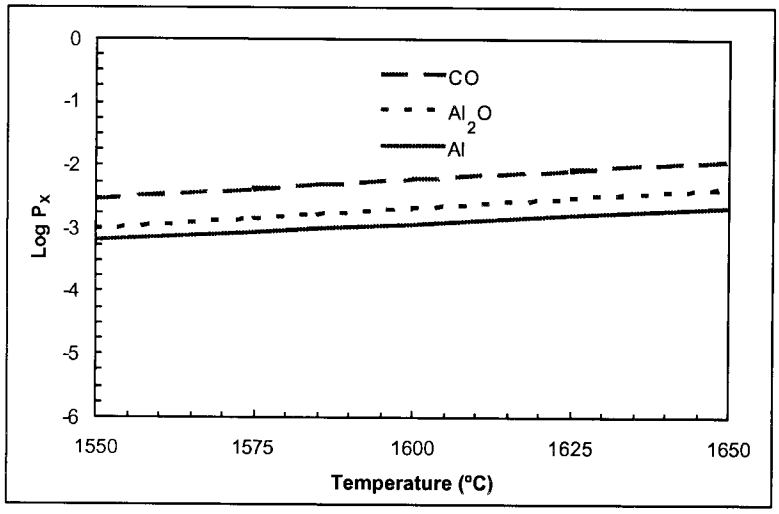

Figure 6
Evolution of gaseous species in the Al-O-C system

Mg-O-C – The addition of 10 wt.% carbon to the Mg-O system leads to the formation of an equal amounts of $Mg_{(g)}$ and $CO_{(g)}$ and therefore both are represented by the same line in the Figure 7. This is because the magnesia reduction reaction produces equal moles of the products:

$$MgO_{(s)} + C_{(s)} = Mg_{(g)} + CO_{(g)} \quad \text{.....(14)}$$

The degree of instability of magnesia and graphite at steelmaking temperatures is apparent from Figure 7, as the partial pressure of each of the two species formed is nearly 0.1 atm.

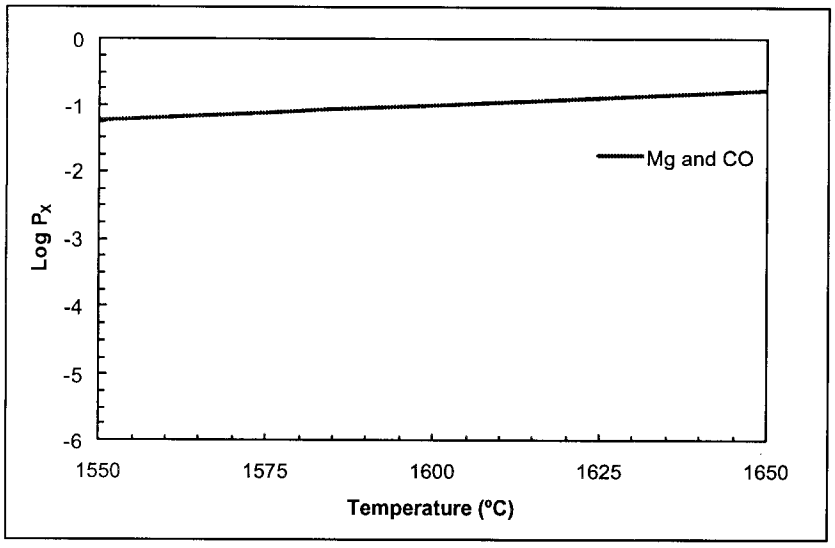

Figure 7
Evolution of gaseous species in Mg-O-C system

Zr-O-C - The addition of 10 wt.% carbon to the zirconia system results in a predominant vapor species of $CO_{(g)}$ with lower concentrations of $Zr_{(g)}$ and $ZrO_{(g)}$ as shown in Figure 8. The addition of carbon to this system resulted in a similar increase in vapor pressure over the carbon-free case, as was observed in the Al-O and Mg-O systems. However, the partial pressures observed in the Zr-O-C system were atleast three orders of magnitude lower than any other carbon containing system. This would make it a good carbon-containing candidate to prevent accretion formation. Formation of these species is described by the following reactions.

$$ZrO_{2(s)} + C_{(s)} = ZrO_{(g)} + CO_{(g)} \quad .....(15)$$

$$ZrO_{2(s)} + 2C_{(s)} = Zr_{(g)} + 2CO_{(g)} \quad .....(16)$$

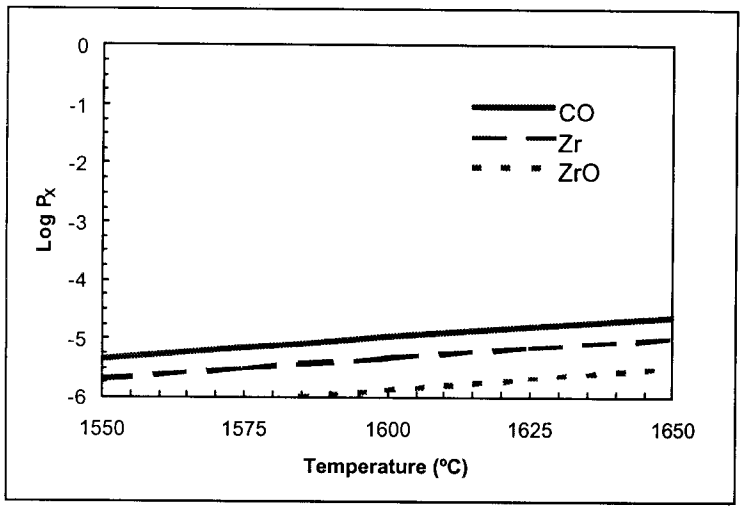

Figure 8
Evolution of gaseous species in the Zr-O-C system

Al-O-C-Si - Most alumina-graphite nozzles contain a significant (up to 10 wt.%) amount of silica, either as an impurity phase or as an addition in the form of SiC or SiO_2. When silica is present (10 wt.%) with 70 wt.% alumina and 20 wt.% carbon, the predominant gaseous species are $SiO_{(g)}$ and $CO_{(g)}$ as shown in Figure 9, even though the system contains considerably more alumina than silica. The reactions that describe the formation of $SiO_{(g)}$ and $Si_{(g)}$ are as follows:

$$SiO_{2(s)} + C_{(s)} = SiO_{(g)} + CO_{(g)} \quad \text{....(17)}$$

$$SiO_{2(s)} + 2C_{(s)} = Si_{(g)} + 2CO_{(g)} \quad \text{.....(18)}$$

The formation of $Al_{(g)}$ likely follows the reaction described in (13).

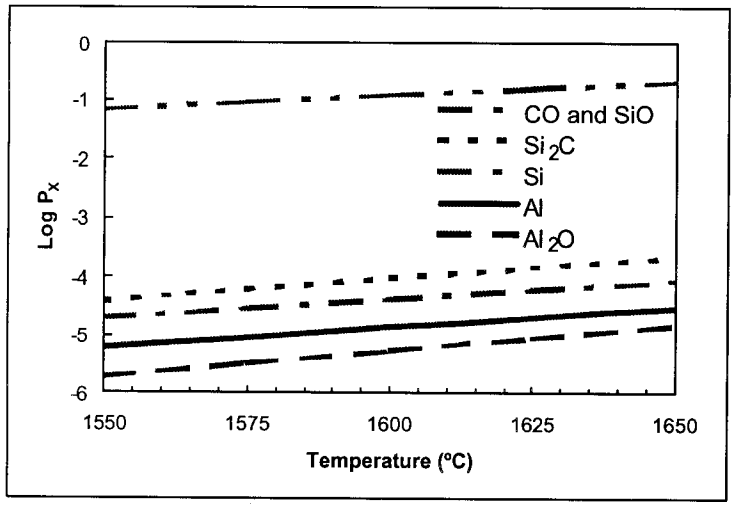

Figure 9
Evolution of gaseous species in the Al -O-C-Si system

Refractory/Steel Interactions

The previous section discussed the products of the refractory module (refer to Figure 2). To determine the magnitude of refractory/steel interactions, the gaseous species generated within one mole of refractory were transported to the steel module and reacted with ten moles of steel. Two steels were considered, ULC with no aluminum (350-400 ppm O content based on temperature) and ULC-AK with 0.12% aluminum (3-5 ppm O content based on temperature). These two steels represent the extremes of typical ULC steels, high oxygen (no aluminum or other appreciable deoxidants) and high aluminum (low oxygen).

Each of the carbon-free refractories (Al_2O_3, MgO, and ZrO_2) resulted in insignificant reaction products when the gases evolved in their respective refractory modules were equilibrated with either of the steels. The following discussion concentrates on carbon-containing systems which were far more reactive.

The interactions between alumina-graphite refractories and ULC/ULC-AK steels were pronounced, with significant solid alumina formation as shown in Figure 10. For the AK steel shown in the figure, the formation of $Al_2O_{3(s)}$ can proceed by the following reactions, recalling that the predominate gaseous species for an alumina-graphite refractory were $CO_{(g)}$, $Al_2O_{(g)}$ and $Al_{(g)}$:

$$Al_2O_{(g)} + 2CO_{(g)} = Al_2O_{3(s)} + 2\underline{C} \quad .....(19)$$

$$2Al_{(g)} + 3CO_{(g)} = Al_2O_{3(s)} + 3\underline{C} \quad .....(20)$$

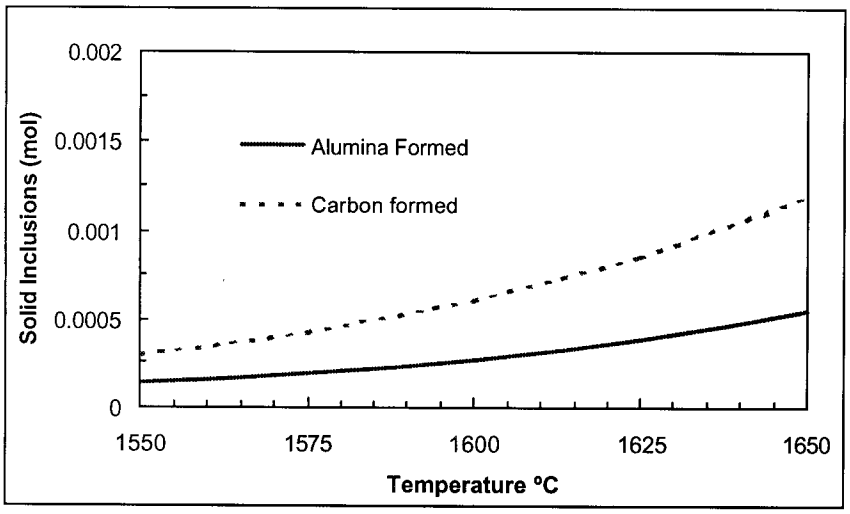

Figure 10
Amount of alumina formed and the increase of carbon in ULC-AK steel by interaction with gaseous species formed with in an alumina-graphite refractory.

It should be noted that alumina is formed from the oxidation of aluminum containing vapors species by CO. Without external sources of oxygen, all alumina formation reactions result in the carbon increasing in AK steel. The reaction of the gaseous species and unkilled steel yields almost exactly the same amount of alumina. However, there is no carbon increase because alumina is formed by the reaction with the dissolved oxygen in the steel:

$$Al_2O_{(g)} + 2\underline{O} = Al_2O_{3(s)} \quad .....(21)$$

$$2Al_{(g)} + 3\underline{O} = Al_2O_{3(s)} \quad \text{.....(22)}$$

The data indicate that the amount of alumina formed increases by more than a factor of three over the 100°C temperature range considered. This increase in alumina is directly related to the gaseous species formed in the refractory. Increases in casting temperatures have long been thought to be one way of decreasing nozzle accretions. If refractory interactions play a significant role in nozzle clogging, thermodynamics indicate the opposite effect might be true with increased temperatures resulting in more alumina available for accretions.

A similar procedure was completed for all of the refractory systems considered. Instead of plotting each system separately, the moles of inclusions were compared for the Al-O-C, Mg-O-C, and Al-O-C-Si systems for ULC-AK steels in Figure 11. Note that the moles plotted on this figure are based on the moles of base refractory and not moles of inclusion, (e.g. one mole of mullite - is plotted as five moles of base refractory since it consists of three moles alumina and two moles of silica).

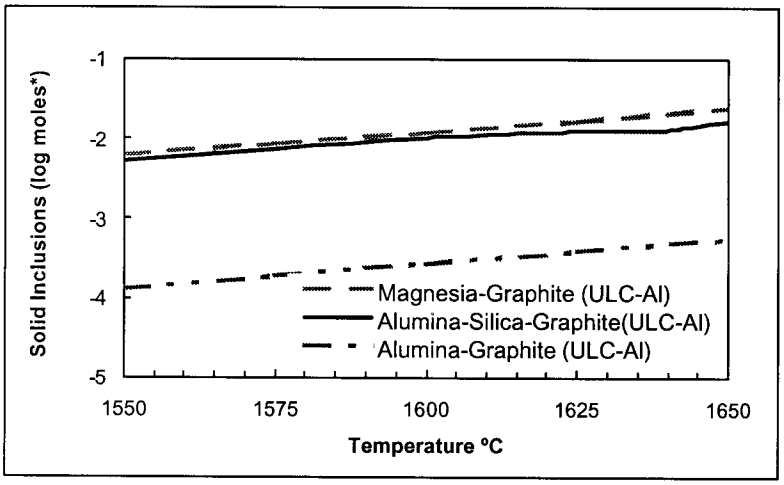

Figure 11
Solid inclusions in ULC-AK steel based on refractory type. Magnesia-graphite (mainly magnesia with some spinel inclusions); alumina-silica-graphite (alumina inclusions with significant mullite at high temperature. Note the slope change at 1640°C); and alumina-graphite (alumina inclusions).

One important refractory system not shown in Figure 11 is the zirconia-carbon system, which yielded no solid inclusions in the thermodynamic analysis. This is important because of the large effect carbon had on the other systems (magnesia, alumina, and silica). Zirconia-carbon nozzles would be expected to be an excellent choice for nozzles that would resist accretion formation.

The highest amounts of solid inclusions were predicted to form when ULC-AK steel interacts with magnesia-graphite refractory or alumina-silica-graphite refractories refractories. Although not shown in the graph , ULC unkilled steels resulted in slightly higher amounts of soild inclusions due to the higher dissolved oxygen content. Silica additions to alumina-graphite refractories not only increased the volume of solid inclusion but also the dissolved silicon content of the steel as shown in Figure 12. The formation of alumina and dissolved silicon is described by the following reactions:

$$3SiO_{(g)} + 2\underline{Al} = Al_2O_{3(s)} + 3\underline{Si} \quad .....(23)$$

$$3CO_{(g)} + 2\underline{Al} = Al_2O_{3(s)} + 3\underline{C} \quad .....(24)$$

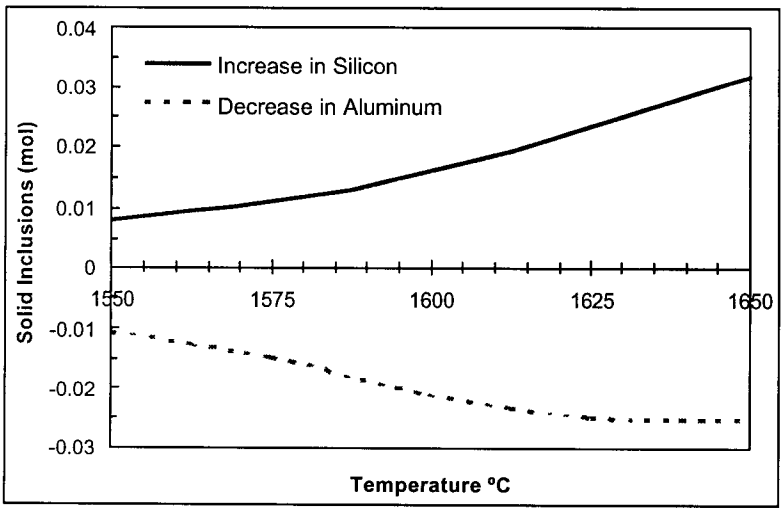

Figure 12
Aluminum and silicon changes in ULC-AK with alumina-graphite-silica refractories. Note the change in the Al slope at high temperatures due to mullite formation.

EXPERIMENTAL VERIFICATION

Experimental Procedure

Oxide refractory materials were fabricated by mixing appropriate combinations of reagent grade powders according to Table I and pressing them in an isostatic press at approximately 350 MPa. The resulting compact was fired at approximately 1600°C (2912°F) for six hours or 225°C (437°F) for 8 hours when graphite-containing. Upon cooling, holes of 0.64 cm (¼") diameter and 2.54 (1") depth were machined into the surface of the refractory to allow multiple steel chemistries to be tested with each refractory composition.

Table I: Refractory Compositions (wt%)

Refractory	Al_2O_3	C	SiO_2	MgO	ZrO_2
Al_2O_3	100	-	-	-	-
MgO	-	-	-	100	-
ZrO_2	-	-	-	-	100
Al_2O_3-C	80	20	-	-	-
MgO-C	-	10	-	90	-
ZrO_2-C	-	10	-	-	90
Al_2O_3-SiO_2-C	70	20	10	-	-

Steels indicated in Table II were obtained by melting a combination of electrolytic iron and low residual bar stock in an induction furnace under an argon atmosphere. Appropriate additions of carbon and aluminum were made to the melt and steel rod samples were extracted at suitable intervals by suction into quartz tubes of 0.476 cm (3/16") diameter. Steel compositions were confirmed through chemical analysis.

Table II: Steel Compositions (wt%)

Steel	C	Al
ULC	0.003	0.00
ULC-AK	0.003	0.12

A 2.54-cm (1") length of each steel rod was cut and inserted in the holes of the refractory sample before being placed in an alumina enclosure. Samples were packed in graphite to reduce the oxygen potential in the system and heated under argon to 1585°C and held for a 120 minutes after which the samples were cooled to room temperature in approximately 8 hours. Samples were then impregnated to hold the friable accretions, cut, mounted and polished to 0.5-micron finish for CL, RL and SEM characterization.

Post-mortem Analysis

Post-mortem characterization using CL provides valuable information which is not obtainable in some cases by other readily available techniques especially when used in conjunction with observations made with RL and SEM. The interactions are well characterized by CL images but the boundaries of steel and refractory cannot be accurately defined in the CL image, as steel is not luminescent. However, these boundaries are well defined in RL images and hence it becomes necessary to use both the images to preserve the information. For all photomicrographs in this paper, the top 25% is RL and the bottom 75% is CL (see Figure 13).

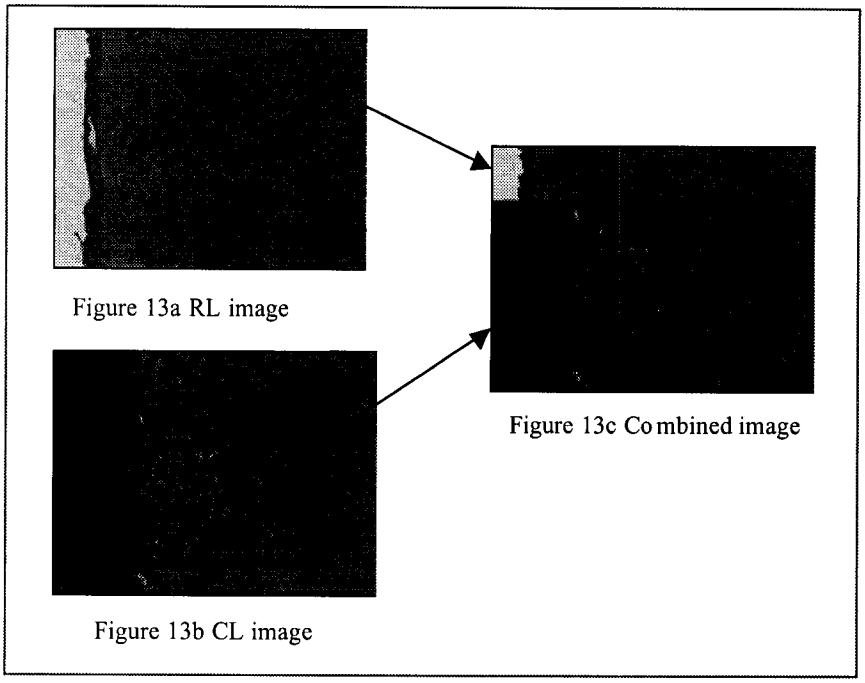

Figure 13
Interpretation of CL images

Post characterization of samples from experiments with alumina refractories revealed a "clean" interface as shown in Figure 14. Both refractories were stable with steel, the only interaction being ionic diffusion of FeO_x into the refractory, converting a thin layer of surface (~150 micron) to well-sintered hercynite ($FeAl_2O_4$). There was little difference in the level of FeO_x penetration between the two refractories as shown in Figure 14 and no inclusions were observed.

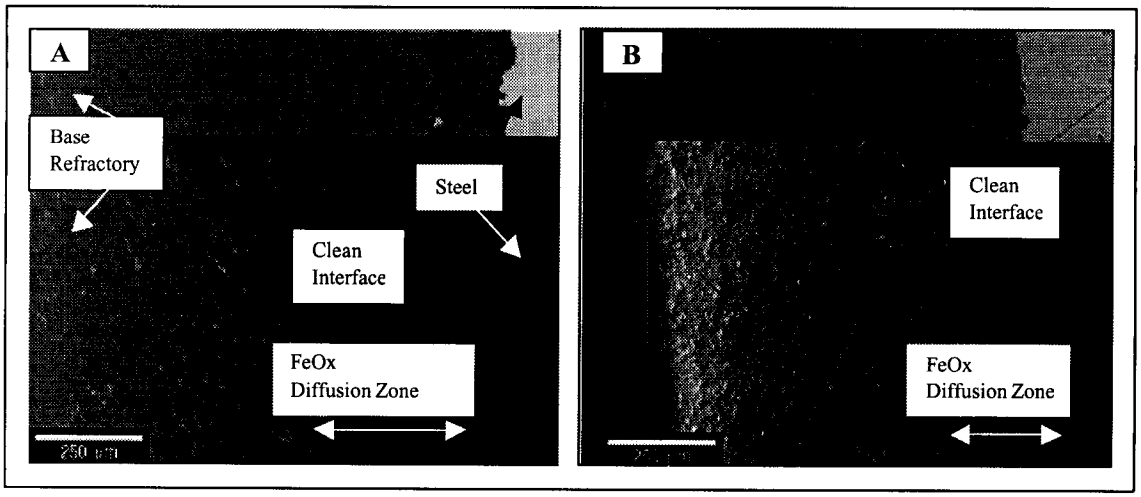

Figure 14

A. RL/CL micrograph of interface between white fused alumina refractory and ULC-AK steel.
B. RL/CL micrograph of interface between tabular alumina refractory and ULC-AK steel

Magnesia and zirconia refractories reacted similarly to the alumina refractories with no significant interactions observed. As with alumina, both had slight penetration of FeO_x and neither introduced detectable inclusions into the steel.

Graphite-containing refractories were considerable more reactive with the steel. Reduction and reoxidation reactions leading to deposition of oxides at the steel/refractory interface were common in graphite-containing refractories. Steel that was originally inclusion-free (characterized and confirmed by CL microscopy) contained a number of alumina inclusions upon interaction with an alumina-graphite refractory as shown in Figure 15. Figure 15a shows that the inclusions were mainly located near the refractory/steel interface and had needle-like morphology. Inclusions of alumina were also found in steel samples that did not contain aluminum additions (Figure 15a), confirming the redox reactions in the refractory. Alumina is reduced by carbon in the refractory to form aluminum-containing gases according to equations (12) and (13),

which react with the oxygen dissolved in steel to form alumina according to equations (19) - (21). Some discontinuous accretions were observed at the interface.

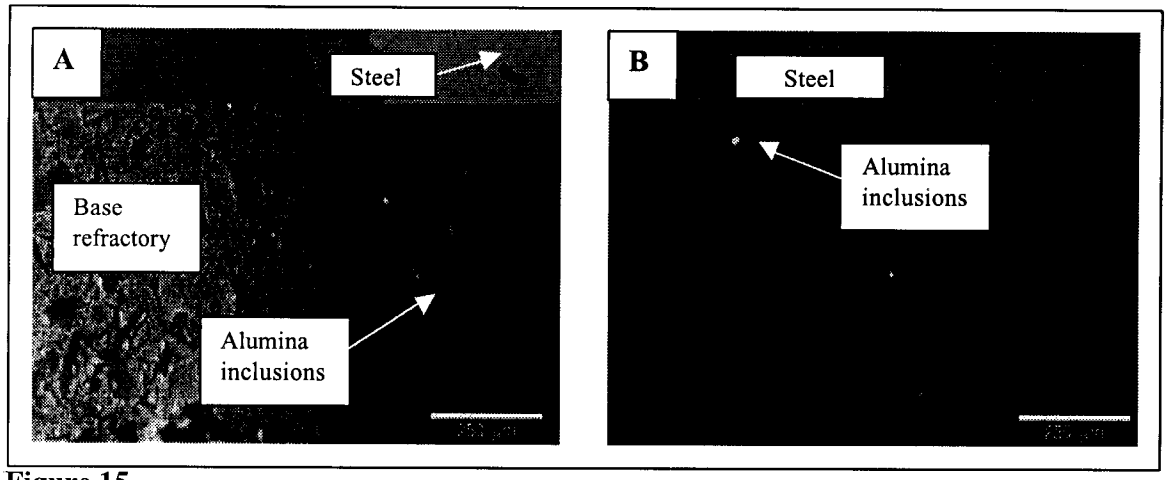

Figure 15
A.RL/CL micrograph of ULC steel /alumina-graphite refractory interface (note numerous alumina inclusions in the steel). B. RL/CL micrograph of ULC-AK steel bulk after experiment (note numerous alumina inclusions in the steel)

Substantial interactions were also observed with magnesia-graphite refractories. Few inclusions were observed in the bulk steel, but the inclusions observed displayed green luminescence color characteristic of magnesium aluminate spinel ($MgAl_2O_4$). A 50-75 micron thick oxide accretion was observed at the interface. comprised of magnesia, and traces of magnesium-calcium-silicate and entrapped steel as shown in Figure 16. The MgO powder used for fabricating the refractory for this experiment had trace amounts of calcium silicates, which accounts for the magnesium-calcium–silicate present at the interface.

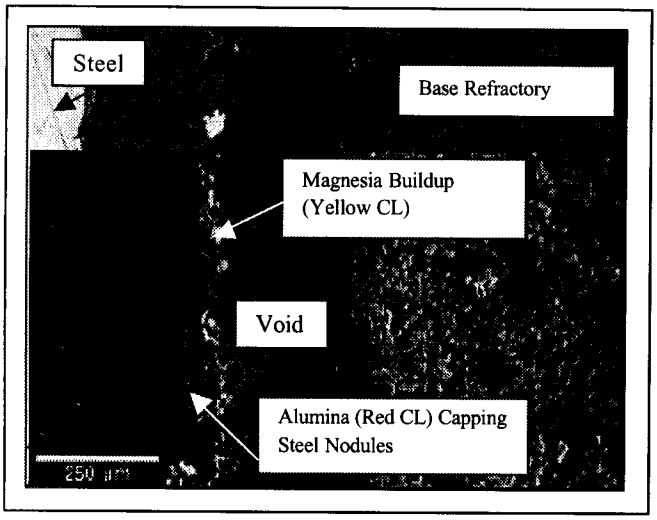

Figure 16
RL/CL photomicrograph of interface between magnesia-graphite refractory and ULC-AK steel

Among all the alumina-based refractories evaluated, alumina-silica-graphite refractories were the most reactive in terms of accretions at the interface in agreement with the thermodynamic analysis. The base refractory had a decarburized layer that was about 200 micron thick. The reaction layer adjoining the decarburized layer was roughly the same thickness. The accretion layer was uniform and contained alumina, silica and some entrapped steel. A silica increase was also observed in both ULC unkilled and ULC-AK steels using energy dispersive spectroscopic (EDS) analysis. This was expected from the thermodynamic analysis. Some areas consisted of a thin glassy silica matrix with recystallized alumina as shown in Figure 17, as predicted by thermodynamics.

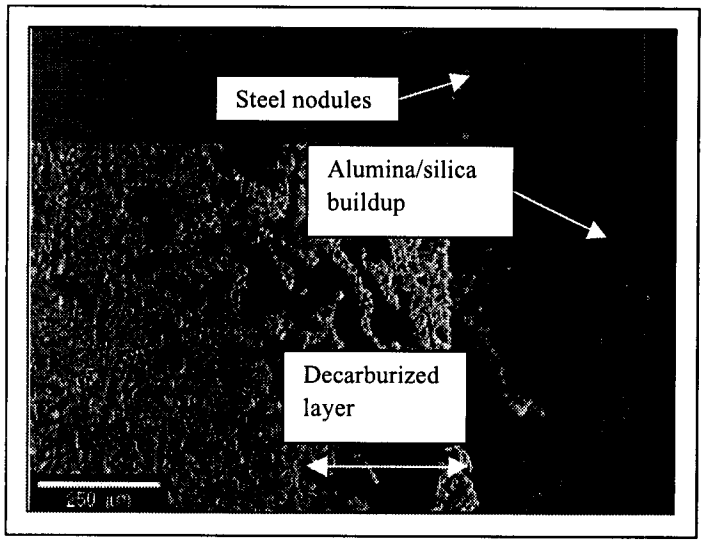

Figure 17
RL/CL photomicrograph of interface between alumina-silica-graphite refractory and ULC steel

DISCUSSION

Results from the static experiments clearly indicate that the greatest amounts of accretion/inclusion formation were observed in the Mg-O-C (Figure 16) and Al-O-C-Si (Figure 17) systems in agreement with thermodynamic predictions (see Figure 10). Both of these systems had refractories that generated substantial vapor species as shown in Figures 7 and 9. This is a clear indication that the amount of gaseous species generated by a refractory can directly impact the tendency to accrete. Conversely, systems resulting in insignificant levels of vapor species, partial pressures less than approximately 10^{-6} atm (Al_2O_3, MgO, and both carbon-free and carbon-containing ZrO_2 refractories), showed no signs of accretions/inclusions in the static experiments.

Another important result relates to the presence of additives/impurities in the refractories. Considering the Al-O and Al-O-C systems, there is a substantial difference (~7 orders of magnitude) in the amount of gaseous species evolved by the addition of 20 wt.% carbon. Recall that thermodynamic predictions indicate that the entire metallic

vapor phase will be deposited in the steel as accretions/inclusions, a result that is substantiated by the static accretion experiments (see Figure 15). Given that graphite reduced the alumina, one of the most stable refractory oxides, it is expected that less stable oxides will generate even greater amounts of vapor, eventually leading to accretions/inclusions. Both thermodynamic predictions and static accretion experiments substantiate this expectation as shown in the case of Al-O-C-Si (see Figures 9 and 17). Most refractories also contain impurities such as Na_2O, CaO, K_2O etc., in addition to silica. These impurities would also be reduced by graphite, generating additional gaseous species. Upon interaction with aluminum-killed steel, these gases will react to form additional alumina inclusions/accretions.

The results of this study indicate the potential for clogging due solely to the refractory material. Although mass balance calculations indicate that refractory reactions cannot generate sufficient solid inclusions to completely clog a nozzle, the amount is not insignificant. In fact, the nature of the reactions is such that the resulting solid inclusions will form near the refractory surface likely impacting, if not directly causing, the onset of nozzle clogging.

CONCLUSIONS

Thermodynamic calculations and static accretion experiments showed that refractory/steel interactions could contribute to nozzle accretion formation as well as increase the inclusions in the steel. Although the exact amount is difficult to verify from this study, it was shown that:

1. The gaseous species generated in the refractories are the root cause of accretions/inclusions observed in static experiments.

2. Graphite-containing refractories generate significantly higher amounts of gaseous species than graphite-free materials, due to reduction of the refractory oxides.
3. The formation of accretions and inclusions are directly related to the amount of gaseous species generated. Pure refractory oxides (Al_2O_3, MgO, and ZrO_2) and graphite-containing zirconia showed no signs of accretions/inclusions in the static experiments (nor would they be expected from thermodynamic analysis). However, the presence of unstable impurities and reducing agents resulted in significantly greater interactions and accretions.
4. Static experiments confirmed thermodynamic predictions that silica- and graphite-containing refractories induce silicon in the steel.
5. Thermodynamic calculations predict that there is a significant increase in the alumina formed at higher temperatures, which could offset some of the expected improvements in fluidity from raising the casting temperature.

ACKNOWLEDGEMENTS

The authors wish to thank the American Iron and Steel Institute and the U.S. Department of Energy for their support of this research.

REFERENCES

1. K.Sasai, Y.Mizukami, ISIJ International, Vol. 34, pp. 802-809, 1994.
2. V.Brabie, Steel Research, Vol. 68, pp. 54-60, 1997.
3. Y.Fukuda, Y.Ueshima, S.Mizoguchi, ISIJ International, Vol. 32, pp. 164-168, 1992.
4. S.Ogibayashi, M.Uchimara, et al., 75th Steel Making Conference Proceedings, pp. 304, 1992.

5. K.Sasai, Y.Mizukami, ISIJ International, Vol. 40, pp. 40-47, 2000.
6. N.Yu.Novozhilov, V.V. Khlynov, I.D.Kashcheev, B.V.Tsarevskii, Refractories, Vol. 26, pp. 78-81, 1985.
7. W.Höller, Veitsch-Radex, Vol. 6, #1, pp. 30-39, 1999.
8. J.D.Smith, K.D.Peaslee, et al., 38th Conference of Metallurgists and 29th Hydrometallurgical meeting of CIM, Quebec City, Quebec, Canada, August 23,1999.
9. K.Harold, A.Elksmitis, K.Oguri, International Symposium on Advances in Refractories for the Metallurgical Industries III, pp. 163-175, 1999.
10. V.Yves, C.Bert, B.Bart, et al., Steel Making Conference Proceedings, 2000.
11. Tsujino, Tanka, ISIJ International, Vol. 34, pp. 853-858, 1994.
12. J.Poirier, M.A.Guiban, UNITECR'95 Conference Proceedings, pp.79-86, 1995.
13. F.Hauck, J.Markert, J.Pötschke, [eds] Y.Sahai, G.R.Pierre, Advances in Transport Processes in Metallurgical Systems, Elsevier Science Publishers, 1992.
14. K.K.Strelov, I.D.Kashcheev, E.A.Visloguzova, Refractories, Vol. 26, No.7-8, pp. 331-334, 1985.
15. V.Brabie, Scandinavian Journal of Metallurgy, Vol. 25, No.4, pp.148-160, 1996.
16. P.M.Benson, Q.K.Robinson, C.Dumazeau, UNITECR'93 Congress, pp. 1087-1096, 1993.
17. Gao, Sorimachi, ISIJ International, Vol. 33, pp. 291-297, 1993.
18. S.N.Singh, Metallurgical Transactions, Vol. 5, pp. 2165-2178, 1974.
19. A.F.Dick, et al., ISIJ International, Vol. 37, No.2, pp. 102-108, 1997.
20. S.Dawson, Steelmaking Conference Proceedings, pp. 15-31, 1990.
21. L.M.Aksel'rod, Refractories, Vol.34, No. 5-6, pp. 287-290, 1993.
22. T.Smith, Steel Times, Vol.226, No.11, pp. 389-391, 1998.

15.0 Appendix I

Role Of Refractories In Nozzle Clogging During Continuous Casting

Sujatha Ramachandran

Kent D. Peaslee

Jeffrey D. Smith

Department of Metallurgical Engineering

University of Missouri-Rolla

Abstract

Accretions on the inner wall of submerged entry nozzles (SENs), tundish nozzles, or ladle nozzles are affected by interactions between the molten steel and the nozzle's refractory material. Thermochemical reactions that qualitatively explain these interactions were investigated by melting steel with and without aluminum and titanium in crucibles made from commonly used refractory materials. The refractory systems analyzed were, Al_2O_3, Al_2O_3-SiO_2, MgO, ZrO_2 and $MgAl_2O_4$ spinel (stoichiometric and high alumina) with and without graphite. Samples were characterized using cathodoluminescence microscopy (CLM), reflected light microscopy (RLM) and scanning electron microscopy (SEM). Microscopic data indicated that graphite-containing refractories, especially magnesia-graphite or alumina-silica-graphite, resulted in the greatest degree of interaction with steels leading to the buildup of an accretion. All of the carbon-free materials resulted in significantly lesser interactions.

1. Introduction

Clogging of SENs and tundish well nozzles has been a productivity and quality problem facing the steel industry for many years. Clogging is affected by a number of factors including oxide precipitation and deposition, steel chemistry, cleanliness, air aspiration through the refractory and refractory/steel interactions.

Several researchers[1-12] have investigated clogging using a variety of tools including post mortem studies of used nozzles. These studies have provided a better understanding of clogging, but a number of fundamental questions regarding the basic steel/refractory interactions and underlying reaction mechanisms remain unanswered. Some of these investigations have studied the effects of refractory/steel interactions on clogging. They showed that the nature of these interactions depends on the chemistry of the refractory and of the steel.

One of the earliest works by Hauck et al.[13] proposed that the alumina deposit originate from Al_2O gas that evolves from the reduction of alumina by carbon in the refractory nozzle. Strelov et al.[14] emphasized the significance of oxygen transport between molten steel and the oxides within the refractories. The work also postulated the presence of a gas phase in equilibrium with the refractory due to the dissociation of the oxides at high temperature according to the general equation:

$$2MO_{(s)} \Leftrightarrow 2M_{(g)} + O_{2(g)} \quad \text{and/or} \quad MO_{(s)} \Leftrightarrow M_{(g)} + O_{(g)} \tag{1}$$

Fukuda et al.[3] conducted an immersion test to understand the mechanism of network alumina formation. In the experiment, an alumina graphite rod was immersed in

an aluminum-killed steel melt and held at 1873K for 4 hours. A thin layer of alumina formed and deposited on the surface of the alumina graphite rod in contact with the steel melt. They suggested that the alumina in the alumina graphite rod is reduced by graphite in the refractory to suboxide gas, and the suboxide gas diffuses to the contact interface with molten steel and is reoxidized to form alumina. They proposed that this reaction is accelerated by the presence of silica in the refractory and the dense network of alumina formed on the surface of the refractory served as a site for deposition of suspended inclusions in the steel melt. Sasai et al.[1,5] conducted experiments that also supported this hypothesis.

Ogibayashi and colleagues[4] examined used industrial SENs and observed network alumina on the nozzle side of the interface and cluster-containing metal and chalky alumina on the molten steel side, as shown in **Figure 1**. They believed that network alumina was formed when silica in the refractory was reduced to SiO gas by graphite in the nozzle. The SiO gas formed would then react with aluminum in molten steel to form alumina and silicon as described in the following reactions:

(2) $SiO_{2(s)} + C_{(s)} = SiO_{(g)} + CO_{(g)}$ [inside the refractory]

(3) $3SiO_{(g)} + 2\underline{Al} = Al_2O_3(s) + 3\underline{Si}$ [Steel/refractory interface]

(4) $3CO_{(g)} + 2\underline{Al} = Al_2O_3(s) + 3\underline{C}$ [Steel/refractory interface]

(5) $3SiO_{2(s)} + 3C_{(s)} + 4\underline{Al} = 2Al_2O_{3(s)} + 3\underline{Si} + 3\underline{C}$ [Overall reaction]

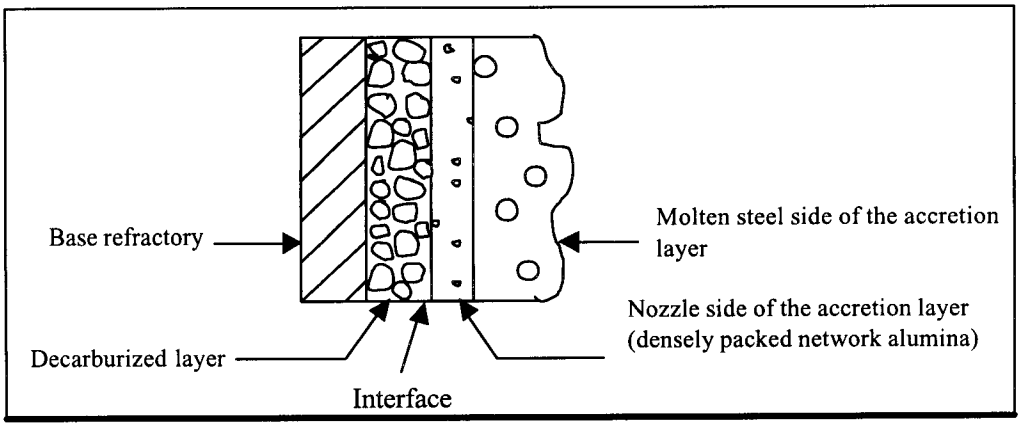

Figure 1. *Schematic of accretion morphology on industrial SENs.*

Tsujino et al.[11] investigated the conditions necessary for alumina deposition on a ZrO_2-CaO-C refractory and compared it to a similar deposition on a Al_2O_3-C refractory using rotating-immersion tests. In these tests, a refractory sample was immersed in a steel melt and rotated at 100 rpm for 15 sec to 30 min. They proposed that deposition on the nozzle proceeded in two steps. First, a fine oxide layer (the network alumina) was formed shortly after immersion at the hot face of the refractory. They believed that the fine oxide layer was formed due to the reaction between molten steel and the refractory Second, non-metallic inclusions were deposited onto the fine oxide layer.

Poirier et al.[12] focused on the influence of refractory composition on buildup of alumina accretions. This study described the mechanism of alumina deposition as a result of the thermochemical reduction of nozzle constituents coupled with oxidation of aluminum in the steel. This study presented a three-step mechanism on the deposition of alumina.

1) Formation of a decarburized zone within the refractory, due to reaction of the refractory oxides with graphite.

2) Buildup of a deposit made of alumina and a vitreous phase. This was due to the reduction of the refractory alumina and impurities such as SiO_2, Na_2O, and K_2O by graphite at steelmaking temperatures. The reduction reactions generate gaseous species according to reaction (1), which migrate to the interface due to lower partial pressure, reoxidize and condense to form the deposit.

3) Oxidation of aluminum in steel by carbon monoxide formed from the reduction reactions occurring within the refractory.

This study clearly showed that carbon in the refractory might be responsible for the deposition of alumina at the refractory/steel interface and removal of the carbon should eliminate the alumina deposition.

Brabie[15] studied the possibility of carbon monoxide absorption and precipitation of inclusions in molten steel, when aluminum deoxidized molten steel was held in contact with a carbon monoxide atmosphere. Experiments were conducted in which droplets of aluminum-deoxidized steel were levitated in different CO-He atmospheres. The droplets of aluminum-deoxidized steel were found to have a thin film of alumina after the experiments. His work indicated that, at lower aluminum contents, the film was compact and prevented further absorption of carbon monoxide while at higher aluminum contents the film was friable and could be easily detached and entrapped into molten steel as oxide inclusions.

Brabie[2] also studied the mechanism of reaction between refractory materials and aluminum deoxidized molten steel by static experiments in which steel was melted in MgO-C crucibles cut from a commercial brick. The buildup at the refractory/steel

interface consisted of pure MgO or $MgO{\cdot}Al_2O_3$, which was attributed to reaction between magnesium vapor and the carbon monoxide generated from the reduction of magnesia by carbon in the crucible walls. The oxide inclusions in the steel were mainly magnesia or alumina or a mixture of both. These studies showed that static experiments could produce accretions similar to those found in industrial nozzles.

Recent works by Holler[7] and Yves et al.[10] also confirmed that the first reaction layer, depicted as the nozzle side of the accretion layer in Figure 1, formed due to the reduction reaction within the refractory. Holler's work explored the application of a ceramic bonded inner layer for submerged nozzles to reduce the adherence of alumina on the refractory. Application of a carbon free inner layer was also discussed. Yves et al. [10] attempted to plasma coat alumina onto an alumina-graphite refractory and showed that the technique has anti-clogging potential. This idea was proposed earlier by Benson et al.[16] who performed thermochemical analyses to calculate the limiting equilibrium that occur in carbon bonded refractories. Benson et al. proposed that carbon monoxide gas affects alumina formation in aluminum-killed steel and indicated that a carbon-free liner would help in the prevention of alumina buildup.

Refractory composition may have various implications on the clogging process. First, the interaction of the nozzle refractory with the melt, which directly depends on the refractory composition, leads to accretion formation on the nozzle walls or alterations of the chemistry of the melt. In addition, the mere surface alteration of the nozzle facing the molten steel as a result of the chemical reaction could provide a site for nucleation of inclusions in the melt. The contributions of these factors to the actual clogging process are not clearly understood. This study aims at understanding the effect of refractory

composition on accretion formation, which could lead to nozzle clogging. Although some fundamental studies were performed in the previous works cited, more work needs to be done to understand the effect of the different components in the refractory and the nature of interactions and the thermochemical reactions in each case.

This paper presents the results of experiments conducted to establish the effect of refractory composition on accretion formation. The experiments were conducted with various refractories, fabricated with controlled additives, which were then tested for their interactions with molten steel. The interactions between commonly used refractory materials and molten steel are explained. The strategy used in the study was to perform static experiments with molten steel of different compositions in crucibles made of various refractories, followed by a post mortem characterization using cathodoluminescence microscopy (CLM), reflected light microscopy (RLM) and scanning electron microscopy (SEM).

2. Experimental

2.1 Materials

In an attempt to simulate and understand the interaction of steel with nozzle materials, experiments were conducted using the common refractories shown in **Table 1**. Refractories were fabricated in-house by mixing 99+% pure powders (see **Table 2**) with phenolic binder in the case of carbon-bonded refractories, and pressing to an aim pressure of 345 MPa (50 ksi) in an isopress. Non-carbon containing green refractory compacts were fired at 1600-1625°C. Carbon-bonded refractories were heated to 225°C to allow for phenolic binding. The refractories produced were 85-90% of the theoretical density. Four holes, 0.635 cm (¼") diameter and 2.54 cm (1") deep were machined in each refractory

sample as shown in **Figure 2**. Each hole represents a separate crucible allowing four steel chemistries to be tested with each refractory composition.

	Refractory	Al_2O_3	C	SiO_2	MgO	ZrO_2
Non-carbon Containing	Al_2O_3 (Tabular or Whitefused)	100	-	-	-	-
	Al_2O_3-SiO_2 (Tabular)	90	-	10	-	-
	MgO	-	-	-	100	-
	ZrO_2	-	-	-	-	100
	$MgAl_2O_4$ (Stoichiometric)	56 (As spinel)	-	-	44 (As spinel)	-
	$MgAl_2O_4$ (High Alumina)	64 (As spinel)	-	-	36 (As spinel)	-
Carbon Containing	Al_2O_3-C (Tabular)	80	20	-	-	-
	MgO-C	-	10	-	90	-
	ZrO_2-C	-	10	-	-	90
	Al_2O_3-SiO_2-C (Tabular)	70	20	10	-	-
	$MgAl_2O_4$-C (Stoichiometric)	50.4 (As spinel)	10	-	39.6 (As spinel)	-
	$MgAl_2O_4$-C (High Alumina)	57.6 (As spinel)	10	-	32.4 (As spinel)	-

Table 1: *Refractory compositions (wt%)*

Raw Material	Purity	Impurities
Alumina (tabular and white fused)	99.0	CaO, Na_2O
Silica	99.5	CaO
Magnesia	98.2	CaO, SiO_2
Zirconia	99.2	CaO
Stoichiometric Spinel	99.0	CaO, Na_2O
High Alumina Spinel	99.0	CaO, Na_2O
Graphite	99.0	SiO_2

Table 2: *Purity of raw materials*

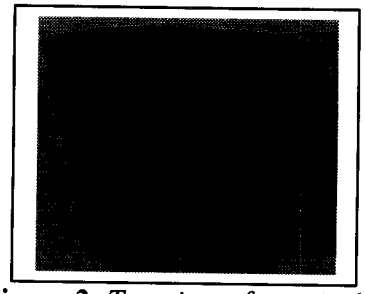

Figure 2: *Top view of a typical refractory sample with holes drilled*

Steels of four compositions (see **Table 3**) were obtained by melting a combination of electrolytic iron and low residual bar stock (ARMCO 1001 HP) in an induction furnace under an argon atmosphere. After the entire charge was molten, the steel was held at 1585°C for 3 minutes and an oxygen measurement obtained. Aluminum additions were based on complete deoxidation using the oxygen reading and the final chemistry (assumed 95% recovery). Titanium was added after the aluminum based on a 95% recovery. After the additions were made, the melt was allowed to stir by maintaining temperature with the induction power for 30 seconds followed by taking a chemical sample. Steel rods to be used in the experiments were obtained using a venturi sampler attached to 0.476 cm (3/16") diameter quartz tubes. Steel was drawn into the quartz tubes and several rods of 20-25 cms in length were obtained. A final chemical sample was obtained to quantify any fade of aluminum as shown in Figure 3.

Steel Type*	Aim			Actual**		
	C	Al	Ti	C	Al	Ti
ULC (B)	0.003	0.00	0.00	0.0040	-	-
ULC-Al (B)	0.003	0.12	0.00	0.0030	0.1235	0.0006
ULC-Al (A)	0.003	0.12	0.00	0.0027	0.1197	0.0006
ULC-Al-Ti (B)	0.003	0.12	0.10	0.0024	0.1162	0.1169
ULC-Al-Ti (A)	0.003	0.12	0.10	0.0033	0.1134	0.1157
MC-Al-Ti (B)	0.20	0.12	0.10	0.2360	0.1137	0.1083

Table 3: *Steel compositions (wt%)*

* "B" in parentheses indicates that the chemical sample was acquired before the actual tube samples; "A" indicates after. ** All heats low residual (average): Mn: 0.0403, P: 0.0051, S: 0.0054, Si: 0.0099, Cu: 0. 003, Ni: 0.0069, Cr: 0.0031, Mo: 0.0009, Sn: 0.0013, Nb: 0.0014

2.2 Procedure

A 2-3 g (~2.54 cm long) steel sample from each of the four steels was placed in the holes in the refractory samples. The refractory was placed in an alumina enclosure and graphite was packed around the sample to reduce the oxygen potential in the system (see **Figure 3**). After covering the alumina enclosure with an alumina lid, argon (high purity) was fed through a tube in the lid to provide an inert environment. The experimental apparatus was placed in a resistance furnace and heated at the rate of 130°C/hour to 1585°C, held for a 120 min, and furnace cooled for about 8 hours. Samples were impregnated with a low viscosity resin to hold the friable accretions, cured, cut, mounted and polished to 0.5-micron finish for cathodoluminescence/reflected light/scanning electron microscopy.

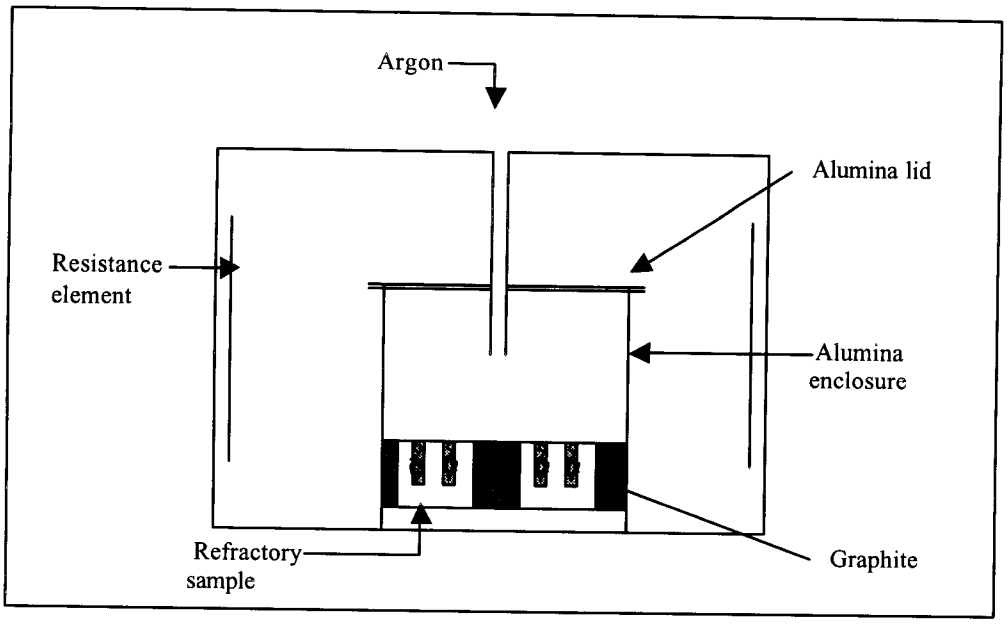

Figure 3: *Schematic of the experimental apparatus*

2.3. Post-characterization

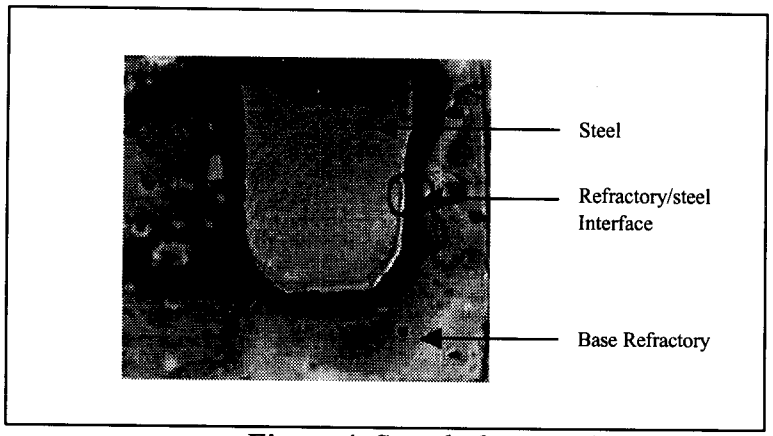

Figure 4: *Sample for post characterization*

Figure 4 is a typical sample prepared for post-characterization of the interaction zone and the base refractory. The area circled in the figure was the refractory/steel interface where most of the interactions are observed. The characterization of the samples was usually done using scanning electron microscopy (SEM), reflected light microscopy (RL) or other techniques. However, in this study cathodoluminescence microscopy (CLM) is employed for post characterization. CLM is relatively new for applications in

steel and refractory research, but has proved to be very effective tool. CLM is a technique in which samples are bombarded with energetic electrons from an electron gun. The application of CLM to post mortem characterization of spent nozzles has previously been discussed by Smith et al. [8]. In some cases, valuable information can be obtained by CLM, which is not obtainable by other readily available techniques. The CLM observations provide precious information when used in conjunction with observations made with RLM and SEM.

The interactions are well characterized by CLM images but the boundaries of steel and refractory cannot be accurately defined in the CLM image, as steel is not luminescent. However, these boundaries are well defined in RLM images and hence it becomes necessary to use both the images to preserve the information. In light of the above discussion, the top 25% of all micrographs is RLM and the bottom portion is CLM (see **Figure 5**).

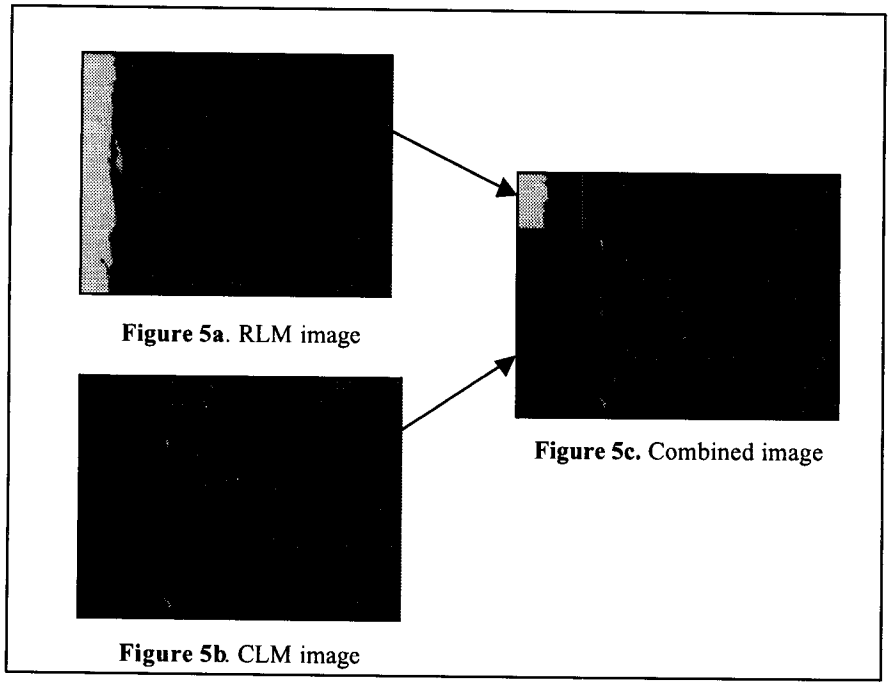

Figure 5: *Interpretation of micrographs*

3. Results and discussion

3.1 Carbon-free refractories

3.1.1 Alumina (tabular/white fused)

Tabular alumina is aluminum oxide that has been heated to temperatures above 1,650°C (3,000°F). Composed of tablet-like crystals, it has high heat capacity and thermal conductivity as well as exceptional strength and volume stability at high temperatures. For these reasons, a major use of tabular alumina is in the production of high-quality refractories. Fused aluminas are currently used in special refractories for the glass industry. Fused alumina is calcined alumina that is melted in electric-arc furnaces, cooled, crushed, and recast into desired shapes. Both tabular and white fused alumina was tested for their interaction with steel with a motive of determining the difference in performance between different forms of the same material.

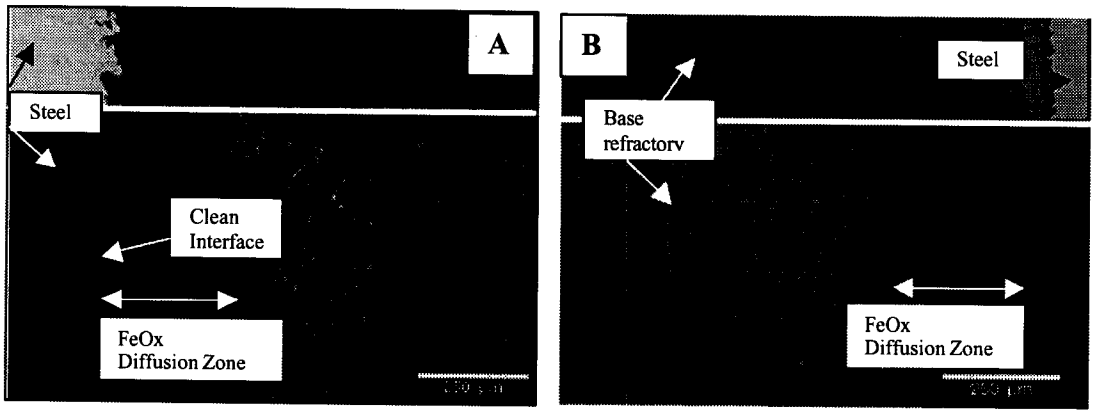

Figure 6A. *RL/CL micrograph of white fused alumina / ULC-Al steel interface.* ***Figure 6B.*** *Tabular alumina/ULC-Al steel interface*

The post characterization of samples from the experiments with tabular and white fused alumina revealed a "clean" interface with all the steel chemistries. Both the refractories were very stable and the only interaction was ionic diffusion of FeO_x into the

refractory surface, converting a thin layer of refractory (~150 micron) to well-sintered hercynite ($FeAl_2O_4$). There was no remarkable difference in the level of FeO_x penetration between the refractories (see **Figure 6**).

3.1.2. Alumina-silica

Aluminosilicate refractories did not exhibit obvious reactions with any of the steels. However, dissolution of silica in steel was detected by SEM/EDS analysis. The concentration of silicon was highest near the interface and progressively decreased in the bulk. There was no significant difference in their interaction with different steel chemistries. FeOx diffusion into the base refractory was observed to a very small extent as shown in **Figure 7**.

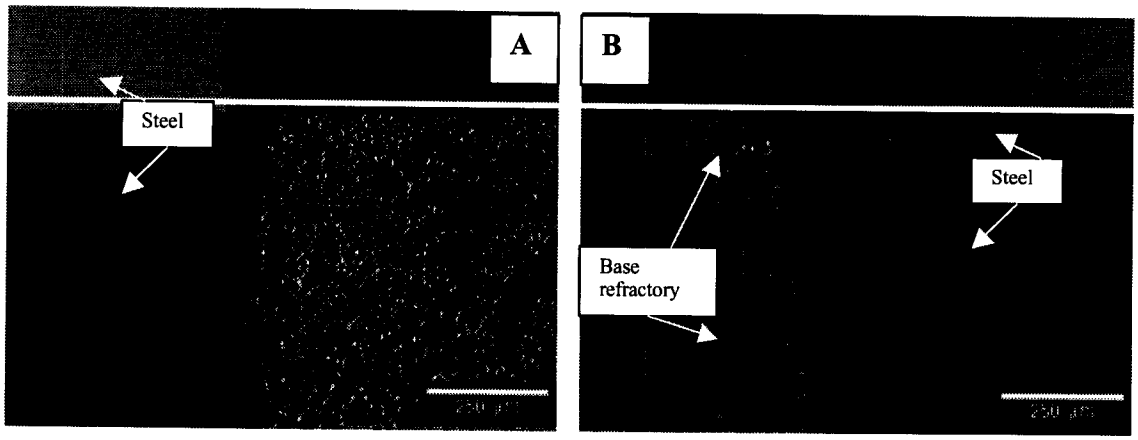

Figure 7A. *RL/CL micrograph of alumina-silica refractory / ULC-Al-Ti steel interface.* ***Figure 7B.*** *Alumina-silica refractory /MC-Al-Ti steel interface*

3.1.3 Magnesia

Pure MgO refractories did not have a pronounced interaction with steel although very high diffusion of FeO_x was observed (see **Figure 8**). The diffused FeO_x enters into a solid solution with MgO. The penetrated zone is well sintered and the refractory as well

as the steel surface was very smooth. Similar interaction was observed in all steel chemistries.

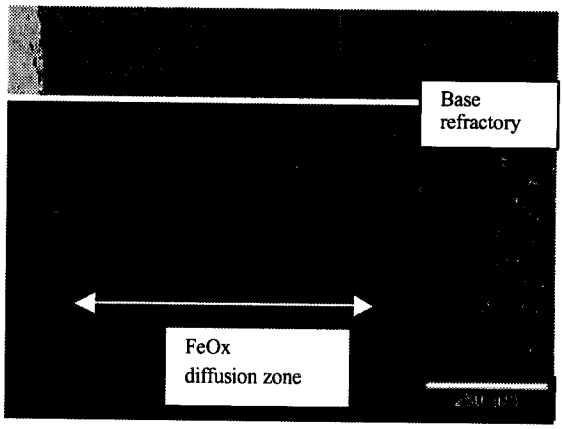

Figure 8: *Magnesia refractory/ULC-Al steel interface*

3.1.4 Zirconia

Zirconia refractories were found to be chemically very stable in contact with all molten steel chemistries as can be seen in **Figure 9**. No buildup was observed and the refractory and steel surface was clean. A thin layer of FeO_x diffusion was observed.

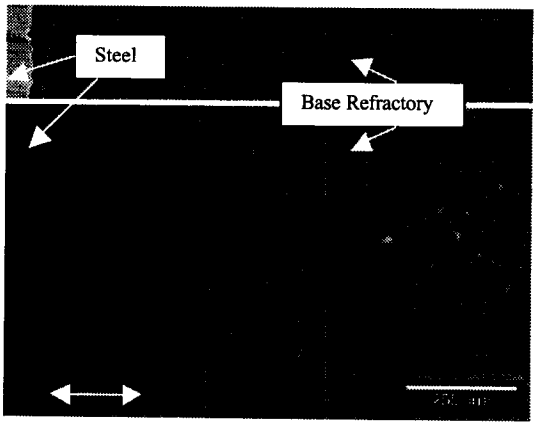

FeOx Diffusion Zone

Figure 9: *Zirconia/steel interface*

3.1.5 Magnesium aluminate spinel (stoichiometric and high alumina)

Magnesium aluminate spinels were also tested for their interaction with molten steel. Although no accretions were observed on interaction with any of the steel chemistries, diffusion of magnesia in the refractory towards the interface was typical. This can be well observed in micrographs from high alumina spinel-graphite systems (**Figure 10A**). A thick alumina rich band (Red CL) can be observed in the refractory near the interface. The stoichiometric spinel systems behave similarly, though it is not obvious from the micrograph, **Figure 10B.**

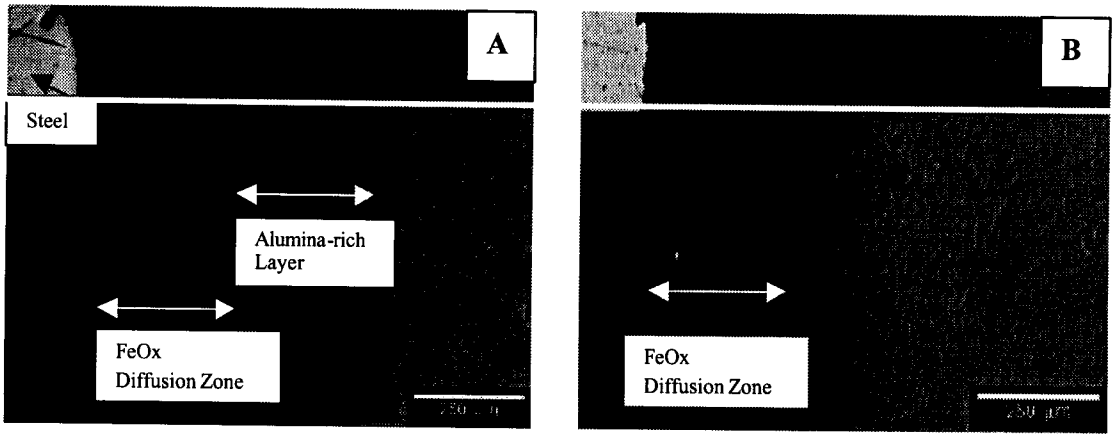

***Figure 10A**: High alumina spinel/ULC-Al system.* ***Figure 10B**: Stoichiometric spinel/ ULC-Al steel interface*

The reason behind the difference in the appearance between the two spinel systems can be explained based on the phase diagram provided in **Figure 11**. In this diagram, the initial composition of the stoichiometric spinel and high alumina spinel are marked as green and red dots respectively. As the experiment proceeded the diffusion of magnesia towards the interface took effect and the loss of magnesia from the stoichiometric spinel

system did not affect the CL color as the system was still in the spinel region as shown by the arrow. However, in the high alumina spinel system, the start point is the spinel corundum binary phase field and as magnesia diffuses out, the refractory becomes corundum rich exhibiting red CL. This magnesia reacts with the FeO_x diffusing in and the base refractory to form a complex $FeO\text{-}MgO\text{-}Al_2O_3$ spinel region within the refractory.

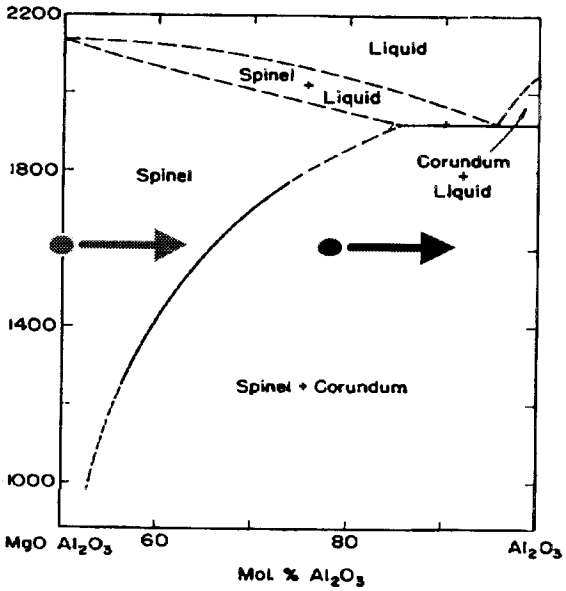

Figure 11: *Spinel-alumina phase diagram*

3.2 Carbon-bonded refractories

3.2.1 Alumina-silica-graphite

Among all the alumina-based refractories that were tested, alumina-silica-graphite refractories were the most reactive in terms of buildups at the interface. The base refractory that was exposed to the steel shows the presence of a decarburized layer of about 200 micron thick. The reaction layer was adjoining the decarburized layer and was roughly about the same thickness as the decarburized layer. The accretion layer was not

perfectly continuous and was found to consist of alumina, silica, and entrapped steel. An increase in the silicon content in steel was also detected with SEM/energy dispersive spectroscopy (EDS) analysis. Alumina accretions with steel entrapped were more common, while in some areas a thin glassy silica matrix with recystallized alumina was observed (see **Figure 12**). In case of Al killed steels, several alumina inclusions were observed in the steel as it can be seen in **Figure 12A**.

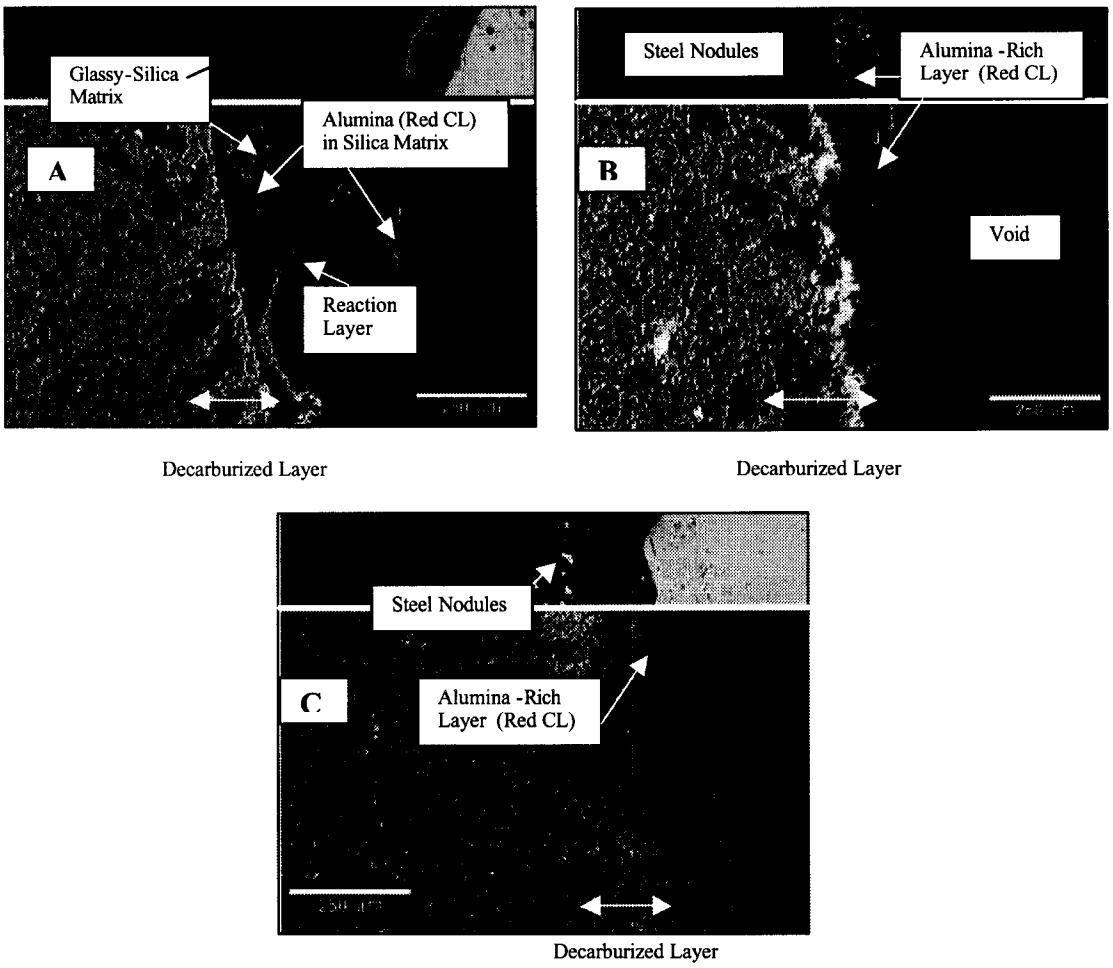

Figure 12A&B: *Reaction front in Al_2O_3-SiO_2-C graphite refractory/ULC-Al steel showing alumina buildup and glassy silica matrix.*
Figure 12C: *Interface between Al_2O_3-SiO_2-C graphite refractory/ULC steel*

The formation of the accretion at interface can be attributed to the reduction reactions that occur in the refractory. The alumina and silica in the refractory are reduced by carbon in the refractory to produce alumina and silica suboxide gases respectively. These gases migrate to the interface owing to the lower pressure and reoxidizes to alumina and silica as explained in the following reactions:

(6) $SiO_2\,(s) + C\,(s) = SiO\,(g) + CO\,(g)$

(7) $Al_2O_3\,(s) + 2C\,(s) = Al_2O\,(g) + 2CO\,(g)$

The SiO and Al_2O suboxide gases are not the only gases that form at the temperature. These are the major species while there are other suboxide gases, which undergo the same reactions. These gases diffuse to the interface and are reoxidized to silica and alumina by reacting with the dissolved oxygen in steel or oxygen leaked in to the system. The SiO and CO also reacts with the aluminum dissolved in steel to form alumina according to the following reactions:

(8) $SiO\,(g) + \underline{Al} = Al_2O_3\,(s) + \underline{Si}$

(9) $3CO\,(g) + 2\underline{Al} = Al_2O_3\,(s) + 3\underline{C}$

An increase in silicon content in steel as predicted by equation (8) was observed in the experiments conducted and was confirmed by SEM/EDS analysis.

3.2.2 Alumina-graphite

Experiments with Al_2O_3-C refractories resulted in a defined accretion layer of alumina as shown in **Figure 13**. However, the interactions were not as severe and the reaction layer was relatively thin (~ 25-40 micron).

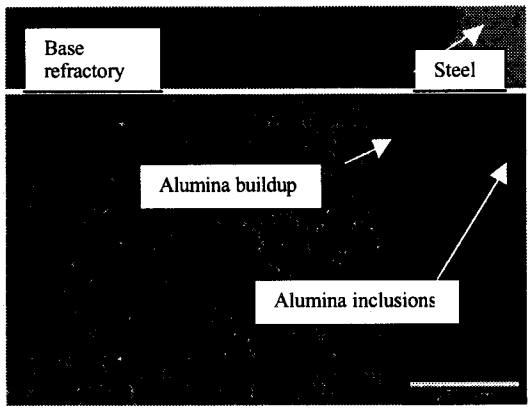

Figure 13: *ULC-Al-Ti steel/ Al_2O_3-C refractory interface*

The clean steel (characterized and confirmed by CLM) that was used for the experiments now contained some prominent alumina inclusions, mainly near the interface, however more inclusions were observed in the bulk steel in case of Al killed steels. No measurable difference was observed in case of medium carbon steels. These inclusions had needle-like morphology and were reaction products from refractory/steel interaction. Deposits of alumina were found bordering even those steel samples, which did not contain any aluminum additions, confirming the redox reactions in the refractory. The alumina in the refractory is reduced by carbon in the refractory to form aluminum suboxide and metal gases (Al_2O, Al), which reoxidizes at the interface and/or reacts with the oxygen dissolved in steel to form alumina.

3.2.3 Magnesia-graphite

A large number of interactions were observed with MgO-C refractories. Few inclusions, which showed green luminescence color, were observed in the steel bulk. These were found to be magnesium aluminate spinel ($MgO.Al_2O_3$). A 50-75 micron thick oxide layer was observed at the interface. In some cases, steel was observed in the oxide layer. The oxide layer was found to be very discontinuous and comprised of magnesia and with traces of magnesium-calcium-silicate as shown in **Figure 14**. The MgO powder used for fabricating the refractory for this experiment had trace amounts of calcium silicates, which explains the magnesium-calcium–silicate that was found at the interface.

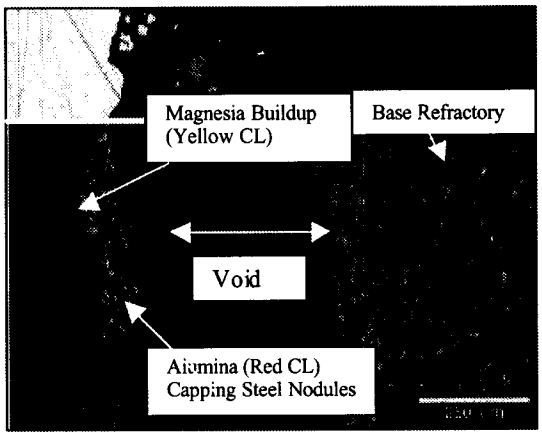

Figure 14: *Reaction front of MgO-C refractory / ULC-Al-Ti steel*

There are many reactions that successively proceed to cause these interactions. The first step was the reduction of MgO by carbon in the refractory to yield Mg (g) and CO (g). According to Brabie [2], magnesium can be characterized by a very high vapor pressure and low solubility at steelmaking temperatures along with a high affinity for oxygen. This explained the buildup of magnesia at the interface and CO formation. The CO also reacted with the aluminum dissolved in steel (in all Al killed steels) to form alumina. This alumina further reacted with diffused $Mg_{(g)}$ and oxygen to form magnesium aluminate

spinel. The steel nodules trapped in the oxide layer is bordered by alumina, is a strong proof of the reaction between carbon monoxide and aluminum dissolved in the steel (reaction 9).

3.2.4 Zirconia-graphite

ZrO_2-C refractories were more stable to reduction by carbon. However, the stabilizer (CaO) used for zirconia was reduced. The oxide gases migrated to the interface and was reoxidized and deposited on the surface of the refractory on interaction with all steel chemistries as shown in **Figure 15**.

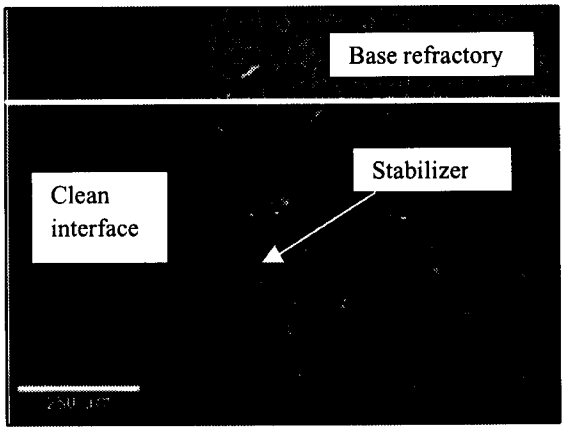

Figure 15: *Interface between Zirconia-graphite refractory and MC-Al-Ti steel*

3.2.5 Magnesium aluminate spinel - graphite

The magnesium aluminate spinel-graphite systems led to complex reactions. Both stoichiometric spinel-graphite and high alumina spinel-graphite were tested for their interaction with molten steel (both ULC and ULC-AK). Accretions of spinel and alumina were observed at the interface along with steel nodules in the case of stoichiometric

spinel (**Figure 16A**) while recystallized spinel was observed on the refractory surface exposed to steel in case of high alumina spinel (**Figure 16B**). The formation of the accretions was similar to that discussed for the other carbon bonded refractories.

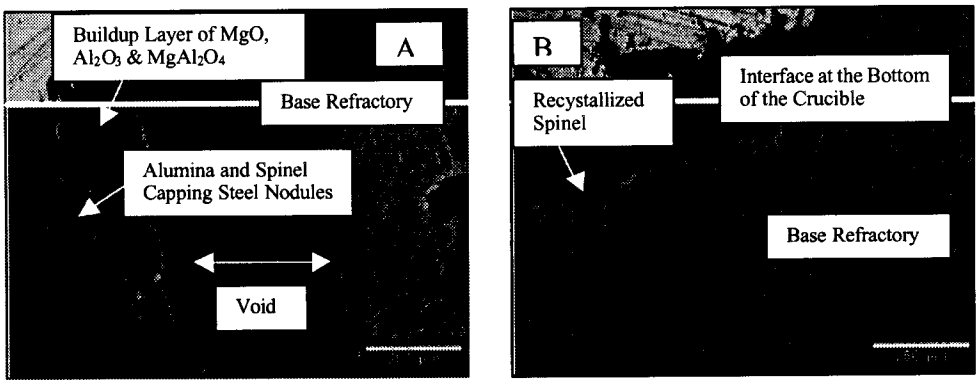

***Figure 16A**: Oxide layer found in stoichiometric spinel-graphite system. **Figure 16B** (Right) shows the interface in the high alumina spinel-graphite systems*

4.Conclusions

This study focused on nozzle refractory materials and their relationship to the accretion buildup mechanism. Although the actual contribution of the nozzle refractory to clogging cannot be accurately measured, accretions formed might be the onset or initiation site for buildups that eventually clog nozzles.

Some conclusions for the study are:

1. The addition of carbon to refractory materials leads to accretion formation on the nozzle wall and also introduces solid inclusions into the melt. The reduction of the base refractory by graphite leading to the formation of suboxide gases and metal gases, which are transported to the interface where they are oxidized, caused these accretions.

2. Pure refractory oxides without common additives or impurities such as carbon and silica, had the least interaction with steel, although the magnitude of interaction between the different refractory oxides and steel varied. Among the other refractories that were tested, pure zirconia was found be very stable in contact with molten steel. Also, pure alumina and magnesia refractories exhibited considerable stability and no significant interactions were observed..
3. Alumina-silica-graphite and magnesia-graphite resulted in the greatest degree of interaction with steels leading to accretions.
4. In the spinel refractory systems, internal diffusion of MgO towards the interface was observed. This MgO reacts with the FeO_x that diffuses into the refractory surface to form complex $FeO\text{-}MgO\text{-}Al_2O_3$ spinels.

Acknowledgements

The authors wish to thank the American Iron and Steel Institute and the U.S. Department of Energy for their continual support for this research. We are also grateful to AISI-member companies for their help with the chemical analysis of the samples.

References

1. Sasai, K.; Mizukami, Y.; "Reaction Mechanism between Alumina Graphite Immersion Nozzle and Low Carbon Steel'. ISIJ International, Vol. 34, pp. 802-809, (1994).
2. Brabie, Voicu; "A Study on the Mechanism of Reaction Between Refractory Materials and Aluminum Deoxidized Molten Steel". Steel Research, Vol. 68, pp. 54-60, (1997).

3. Fukuda, Y.; Ueshima, Y.; Mizoguchi, S.; " Mechanism of Alumina Deposition on Alumina Graphite Immersion Nozzle in Continuous Caster". ISIJ International, Vol. 32, pp. 164-168, (1992).
4. Ogibayashi, S.; Uchimara, M. et al. " Mechanism and Countermeasure of Alumina Buildup on Submerged Nozzle in Continuous Casting". 75th Steel Making Conference, Proceedings, pp. 304, (1992).
5. Sasai, K.; Mizukami, Y.; "Reoxidation Behavior of Molten Steel in Tundish". ISIJ International, Vol. 40, pp. 40-47, (2000).
6. Novozhilov, N.Yu.; Khlynov, V.V.; Kashcheev, I.D.; Tsarevskii, B.V.; "Selecting a Refractory Coating on the Basis of its Interaction with a Metal". Refractories, Vol. 26, pp. 78-81, (1985).
7. Höller, Wolfram. "Prevention of Alumina Clogging in Submerged Entry Nozzles". Veitsch-Radex, Vol 6, #1, pp. 30-39, (1999).
8. Smith, J.D.; Peaslee, K.D. et al.; " Study of Continuous Casting Nozzle Clogging using Cathodoluminescence Microscopy". 38th Conference of Metallurgists and 29th Hydrometallurgical meeting of CIM, Quebec City, Quebec, Canada, August 23,1999.
9. Harold, K.; Elksmitis, A.; Oguri, K. et al.; " The Evolution of Anti-clogging Materials for Submerged Entry Nozzles". International Symposium on Advances in Refractories for the Metallurgical Industries III, pp. 163-175, (1999).
10. Yves, V.; Bert, C.; Bart, B.; "Prevention of Nozzle Clogging during the Continuous Casting of Al-killed Steels". Steelmaking Conference Proceedings, (2000).

11. Tsujino; Tanka; "Mechanism of Deposition of Inclusion and Metal in ZrO2- CaO-C Immersion Nozzle of Continuous Casting". ISIJ International, Vol. 34, pp. 853-858, (1994).

12. Poirier, J; Guiban, M.A.; "Development of New Submerged Nozzles to Reduce Alumina Buildup in Continuous Casting". UNITECR'95 Conference Proceedings, pp. 79-86, (1995).

13. Brabie, Voicu; "The Reaction of Carbon Monoxide in Al-deoxidized Molten steel". Scandinavian Journal of Metallurgy, Vol 25, No.4, pp. 148-160, (1996).

14. Askel'rod, L.M. et al; "Interaction of Steel of Refractories Containing Oxygen-Free Additions".

15. Strelov, K.K.; Kashcheev, I.D.; Visloguzova, E.A.; "Distribution of Oxygen Between Molten Steel and Oxide Refractories". Refractories, Vol 26, No.7-8, pp. 331-334, (1985).

16. Hauck, F.; Markert, J; Pötschke, J. et al.; " Interactions Between Refractories and Melts at High Temperature Processes". [eds] Sahai, Y.; Pierre, G.R.; Advances in Transport Processes in Metallurgical Systems, Elsevier Science Publishers, (1992).

17. Gao; Sorimachi; " Formation of Clogging Materials in an Immersion Nozzle during Continuous Casting of Titanium Stabilized Stainless Steel". ISIJ International, Vol. 33, pp. 291-297, (1993).

18. Benson, P.M.; Robinson, Q.K.; Dumazeau, C.; "New technique for the Prevention of Alumina Build-up in Submerged entry Nozzles for Continuous casting". UNITECR'93 Congress, pp. 1087-1096, (1993).

19. Singh, S.N.; "Mechanism of Alumina Buildup in Tundish Nozzles during Continuous Casting of Aluminum-Killed Steels". Metallurgical Transactions, Vol. 5, pp. 2165-2178, (1974).

20. Dick, A.F. et al; "Attack of submerged entry Nozzles by Mould Flux and Dissolution of Refractory Oxides in the Flux". ISIJ International, Vol. 37, No.2, pp. 102-108, (1997).

21. Dawson. S; "Tundish Nozzle Blockage during Continuous Casting of Aluminum-Killed Steels". Steelmaking Conference Proceedings, pp. 15-31, (1990).

22. Aksel'rod, L.M.; "Refractories for the Continuous Casting Machines: Experience in the Solution of Problems and Prospects". Refractories, Vol.34, No. 5-6, pp. 287-290, (1993).

23. Smith, T.; "Continuous Casting – A Mature Technology". Steel Times, Vol.226, No.11, pp. 389-391, (1998).